

STRATIGRAPHIC VARIATION AND FACIES ARCHITECTURE IN
FLUVIAL AND TIDALLY INFLUENCED SANDBODY UNITS OF THE
NON-MARINE PORTION OF THE ILES FORMATION, RIO BLANCO
AND MOFFAT COUNTIES, NORTHWEST COLORADO, USA

by

Jeffrey Alan Thompson

A thesis submitted to the Faculty and the Board of Trustees of the Colorado School of Mines in the partial fulfillment of the requirements for the degree of Master of Science (Geology).

Golden, Colorado

Date _____

Signed: _____
Jeffrey Alan Thompson

Signed: _____
Dr. Donna S. Anderson
Thesis Advisor

Golden, Colorado

Date _____

Signed: _____
Dr. John D. Humphrey
Professor and Head
Department of Geology and Geological Engineering

ABSTRACT

Many subsurface reservoir models in non-marine units are based primarily on point bars and tidal influence is rarely reported in the non-marine portion of the upper Mesaverde Group. However, a detailed outcrop study of the non-marine portion of the Iles Formation north of Rangely, Colorado finds a much greater variety of non-marine sandbodies than just point bars and extensive evidence of tidal influence. This study describes in detail 23 sandstone units, organized into eight major sandbodies, and interprets the depositional history of these units. Thirteen additional sandstone units are documented in lesser detail. These sandstone units are grouped into four fluvial sandbody types, fluvial channel fills, fluvial constructional bars, point bars, and minor crevasse splays and channels, and six tidally influenced sandbody types, tidal bars, tidally influenced channel fills, fill and spill channels, tidally influenced splays, tidal constructional bars, and tidally influenced braided complexes.

There are two types of cyclicity observed in the field area. There are at least three short-term (thousands to tens of thousands years) cycles of mudstone to sandstone dominated intervals which are linked to the migration of the main channelbelt. One longer term (~100,000 years) cycle of decreasing to increasing tidal influence, linked to the migration of the Iles shoreline and relative sea-level, is also observed.

The non-marine Iles Formation in the Rangely area has not been previously correlated to the named members of the Iles Formation. This study correlates the field area into the Rollins and Cozzette members based on a number of sequence stratigraphic indicators commonly used non-marine units in the geologic literature including tidal indicators, evidence of lengthy subaerial exposure, and amalgamation of sandstone units.

TABLE OF CONTENTS

ABSTRACT	iii
LIST OF FIGURES	viii
LIST OF TABLES	xi
ACKNOWLEDGEMENTS	xii
CHAPTER 1: INTRODUCTION	1
1.1 Field Area.....	3
1.2 Methods.....	3
1.3 Local Stratigraphy.....	5
1.4 Regional Stratigraphy	6
1.5 Regional Structure and Tectonics	8
1.6 Thesis Organization	9
CHAPTER 2: FACIES AND FACIES ASSOCIATIONS	17
2.1 Mud-clast Conglomerate Facies	17
2.2 Trough Cross-stratified Sandstone Facies	18
2.3 Planar Tabular Cross-stratified Sandstone Facies.....	20
2.4 Convolute Sandstone Facies	21
2.5 Structureless Sandstone Facies	23
2.6 Sigmoidal Cross-stratified Sandstone Facies.....	24
2.7 Mud-draped Planar Tabular Cross-stratified Sandstone Facies.....	25
2.8 Climbing-rippled Sandstone Facies	26
2.9 Current-rippled Sandstone Facies	27
2.10 Mud-draped Current-rippled Sandstone Facies	28

2.11 Wave-rippled Sandstone Facies	29
2.12 Bioturbated Sandstone Facies	29
2.13 Root-Trace Dominated Sandstone Facies.....	30
2.14 Undifferentiated Mudstone Facies.....	31
2.15 Organic-rich Mudstone Facies	32
2.16 Coal Facies.....	33
2.17 Paleocurrents.....	34
2.18 Summary of Floodplain Facies Association	34
2.19 Summary of Channelbelt Facies Association	35
CHAPTER 3: MAJOR SANDBODIES	55
3.1 Sandbody I	56
3.1.1 Subbody I1	57
3.1.2 Subbody I2	58
3.1.3 Subbody I3	59
3.1.4 Interpretation.....	60
3.2 Sandbody J	61
3.2.1 Subbody J1.....	62
3.2.2 Subbody J2.....	63
3.2.3 Subbody J3.....	64
3.2.4 Interpretation.....	64
3.3 Sandbody A.....	65
3.3.1 Subbody A1	66
3.3.2 Subbody A2	68

3.3.3 Subbody A3	69
3.3.4 Subbody A4	69
3.3.5 Interpretation.....	70
3.4 Sandbody H.....	71
3.4.1 Subbody H1	72
3.4.2 Subbody H2	72
3.4.3 Interpretation.....	73
3.5 Sandbody G.....	74
3.5.1 Subbody G1	74
3.5.2 Subbody G2	75
3.5.3 Subbody G3	76
3.5.4 Subbody G4	77
3.5.5 Interpretation.....	77
3.6 Sandbody B/C	79
3.6.1 Subbody B.....	79
3.6.2 Subbody C.....	80
3.6.3 Interpretation.....	81
3.7 Sandbody F	82
3.7.1 Subbody F1	83
3.7.2 Subbody F2	84
3.7.3 Subbody F3	84
3.7.4 Interpretation.....	85
3.8 Sandbody D/E	86

3.8.1 Subbody D/E1	86
3.8.2 Subbody D/E2	87
3.8.3 Interpretation.....	89
3.9 Sandbodies in Secondary Field Area	91
CHAPTER 4: DISCUSSION AND CONCLUSIONS	124
4.1 Sandbody Types within Primary Field Area.....	124
4.2 Comparison to Similar Studies	125
4.2.1 Splay Sandbody Types.....	126
4.2.2 Bar Sandbody Types	127
4.2.3 Channel Sandbody Types	128
4.2.4 Discussion.....	129
4.3 Local Stratigraphy.....	130
4.4 Implications for Regional Stratigraphy.....	131
4.5 Conclusions.....	134
REFERENCES CITED	142
APPENDIX: MEASURED SECTIONS.....	CD

LIST OF FIGURES

Figure 1.1 Field area location and regional geology.....	10
Figure 1.2 Stratigraphic column of Upper Cretaceous and Lower Tertiary units	11
Figure 1.3 Field areas.....	12
Figure 1.4 Composite measured section	13
Figure 1.5 Sandstone and Mudstone dominated intervals in field area	14
Figure 1.6 Transgressive and regressive limits for the members of the Iles Formation	15
Figure 1.7 Map of interpreted landward and seaward Iles shoreline locations	16
Figure 2.1 Photographs of mud-clast conglomerate facies	38
Figure 2.2 Photographs of trough cross-stratified sandstone facies	39
Figure 2.3 Photographs of planar tabular cross-stratified sandstone facies.....	40
Figure 2.4 Photographs of convolute sandstone facies.....	41
Figure 2.5 Photographs of structureless sandstone facies.....	42
Figure 2.6 Photographs of sigmoidal cross-stratified sandstone facies	43
Figure 2.7 Photographs of mud-draped planar tabular cross-stratified sandstone facies	44
Figure 2.8 Photograph of climbing-rippled sandstone facies	45
Figure 2.9 Photographs of current-rippled sandstone facies.....	46
Figure 2.10 Photograph of current-rippled sandstone facies in lateral contact with convolute laminations	47
Figure 2.11 Photograph of mud-draped current-rippled sandstone facies	48
Figure 2.12 Photograph of wave-rippled sandstone facies	49
Figure 2.13 Photographs of bioturbated sandstone facies	50
Figure 2.14 Photograph of root-trace dominated sandstone facies	51

Figure 2.15 Photographs of undifferentiated mudstone facies	52
Figure 2.16 Photograph of undifferentiated mudstone facies with permineralized log	53
Figure 2.17 Photographs of organic-rich mudstone and coal facies	54
Figure 2.18 Proportion of paleocurrent measurements per compass quadrant and current rose of all measurements	55
Figure 3.1 Cross-section of Sandbody I.....	93
Figure 3.2 Relative abundance of facies in Sandbody I.....	94
Figure 3.3 Incision at the base of Subbody I1 and internal scour surfaces in Subbody I3	95
Figure 3.4 Cross-section of Sandbody J	96
Figure 3.5 Relative abundance of facies in Sandbody J	97
Figure 3.6A Cross-section of Sandbody A	98
Figure 3.6B Cross-section of the eastern side of Subbody A1	99
Figure 3.6C Cross-section of the western side of Sandbody A	100
Figure 3.7 Relative abundance of facies in Sandbody A	101
Figure 3.8 Accretion surfaces on Subbody A1	102
Figure 3.9 Accretion surfaces on Subbody A2	103
Figure 3.10 Cross-section of Sandbody H	104
Figure 3.11 Relative abundance of facies in Sandbody H	105
Figure 3.12 Accretion surfaces on Subbody H2	106
Figure 3.13 Cross-section of Sandbody G	107
Figure 3.14 Relative abundance of facies in Sandbody G	108
Figure 3.15 Contact between Subbodies G2 and G3	109
Figure 3.16 Cross-section of Sandbody B/C	110

Figure 3.17 Relative abundance of facies in Sandbody B/C	111
Figure 3.18 Accretion surfaces on the eastern side of Subbody B	112
Figure 3.19 Cross-section of Sandbody F.....	113
Figure 3.20 Relative abundance of facies in Sandbody F.....	114
Figure 3.21 Photographs of Sandbody F.....	115
Figure 3.22 Cross-section of Sandbody D/E.....	116
Figure 3.23 Relative abundance of facies in Sandbody D/E	117
Figure 3.24 Life position tree stump at base of Subbody D/E2	118
Figure 3.25 Preserved barforms in subbody D/E2.....	119
Figure 3.26 Isopach map for Subbody D/E2	120
Figure 3.27 Thin wave-rippled sandstone beds in Sandbody Z.....	121
Figure 3.28 Photograph of hillside in secondary field area	122
Figure 3.29 Sandbody Y incised through Sandbody Z	123
Figure 4.1 Composite cross-section of major sandbodies	138
Figure 4.2 Generalized cross-sections of sandbody types	139
Figure 4.3 Composite stratigraphic column showing key stratigraphic surfaces and cycles interpreted within the field area	140
Figure 4.4 Map of field area showing location of permineralized wood fossils.....	141

LIST OF TABLES

Table 2.1 Facies identified in field area.....	37
Table 4.1 Comparison of sandbody types in this study to similar studies.....	137

ACKNOWLEDGEMENTS

I would like to thank my advisor, Dr. Donna Anderson. Her insights and contributions have been invaluable throughout this project. I would also like to acknowledge the contributions of the members of my committee: Dr. Jennifer Aschoff, Dr. Piret Plink-Bjorklund, and Dr. Steve Sonnenberg. For consultations relating to the paleontology of my field area, I wish to thank Dr. Kenneth Carpenter, Dr. Sue Ann Bilbey, Dr. Harley Armstrong, Peter Bucknam, and Maria Brunhart-Lupo.

Funding for this project was provided by the Anadarko Fellowship and ITF through the 3DTIGHT consortium.

CHAPTER 1: INTRODUCTION

Subsurface models in fluvial reservoirs are often based on point bars, but previous work both in the modern and the ancient have described a greater variety of sandbodies. This variety includes crevasse splays (Fielding, 1984; Anderson, 2005; Tooth, 2005; Ponten and Plink-Bjorklund, 2007), mid-channel bars (Cant, 1978; Bridge and Tye, 2000; Best et al., 2003; Lunt and Bridge, 2004), and channel backfill deposits (Caldes, 2005; Cole and Cumella, 2005; Gibling, 2006; Pranter et al., 2009). Because all of these body types vary in geometry and positions within and outside of the channelbelts, subsurface geologic models based on a single body-type do not represent the full spectrum of reservoir possibilities. In addition, subsurface geologic models sometimes treat the vertical organization, or stratigraphy, of thick (>300 m) fluvial successions as somewhat random. A better understanding of the types of sandbodies present and their lateral and vertical spatial relationships within fluvial systems would benefit the exploration and exploitation of petroleum resources in such systems.

This study documents and interprets a variety of two to three-dimensional exposures of sandbodies in the field area (Figure 1.1) in the non-marine portion of the Iles Formation (Figure 1.2) in northwestern Colorado north of Rangely. The non-marine Iles Formation is usually described as a fluvially dominated sequence (Gale, 1910; Cullins, 1968; Garrigues and Barnum, 1980). Previous field studies of the non-marine Iles Formation in the field area by Anderson (2005) and Payne (1982) and nearby in the Deserado coal area (Brownfield et al., 2000), at Kenney Reservoir (Caldes, 1998; Caldes, 2005) and south of Rangely (Nelson, 1984) document a variety of fluvial sandbodies including point bars, crevasse channels and splays, amalgamated channel sandbodies, and

isolated single-story channel sandbodies. However, only Nelson (1984) reported tidal influence in correlative strata south of Rangely. More recently, Gomez-Veroiza and Steel (2010) documented tidally influenced fluvial systems in grossly correlative strata in the Green River basin north of the Rangely area. Their study is one of the first to discuss tidal influence more than 100 km inland from the coeval shoreline in an ancient low gradient fluvial system, such as the one which existed on the western margin of the Western Interior Seaway of North America. One of the questions addressed by this study is the role of tidal influence in the sandbodies of the non-marine portion of the Iles Formation.

A further objective is to examine the organization and sequence stratigraphic interpretation of the more than 90 m thick stratigraphic succession present within the field area. A number of methods have been developed to correlate marine sequences into their coeval non-marine strata. Rodgers (1998) and Gomez-Verozia (2010) have linked the development of tidally influenced fluvial strata to transgressive surfaces and Shanley et al. (1992) and Plint et al. (2001) correlated the maximum inland extent of tidally influenced fluvial strata to the maximum flooding surface of the marine setting. In a similar manner, some studies have correlated the maximum inland extent of regional coal deposits to marine maximum flooding surfaces (Amorosi and Colalongo, 2005; Fanti and Catuneanu, 2010). Atchely et al. (2004) found that mature paleosols correlated with the position of a sequence boundary. Many studies have linked the degree of fluvial aggradation to changes in accommodation space. When accommodation is high (rising base-level) amalgamation tends to be low conversely when accommodation is low (falling base-level) amalgamation is higher (Shanley and McCabe, 1994; Plint et al., 2001; Atchely et al., 2004; Amorosi and Colalongo, 2005; Cleveland et al., 2010; Fanti

and Catuneanu, 2010). Changes in stratigraphic architecture across the field area should reflect regional relative sea-level changes, setting up correlation of non-marine to coeval successions of the Corcoran, Cozzette, and Rollins members of the Iles Formation (Figure 1.2) to the southeast.

1.1 Field Area

The field area is located approximately 13 km north of Rangely, Colorado on the Rio Blanco/Moffat County line in sections 16 and 21 of T3N, R102W (Figure 1.1). It covers an area of 1 sq-km with a vertical topographic relief of about 90 m. It is located on the gently dipping (3° NNE) north flank of the Rangely anticline. Modern erosion and low dip angles have resulted in three-dimensional exposures of many of the sandbodies.

The field area consists of primary and secondary areas. The primary study area has a stratigraphic thickness of about 50 m and extends about 800 m in the east-west direction. It is located to the northeast and stratigraphically above an area studied by Anderson (2005) (Figure 1.3). The primary field area contains a stratigraphic interval from the top of Anderson's Point Bar G to the top of Sandbody D/E in this thesis. The secondary field area is located northeast of the primary field area. Measured section F (Appendix A) extends 45 m into the secondary field area to the coal marker beds of Garrigues and Barnum (1980), which is interpreted as the base of the Williams Fork Formation (Brownfield et al., 2000).

1.2 Methods

The field area was mapped at 1:500 scale using a handheld GPS receiver with $\pm 3\text{-}6$ meter accuracy (Figure 1.3). GPS points were used to outline the outcrop area of major sandbodies and their subbodies. GPS points were also recorded at the base and top of

each measured section, any significant lateral deviations, and the base and top of any major sandbody intersected. The base of minor sandbodies and locations of fossils, sandbody thickness measurements, and any other significant sedimentary feature were also recorded. Over 900 GPS waypoints were collected during mapping.

A series of 48 measured sections was made at 1:20 scale (Appendix A) with the primary focus on eight major sandbodies discussed in Chapter 3. (The scale of measured section F changes to 1:40 at the 33 m mark.) Most of the measured sections only pass through one or two of the major sandbodies. Two long measured sections were made through the middle (Measured section X) and eastern (Measured section S) portions of the field area (Figure 1.3 and Appendix A) and a composite measured section (Figure 1.4) was made for the western portion of the field area. These long measured sections were used to connect the shorter sections together and place them in a stratigraphic context. Where the sandbody exposures were too steep to climb, thicknesses were measured by tape measure. Paleocurrent and accretion set directions were measured using a Brunton compass and analyzed with GEORient and Microsoft Excel. Photographs were taken of all the facies observed and photo panels were constructed for all the major sandbodies. The photo panels and measured sections were used to document lateral variations in thickness and facies distribution in the sandbodies and the intervening fine-grained rocks. The measured sections and GPS location data were combined with a digital elevation model in ESRI ArcGIS to enable a three-dimensional description of the field area.

Stratigraphic cross-sections were constructed for each of the eight major sandbodies (Chapter 3) and a composite cross-section was also constructed to represent

the entire field area. These cross-sections were projected onto a section line of 305°-125°. Most of the outcrop in the field area is roughly parallel to this section line. Because they do not outcrop parallel to this line, two additional cross-sections with section lines of 189°-9° and 250°-70° were constructed for Sandbody A and one additional cross-section with a section line of 226°-46° was constructed for Sandbody J. All cross-sections were made with 10X vertical exaggeration. Facies proportions were measured from the polygon area of each facies in Canvas 9.

1.3 Local Stratigraphy

The geologic map of the Rangely NE quadrangle (1980) divides the Mesaverde Group into four units: the Sego Sandstone, the Lower Unit, the Coal Unit, and the Upper Unit, in ascending stratigraphic order. The coal unit is further divided with the Main Coal Zone in the approximate middle of the unit (Garrigues and Barnum, 1980). Brownfield et al. (2000) correlates the Lower Unit to the Iles Formation and the Main Coal Zone to the Cameo-Wheeler Coal Zone in the southern Piceance basin. The primary field area is located within the Lower Unit with the top of Sandbody D/E corresponding to the contact with the Coal Unit. The secondary field area is located in the Coal Unit below the Main Coal Zone. Distinctive white sandstone layers, known as the coal marker sands, are found immediately below the mineable coals in the Lower White River Coal Field, which correlate to the base of the Williams Fork Formation (Brownfield et al., 2000). The coal marker sands are located at the top of the secondary field area.

Within the primary field area, the stratigraphy consists of three mudstone dominated intervals and three sandstone dominated intervals (Figures 1.4 and 1.5). Immediately above Point Bar G of Anderson (2005) is a mudstone dominated interval

approximately 4.5 m thick (Figure 1.4), termed M1. The M1 interval is overlain by a sandstone dominated interval, S1, containing Sandbodies I, J, A, and H, in stratigraphic order and is about 10 m thick. The second mudstone interval, M2, overlies S1 and is about 7 m thick. The second sandstone interval, S2, contains Sandbodies G and B/C and is about 5 m thick. The third mudstone interval, M3, is about 3 m thick. The topography across M3 is relatively flat, so it appears thicker in map view. The third sandstone interval, S3, is up to 22 m thick containing Sandbodies F and D/E. Above the primary field area, is a fourth mudstone dominated interval, M4 (Figure 1.5), which is about 45 m thick. Two overlapping sandbodies, Sandbodies Z and Y (Figures 1.4 and 1.5), are present about 8 m up in this interval. The M4 interval is capped by the coal marker sands of Garrigues and Barnum (1980).

1.4 Regional Stratigraphy

The Iles Formation is a member of the Mesaverde Group (Figure 1.2) which is a thick package of lower shoreface to non-marine sediment deposited in and around the Western Interior Seaway during the Campanian and Maastrichtian. The Iles Formation is laterally equivalent with the Mount Garfield Formation in the Grand Junction area. In the southern Piceance basin, the Iles Formation is divided into lower, middle and upper members: the Corcoran, Cozzette and Rollins members, respectively. The Iles Formation dominantly consists of marine shoreface deposits; however, it contains landward coeval non-marine deposits in the western Piceance and Uinta basins. The Corcoran Member is around 30 m thick consisting of sandstone, shale, and coal deposited in a marine shoreface to estuarine environment. The Cozzette Member is about 70 m thick consisting of sandstone, shale, and coal. It contains offshore marine, marine shoreface, estuarine,

and coastal plain strata (Hettinger and Kirschbaum, 2002). The Corcoran and Cozzette members are each composed of two regressive cycles related to relatively minor increases in accommodation space (Cumella and Ostby, 2003) within an overall low accommodation setting (Aschoff and Steel, in press). The upper and lower regressive cycles of the Cozzette member are divided by a thin unit of coal overlain by marine shale (Hettinger and Kirshbaum, 2002). The trend of Corcoran and Cozzette shorelines was northeast-southwest (Figure 1.6) (Johnson, 1989; Cumella and Ostby, 2003; Schwendeman, in press). The Rollins Member ranges from 0-60 m and consisting of near shore sandstone (Hettinger and Kirschbaum, 2002). The Rollins Member consists of a single regressive cycle deposited during a large increase in accommodation space (Cumella and Ostby, 2003). The shoreline of the Rollins Member was also closer to true north-south (Figure 1.6) (Johnson, 1989; Cumella and Ostby, 2003; Schwendeman, in press). The three members of the Iles Formation are divided by thin tongues of Mancos shale (Hettinger and Kirschbaum, 2002). The field area is located about 60 to 130 km from the Iles shoreline, based on the projected shorelines in Gomez-Veroiza and Steel (2010) (Figure 1.7).

Numerical ages are not well constrained in the non-marine portion of the Iles Formation. Paleogeographic reconstructions indicate that the Iles Formation in the field area was deposited during the Upper Campanian (Franczyk et al., 1992). The Upper Campanian is between the base of the *Didymoceras nebrascense* to the base of the *Baculites baculus* ammonite biozones and 76.38 to 70.60 Ma based on radiometric age dating (Ogg et al., 2004).

1.5 Regional Structure and Tectonics

Three major structural events have affected the outcrop area since the Late Cretaceous. First, during the Campanian and Maastrichtian, much of the Rocky Mountain region was undergoing a period of anomalous regional subsidence. This subsidence, centered in Colorado and Wyoming, was the result of shallow subduction of the Farallon plate (Cross, 1986; Aschoff and Steel, in press). Recent models, such as Liu et al. (2005), indicate that the locus of dynamic subsidence was migrating eastward and was decreasing accommodation in the vicinity of the Utah-Colorado state border at this time. Aschoff and Steel (in press) postulate that the eastward migration of dynamic subsidence may have been partially responsible for the development of a low-accommodation setting in this area during deposition of the Iles Formation.

The second relevant structural event is the formation of the Douglas Creek Arch. The field area is located on the north end of the Douglas Creek Arch. The Douglas Creek Arch is a 75 km long and 35 km wide, north-south oriented anticline which extends from the Uncompahgre Uplift to the Rangely anticline (Bader, 2009). The Douglas Creek Arch formed as part of the Laramide orogeny during the Maastrichtian to Eocene (Cross, 1986; Bader, 2009). However, thinning strata across the San Rafael Swell of central Utah indicates that Laramide-style deformation began as early as the middle Campanian, 77 Ma (Aschoff and Steel, in press), and may have had an impact on deposition.

Third, the area was tilted by the formation of two large-scale folds. The field area is located on the north flank of the Rangely anticline and the southern flank of the Red Wash syncline. These large-scale folds formed as subsidiary structures of the Uinta Mountains which were uplifted in the Latest Paleocene to the Middle Eocene and are related to the Laramide orogeny (Ritzma, 1969; Cross, 1986).

1.6 Thesis Organization

Chapter 2 contains detailed descriptions of the facies observed in the field area and organizes them into facies associations. Chapter 3 describes and interprets the depositional patterns observed in the eight sandbodies studied in the primary field area and discusses two sandbodies in the secondary field area. Chapter 4 describes and interprets the local and regional stratigraphic relationships and presents a series of conclusions.

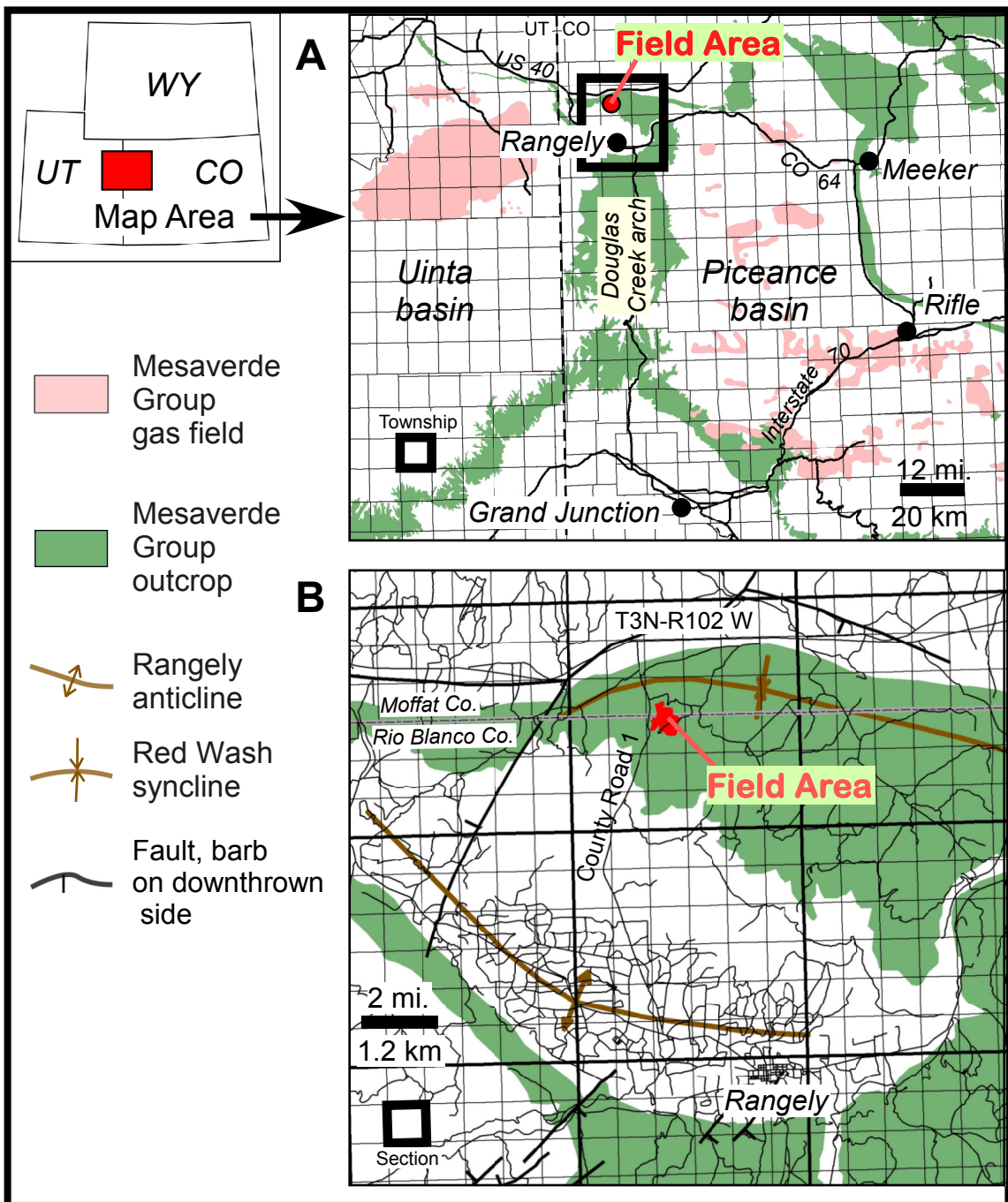
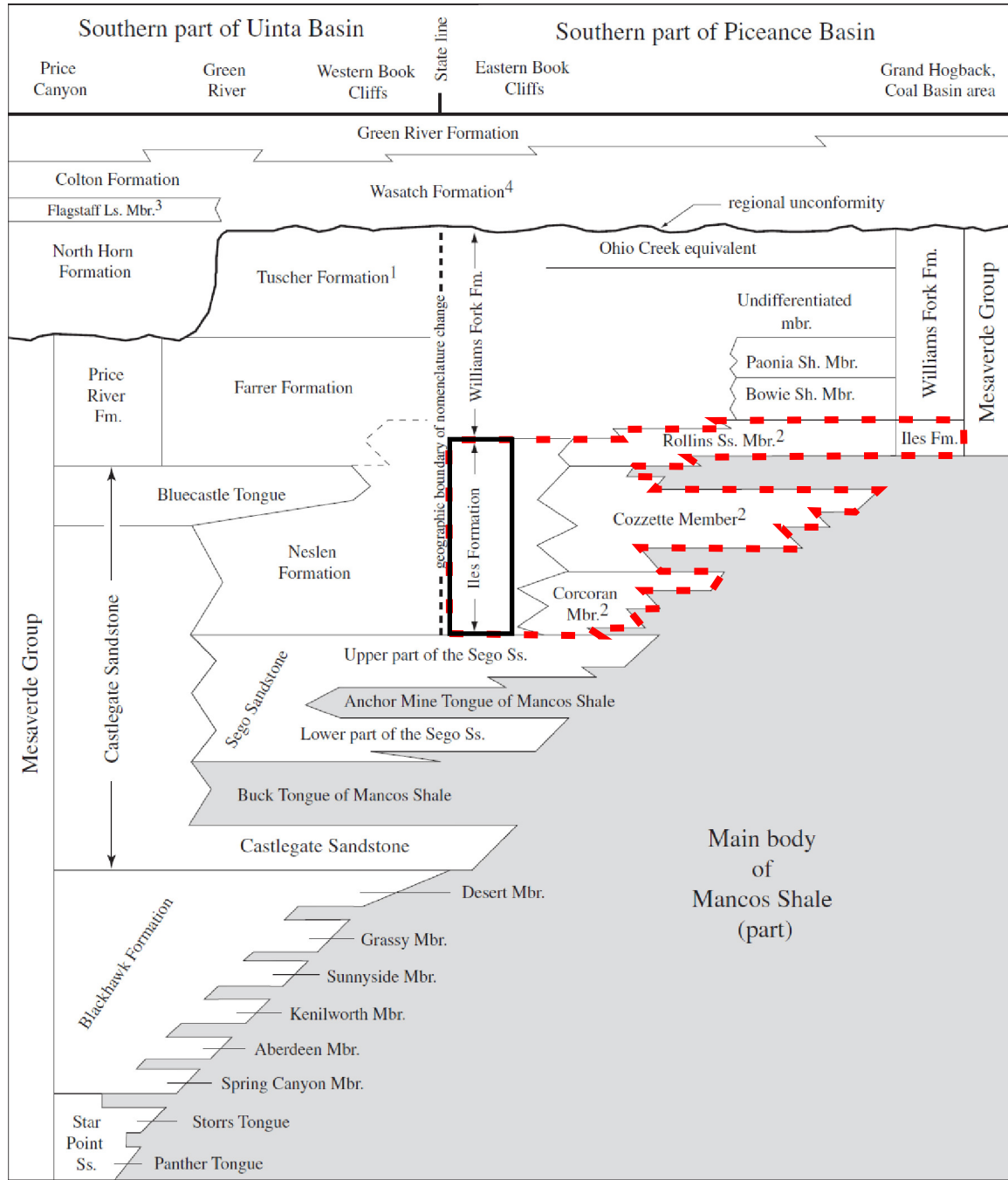


Figure 1.1 Field area location and regional geology. A) The field area is at northern end of the Douglas Creek arch between the Uinta and Piceance basins, where several large gas fields produce from Mesaverde Group strata similar to those in this study. B) The field area is in sections 16 and 21 of T3N, R102W, straddling the Rio Blanco-Moffat county boundary. It is on the gently dipping northern flank of the Rangely anticline and the southern flank of the Red Wash syncline. Geology modified from Sprinkel (1999) and Green (1992); gas fields modified from Sprinkel (1999) and Wray et al. (2005).



¹of the Mesaverde Group

²of the Iles Formation

³of the Green River Formation

⁴includes conglomerate beds at Dark Canyon

Figure 1.2 Stratigraphic column of Upper Cretaceous and Lower Tertiary units in the southern Piceance and Uinta basins. Iles Formation highlighted by dashed line. Studied interval highlighted by solid line. Modified from Hettinger and Kirschbaum (2002).

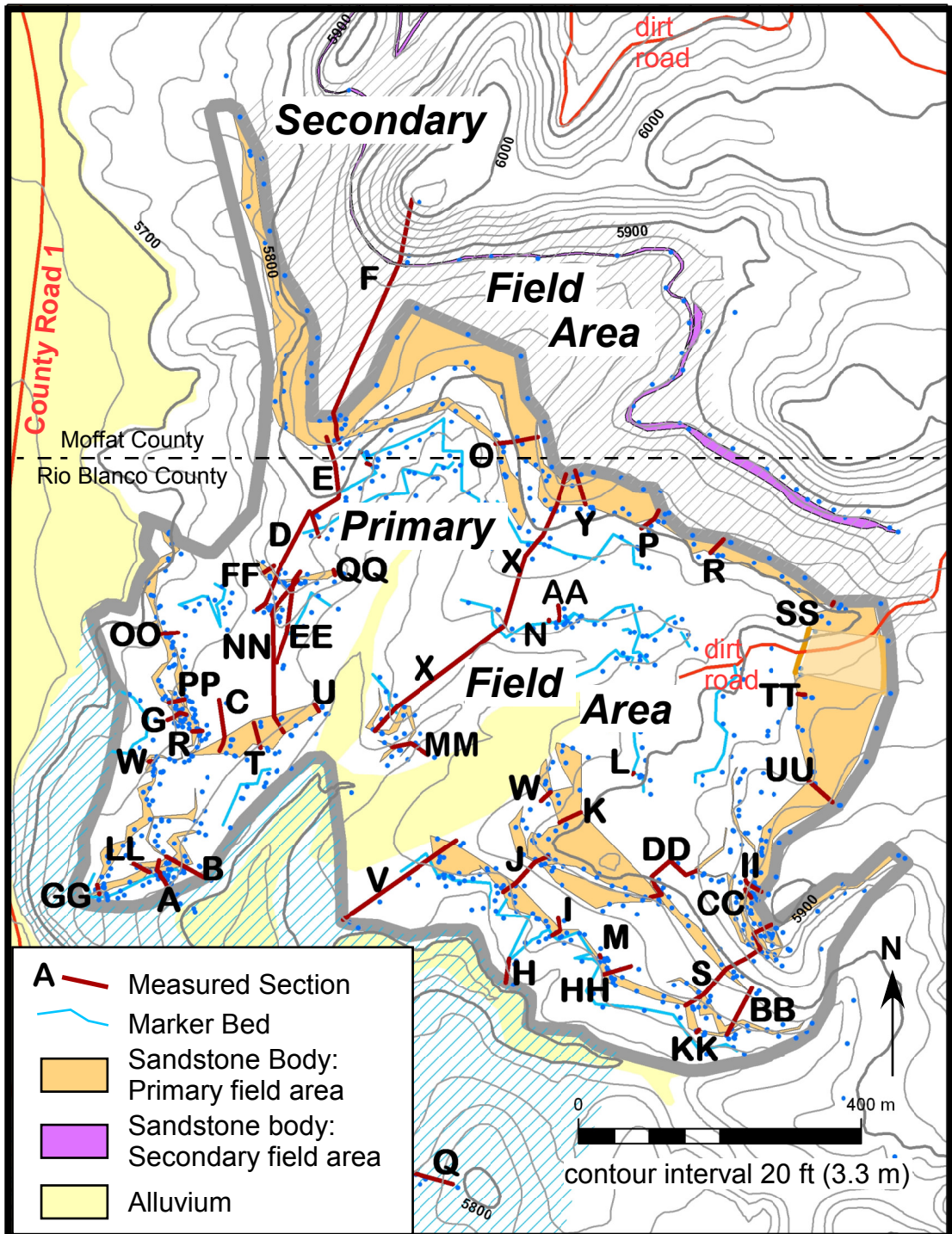


Figure 1.3 Field areas: primary field area outlined by thick gray line; secondary field area within gray hachure: blue hachure is field area of Anderson (2005; discussed in text). Also shown is location of 48 measured sections (labelled) and marker beds (blue lines). Composite measured section (Fig. 1.4) based on sections B, NN, D, E and F, supplemented by X, V and S. Over 900 collected GPS waypoints shown as blue dots Vertical topographic relief across both field areas is almost 300 ft (91 m). Structural dip is 3° NE (040°). Geology modified from Garrigues and Barnum (1980).

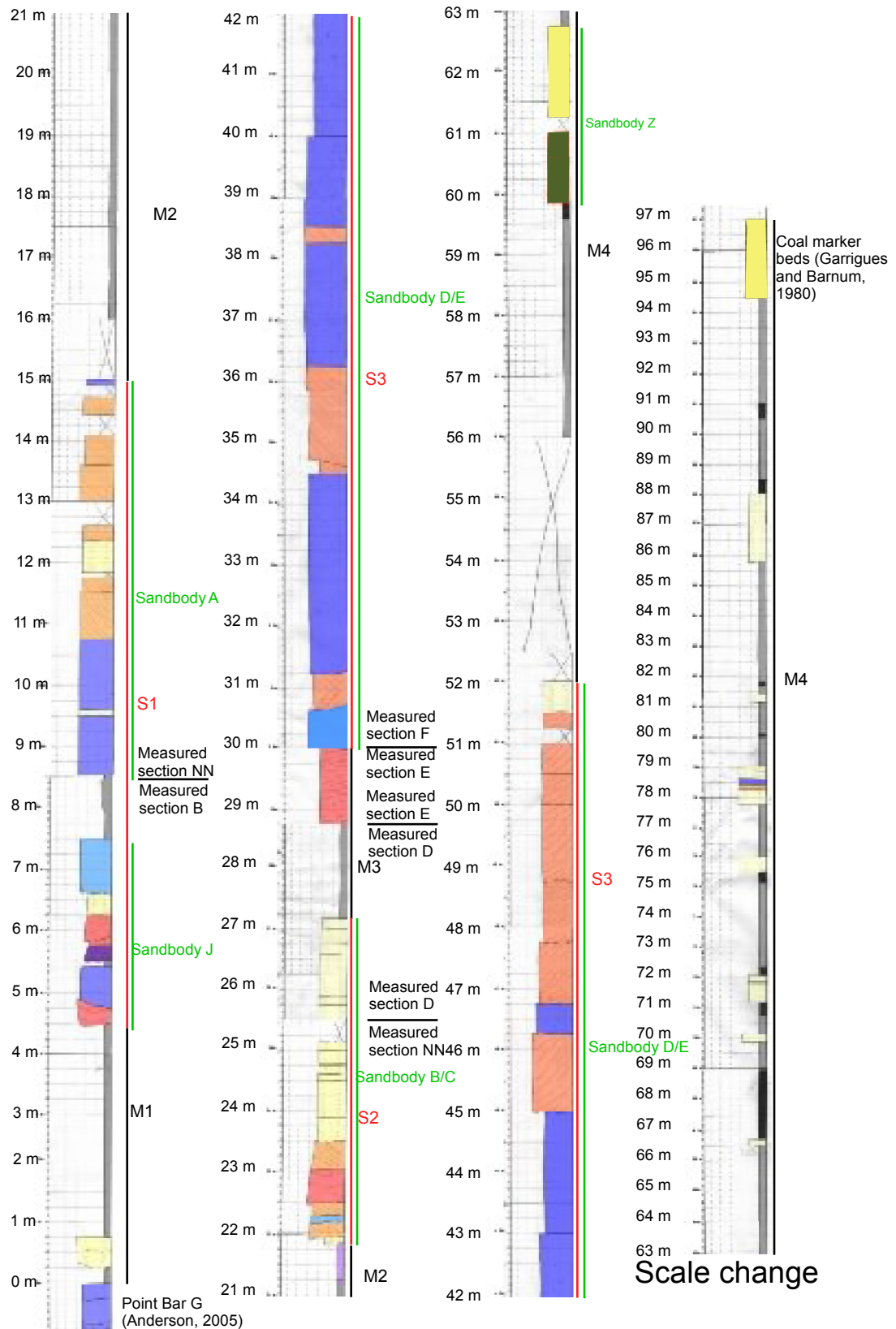


Figure 1.4 Composite measured section of western side of field area. Scale changes at 63 m. Facies are colored following Table 2.1.

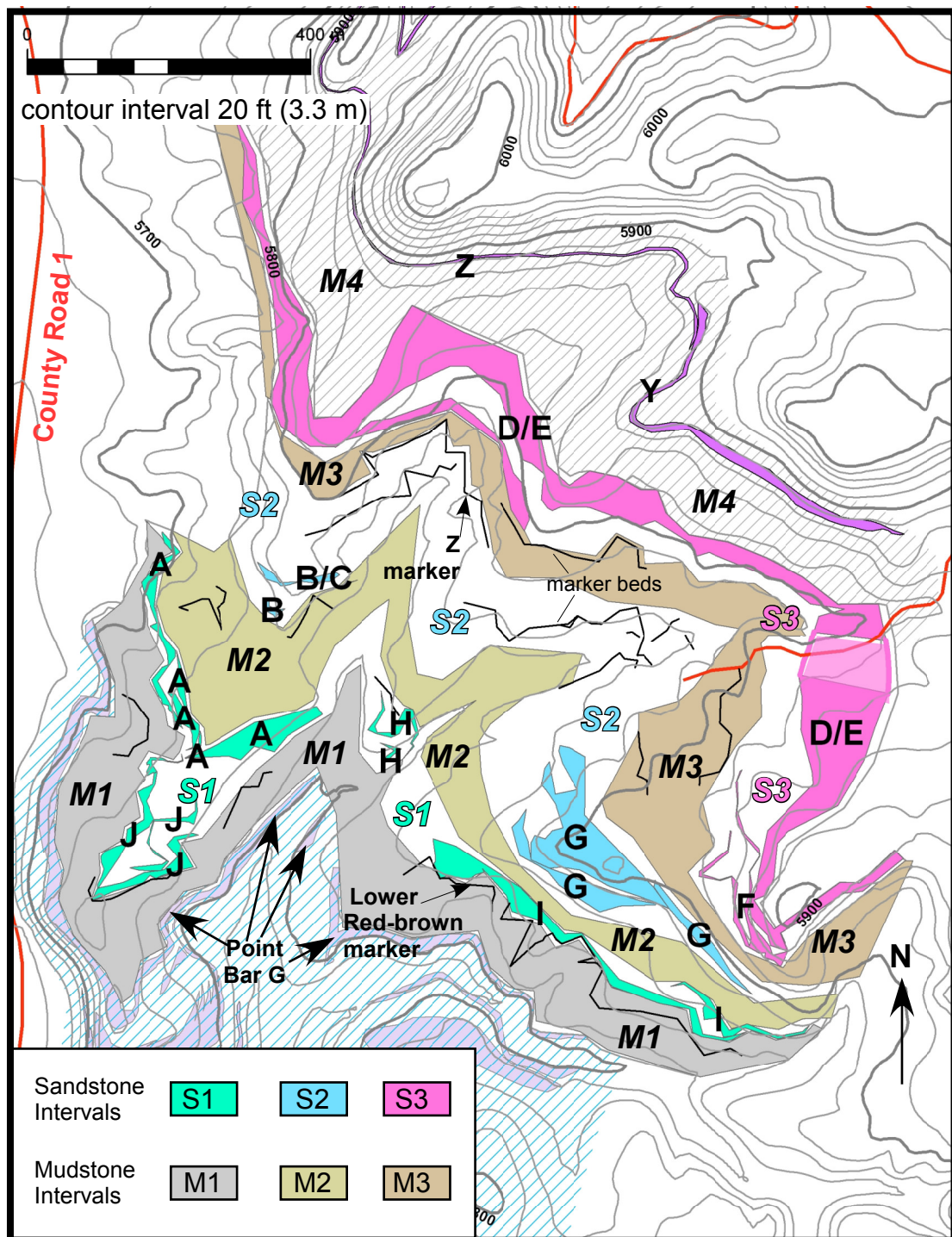


Figure 1.5 Sandstone-dominated intervals (S1, S2, S3) and bodies (letters) and intervening mudstone-dominated intervals (M1, M2, M3, M4) in field area (see text for complete discussion). Older sandstone bodies within blue-hachured area are from Anderson (2005): point bar G is youngest body within her study area and underlies the base of mudstone interval M1. Sandstone bodies J, A, H, I and F occupy sandstone-dominated interval S1. Sandstone bodies B, C and G occupy interval S2. Bodies D and E occupy interval S3. Youngest mudstone interval, M4 overlies Body D/E and contains sandstone bodies Y and Z in the secondary field area (gray hachure). Marker beds as in Figure 1.3.

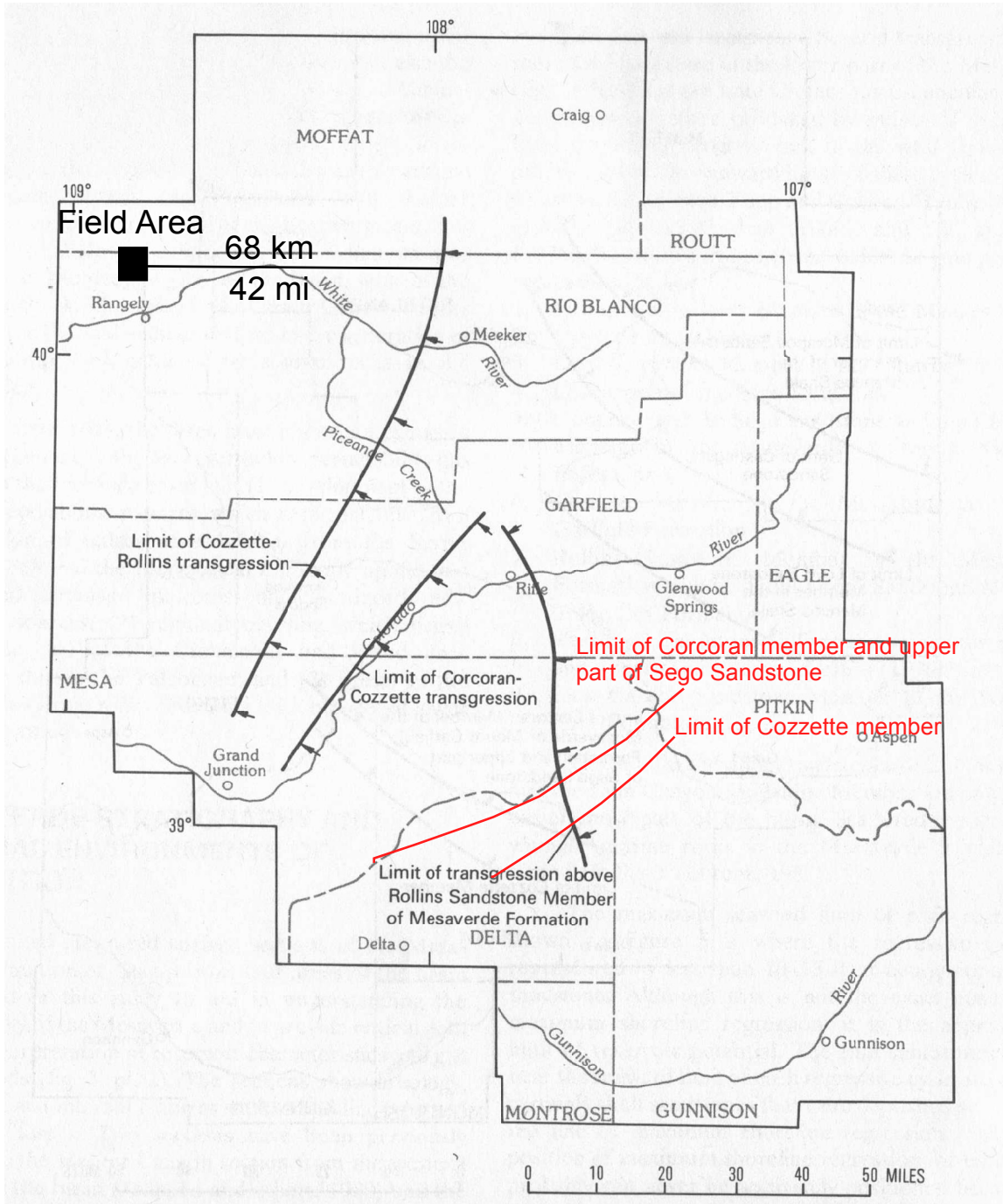


Figure 1.6 Transgressive (in black) and regressive (in red) limits for the members of the Iles Formation showing approximate distance to the shoreline at the Cozzette-Rollins transgression. Field area not shown to scale. Regressive limit of Rollins member to southeast of map area. Modified from Johnson (1989).

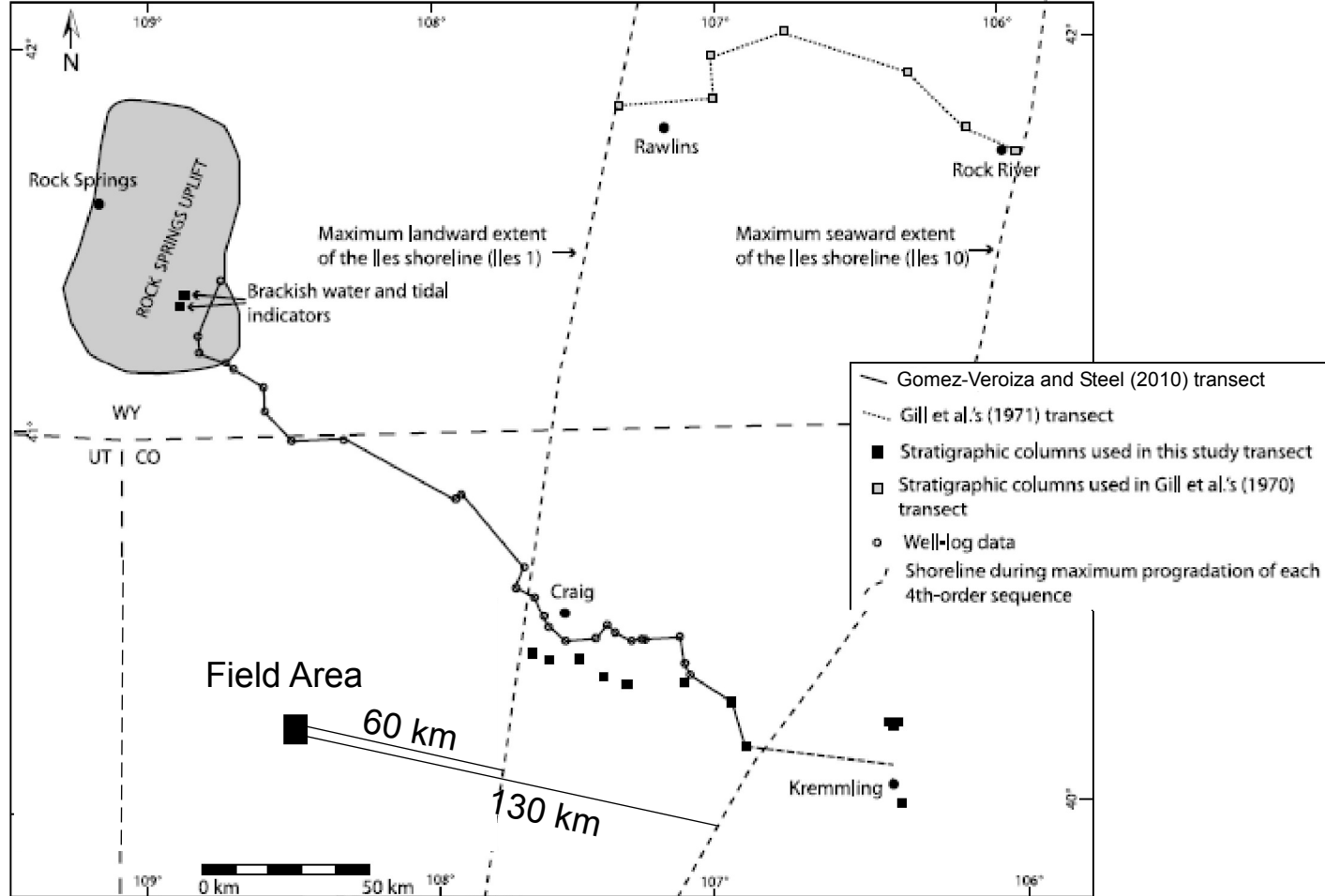


Figure 1.7 Map of interpreted landward and seaward Iles shoreline locations. Note the tidal indicators on the Rock Springs Uplift. Field area not shown to scale. Modified from Gomez-Veroiza and Steel (2010).

CHAPTER 2: FACIES AND FACIES ASSOCIATIONS

This chapter describes and interprets the sedimentary features of the facies present within the field area. Sixteen facies (Table 2.1) were described in the primary and secondary field areas. These facies have been divided into two facies associations: floodplain and channelbelt. Facies are presented in order of decreasing depositional energy.

2.1 Mud-clast Conglomerate Facies

The mud-clast conglomerate facies (Table 2.1) is comprised of pebble to cobble mud clasts in a lower very fine to upper fine sandstone matrix. Rarely mud clasts reach the lower boulder size range (Figure 2.1A). Conglomerates are typically matrix supported. Clast supported conglomerates are rarely present (Figure 2.1B). Clasts may also be permineralized dinosaur bone, turtle bone or logs. A bone from this facies was identified from photographs by Dr. Kenneth Carpenter as a carapace of a trionychid turtle, an exclusively freshwater group (Denver Museum of Nature and Science, personal communication, 2009). Locally, vertebrate bones may account for up to 10% of the clasts (Figure 2.1C). Clasts in a few beds exhibit a-axis imbrication (Figure 2.1D). Bed thickness ranges from 5 cm to 2 m with most beds between 25 to 50 cm thick. Beds extend laterally between 10 and 100 m.

The mud-clast conglomerate facies is associated with the planar tabular cross-stratified sandstone, the structureless sandstone, the undifferentiated mudstone, and the trough cross-stratified sandstone facies, in order of abundance. It may underlie or overlie any of the aforementioned facies except for the undifferentiated mudstone facies which it only overlies. It may also be in lateral contact with the planar tabular cross-stratified

sandstone facies with the planar tabular cross-stratified sandstone facies scouring into the mud-clast conglomerate facies. Basal contacts and bedding planes are typically incised less than 5 cm into the underlying bed, with maximum observed incision up to 15 cm. Some sharp, non-incisive contacts were also observed. This facies is only present within the channelbelt facies association and most commonly occurs at the base of thick sandstone units.

In previous work, this facies is commonly reported at the base of sandstone bodies. Payne (1982) places this facies at the base of Type 1 (distributary channel) and Type 2 (low sinuosity point bar) deposits. It is also found at the base of anastamosing channels in Nelson (1984), low diversity channelbelts in Caldes (1998), and crevasse channels in Anderson (2005). Caldes (1998) attributes this facies to hyperconcentrated turbulent flows or slumps; however, the presence of imbrication in some of the beds indicates that at least those beds must have been deposited at a slower rate. Anderson (2005) attributes this facies to very high energy, upper flow regime traction flows. This interpretation is appropriate for most of the mud-clast conglomerate beds in the field area; however, the beds containing clasts larger than pebbled sized were likely deposited during a bank collapse or levee break. The size and abundance of terrestrial fossils make long transport distances unlikely and provides evidence for a non-marine environment. The presence of a trionychid turtle indicates a freshwater environment, but it is not conclusive as the fossil may be redeposited.

2.2 Trough Cross-stratified Sandstone Facies

The trough cross-stratified sandstone facies (Table 2.1) consists of upper very fine to lower medium sandstone organized into trough cross-sets (Figure 2.2A and B).

Preserved cross-set thickness ranges from 5 to 35 cm with most of the cross-sets in the 10 to 20 cm range. Mud clasts are common and are oriented along foresets, present at the toes of foresets, or line the base of the trough scour pit. Rarely current ripples are observed on the foresets. Dewatering structures, such as convolute lamination, are locally present, but are not abundant in this facies. Mud drapes are extremely rare and only occur on toes of foresets. Cosets of troughs form units between 10 cm and 2.5 m thick, with most cosets in the 25 to 50 cm range. Units extend laterally for approximately 10 to 50 m.

The trough cross-stratified sandstone facies is most commonly associated with the current-rippled sandstone facies, the planar tabular sandstone facies, the structureless sandstone facies, and the undifferentiated mudstone facies, in that order. It is less commonly associated with the convolute sandstone and the mud-clast conglomerate facies. The trough cross-stratified sandstone may be found underlying or overlying any of the previously mentioned associated facies. It rarely underlies the mud-draped planar tabular cross-stratified sandstone facies and overlies the root-trace dominated sandstone facies. Upper and lower contacts with other facies and bedding contacts tend to be incised less than 5 cm. The maximum incision observed at the base of this facies is 15 cm. Gradational contacts and sharp, non-erosive contacts have also been observed with the planar tabular sandstone facies and the current-rippled sandstone facies. It is rarely observed in lateral contact with the structureless sandstone facies where the structureless sandstone has deeply incised into the underlying trough cross-stratified bed. The trough cross-stratified sandstone facies occurs in both the channelbelt and floodplain facies tracts.

Previous workers (Payne, 1982; Nelson, 1984; Caldes, 1998; Anderson, 2005) have all described similar facies in the Rangely area. This author agrees with their previous interpretation that this facies represents deposition by three-dimensional dunes under high energy, lower flow regime conditions. Payne (1982) reports trough cross-stratification in his Type 1, 2, and 3 (anastamosing channel) channels. Nelson (1984) associates it with tidal creek point bars, as well as anastamosing channels. Caldes (1998) divides this facies based on the size of the cross-sets with large scale trough cross-bedding near the base of meandering channels and small scale cross-bedding at the base of crevasse channels. Anderson (2005) associates this facies with point bar and crevasse channel deposits.

2.3 Planar Tabular Cross-stratified Sandstone Facies

The planar tabular cross-stratified sandstone facies (Table 2.1) is one of the most abundant in the field area. It consists of lower very fine to lower medium sandstone organized into planar tabular cross-sets with preserved thicknesses of 5 to 90 cm (Figure 2.3A). The majority of preserved cross-sets are between 10 and 30 cm thick. Mud clasts are common on the foresets and on the bases of beds and cross-sets. Units of this facies may exhibit bi-directional paleocurrents. Permineralized dinosaur bone and terrestrial plants are present. Mud drapes on the toes of foresets are very rare. Convolute laminations are also rarely present. Cosets form units between 10 cm and 3.35 m thick. Most coset units are in the 25 to 75 cm thickness range. Lateral extents are commonly in the 50 to 100 m range.

This facies is most commonly associated with the structureless sandstone facies, the current-rippled sandstone facies, the undifferentiated mudstone facies, the convolute

sandstone facies, the trough cross-stratified sandstone facies, and the mud-clast conglomerate facies, in order of number of associations. It is uncommonly associated with the mud-draped planar tabular cross-stratified sandstone facies and the mud-draped current-rippled sandstone facies. The planar tabular cross-stratified sandstone facies is observed both above and below all of the previously mentioned associated facies. It is rarely observed overlying the organic-rich mudstone facies, underlying the climbing-rippled sandstone facies, and incised into the mud-clast conglomerate facies. The majority of basal contacts and bedding planes exhibit incision of less than 5 cm into the underlying bed. Incision up to 20 cm was observed. Sharp, but non-erosive and gradational contacts are also common. This facies is present in both the channelbelt and the floodplain facies associations.

This facies is commonly documented by previous work in the area (Payne, 1982; Caldes, 1998; Anderson, 2005). Payne describes this facies in his Type 1, 2 and 3 channels. Caldes reports this facies in meandering channelbelts and Anderson reports it in point bar and crevasse splay deposits. Anderson interprets this facies as high energy, lower flow regime deposits. Caldes adds that this facies is indicative of straight-crested downstream accreting dunes. This author agrees with the interpretations of Caldes and Anderson.

2.4 Convolute Sandstone Facies

The convolute sandstone facies (Table 2.1) consists of upper very fine to lower medium sandstone dominated by convolute laminations (Figure 2.4A). Rarely, soft-sediment folding may involve multiple beds and reach a meter in height (Figure 2.4B). A few preserved planar tabular cross-sets were observed. Mud clasts are common and may

be randomly distributed or horizontally oriented, typically along bedding planes. Concretions and wood fragments are rarely present. Beds are between 5 cm and 2.75 m thick, with most between 50 cm and 2 m. Units may extend for more than 100 m laterally, but most are less than 50 m.

This facies is most commonly associated with the planar tabular cross-stratified sandstone facies. It is less frequently associated with the undifferentiated mudstone facies, the current-rippled sandstone facies, the structureless sandstone facies, and the trough cross-stratified sandstone facies. It is observed above and below all of the previously mentioned facies. This facies is also rarely observed underlying the mud-draped current-rippled sandstone facies, grading laterally into the mud-draped planar tabular sandstone, and truncating the root-trace dominated sandstone and undifferentiated mudstone facies. Bedding planes and basal contacts are usually incised less than 5 cm. Incision up to 50 cm was observed. Non-incisive but sharp and gradational contacts were also observed. Lateral terminations are typically gradational into another sandstone facies. This facies is present in both the channelbelt and floodplain facies associations.

Soft-sediment deformation has been previously described in the area by Payne, (1982), Nelson (1984), Caldes (1998), and Anderson (2005). Caldes and Anderson attribute this facies to post-depositional liquefaction destroying the original sedimentary structures. Because it is very commonly associated with the planar tabular cross-stratified sandstone facies and a few remnant planar tabular cross-sets within it, it was most likely deposited as planar tabular cross-strata. This interpretation is further supported by rare convolute laminations within the planar tabular cross-stratified sandstone facies. A few of the beds might have been deposited as another facies as suggested by the presence of

some convolute laminations within the trough cross-stratified and current-rippled sandstone facies.

2.5 Structureless Sandstone Facies

The structureless sandstone facies (Table 2.1) is comprised of lower very fine to lower medium sandstone with no discernable sedimentary structures (Figure 2.5A). Mud clasts are common and are randomly oriented or form horizontal laminations, typically on relict bedding planes. Carbonized wood fragments and root traces were rarely observed. At least two ammonites are also present (Figure 2.5B). Beds range in thickness from 5 cm to 3.75 m. Most beds are between 25 cm and 1 m thick. Units may extend for more than 100 m laterally, but most are less than 50 m.

The structureless sandstone facies is most commonly associated with the planar tabular cross-stratified sandstone facies and the undifferentiated mudstone facies. It is also commonly associated with the current-rippled sandstone, the trough cross-stratified sandstone, the mud-clast conglomerate, and the convolute sandstone facies. Uncommon associations include the mud-draped current-rippled sandstone and the organic-rich mudstone facies. The structureless sandstone facies may underlie or overlie all but the organic-rich mudstone facies, which only underlies the structureless sandstone facies. It also pinches out into and truncates the undifferentiated mudstone. Lateral terminations are commonly gradational into another sandstone facies, usually the trough or planar tabular cross-stratified sandstone or convolute sandstone facies. Basal contacts and bedding planes are usually incised less than 5 cm. Incision up to 30 cm was observed. Sharp, non-incisive and gradational contacts are also present. This facies is present in both the channelbelt and floodplain facies associations.

This facies has been commonly described in previous work (Payne, 1982; Nelson, 1984; Caldes, 1998; Anderson, 2005). It was most likely deposited as planar tabular or trough cross-stratified sandstone and later destroyed by fluidization, as suggested by the abundance of dewatering structures present in the field area. It is unclear if the ammonites were redeposited or transported post-mortem, or indicate salinities high enough to support marine life.

2.6 Sigmoidal Cross-stratified Sandstone Facies

The sigmoidal cross-stratified sandstone facies (Table 2.1) consists of lower fine grained sand organized into sigmoidal cross-strata (Figure 2.6A). Top-sets are distinctly rounded. Preserved cross-strata are about 35 cm thick, which is the entire thickness of the single bed where this facies is observed. Paleocurrents in this bed are oriented to the northwest. This bed forms a mounded shape of less than 5 m lateral extent (Figure 2.6B). Bundling and mud drapes were not observed. This facies is surrounded by the current-rippled sandstone facies. Contacts are sharp and non-erosive. This facies was only observed in the channelbelt facies association in Sandbody I.

This facies was deposited in a moderately high energy, lower flow-regime tidal environment. Rounded top-sets indicate reworking by a subordinate current direction. The lack of mud drapes and bundling indicates deposition occurred in an area with a very brief slackwater period and little effect of neap-spring cyclicity. This facies has not been previously described in the Iles Formation in the Rangely area; however, Caldes (1998) reported a similar facies in tidal units of the Upper Sego Formation below the Iles Formation.

2.7 Mud-draped Planar Tabular Cross-stratified Sandstone Facies

The mud-draped planar tabular cross-stratified sandstone facies (Table 2.1) consists of lower fine to lower medium sandstone organized into planar tabular cross-sets (Figure 2.7A). Preserved cross-sets are between 10 and 60 cm thick. Most cross-sets are less than 20 cm thick. All foresets are mud draped from the top to the toe of the foreset. No double mud drapes were observed. Some cross-sets show a bundled pattern (Figure 2.7A). Bi-directional paleocurrents are present including rare herring-bone cross-stratification (Figure 2.7B). Mud clasts are sometimes observed lining the foresets. Coset units are between 10 cm and 1 m thick with most between 25 and 50 cm thick. Beds extend laterally for about 30 m.

The mud-draped planar tabular cross-stratified sandstone facies is most commonly associated with the structureless sandstone and the planar tabular cross-stratified sandstone facies and may occur above or below either facies. This facies may also underlie the convolute sandstone, mud-clast conglomerate, or current-rippled facies and may overlie the trough cross-stratified sandstone facies. Basal contacts are either sharp, non-incisive or incised less than 5 cm into the underlying bed. These types of contacts occur in roughly equal proportions. Some incisive contacts are lined by a mud clast lag. This facies is also observed in grading laterally into the convolute sandstone facies (Figure 2.7C). This facies occurs in both the channelbelt and floodplain facies associations.

This facies represents deposition by straight crested dunes in a moderately high energy, lower flow regime tidal environment. The abundance of mud drapes suggests periodic near-zero current velocities. The presence of bundling indicates the influence of

neap-spring cyclicity. This facies has not been reported in previous work in the Rangely area.

2.8 Climbing-rippled Sandstone Facies

The climbing-rippled sandstone facies (Table 2.1) consists of upper very fine to upper fine sandstone organized into ripple laminae of less than 5 cm thick (Figure 2.8). Ripples exhibit a steep angle of climb. Ripple foresets may be partially mud draped (Figure 2.8). This facies forms beds from 15 to 40 cm thick that extend for less than 10 m laterally.

This facies is most commonly associated with the current-rippled sandstone facies and may occur either above or below it. The climbing rippled sandstone facies may also overly the undifferentiated mudstone facies and the planar tabular cross-stratified sandstone facies. Basal contacts tend to be sharp, but non-incisive. Incision of less than 5 cm into the underlying bed may also occur. This facies is only present within the channelbelt facies association.

This facies has been previously described by Nelson (1984), Caldes (1998) and Anderson (2005) in the Rangely area. Caldes and Anderson interpret this facies as deposited under low energy traction flow conditions where the deposition rate exceeds the rate of ripple migration and this author concurs with this interpretation. Nelson associates this facies with the upper portion of Gilbert splays. Anderson found this facies on the fringe of a crevasse splay. Caldes also found this facies in crevasse splays as well as his lake facies association.

2.9 Current-rippled Sandstone Facies

The current-rippled sandstone facies (Table 2.1) consists of lower very fine to lower medium sandstone organized into ripple laminae of sets less than 5 cm thick (Figure 2.9A). This facies is one of the most common in the field area. Randomly distributed mud clasts are fairly common and are also common horizontally oriented at the base of beds. A few units are interbedded with thin mud beds (Figure 2.9B). Mud drapes are very rare. A few beds transition to convolute laminations (Figure 2.10). Vertical burrows are rarely observed. Root traces are observed at the top of a few beds. Carbonized wood fragments and permineralized dinosaur bone are also rarely present. Beds are between 5 mm and 2 m thick. Most beds are between 10 and 75 cm thick. This facies may extend laterally for hundreds of meters.

This facies is most commonly associated with the undifferentiated mudstone facies. It is also commonly associated with the planar tabular cross-stratified, trough cross-stratified and structureless sandstone facies. Uncommonly, it is associated with the convolute sandstone, mud-clast conglomerate, climbing-rippled sandstone, sigmoidal cross-stratified sandstone, and organic-rich mudstone facies. In the general field area, on the upper part of measured section F, it is associated with the coal facies. The current-rippled sandstone facies may underlie or overlie any of the previously mentioned facies, except for the organic-rich mudstone facies which it only overlies. It is also observed pinching out into the undifferentiated mudstone and truncated by the planar tabular cross-stratified sandstone facies. Basal contacts and bedding planes are typically sharp, non-incisive or incised less than 5 cm in roughly equal proportions. Incision up to 10 cm and gradational contacts were also observed. This facies is common in both the channelbelt and floodplain facies associations.

This facies has been commonly described in previous work. It is commonly found in the upper portions of channel deposits (Payne, 1982; Nelson, 1984; Caldes, 1998), Gilbert splays (Payne, 1982; Nelson, 1984), and point bars (Anderson, 2005), on the fringes of crevasse splays (Caldes, 1998; Anderson, 2005), and within lake deposits (Caldes, 1998). It is interpreted as low energy, lower flow-regime traction flow.

2.10 Mud-draped Current-rippled Sandstone Facies

The mud-draped current-rippled sandstone facies (Table 2.1) consists of 3-5 cm thick ripple-laminated cosets of upper fine to lower medium sandstone. The top-sets are rounded to appear sigmoidal (Figure 2.11). Ripples have a low climb angle and show a bundled pattern. Mud drapes are common on ripple foresets and they drape from the toe to the top of the foreset. Double mud-drapes are present but rare. This facies forms beds between 25 and 60 cm thick that extend about 10 m laterally.

This facies is most commonly found in association with the planar tabular cross-stratified sandstone facies and can be found directly below and above it. The mud-draped current-rippled sandstone facies has also been observed directly overlying the convolute sandstone facies. Basal contacts tend to be sharp and may incise less than 5 cm into the underlying bed. This facies is found exclusively within the channelbelt facies association in Sandbody I.

The mud-draped current rippled sandstone facies is interpreted as bidirectional low velocity traction flow deposits in a tidal environment. The abundance of mud drapes suggest periodic near zero current velocities. Rounded top-sets indicate reworking by a subordinate current direction. The bundling of cross-lamina may be the result on neap-spring cyclicity. Previous workers have not reported this facies in the Rangely area.

2.11 Wave-rippled Sandstone Facies

The wave-rippled sandstone facies (Table 2.1) is comprised of medium very fine, well sorted sandstone organized into symmetrical ripples (Figure 2.12). Vertical burrows are common. Beds range from 1 cm to 1.5 m thick with most beds less than 10 cm thick. Beds may extend laterally for hundreds of meters.

This facies is associated with the undifferentiated mudstone facies and the coal facies. It may overlie or underlie the undifferentiated mudstone facies. It is also observed loading into the coal facies. Contacts are sharp, but non-erosive. This facies was only observed in the secondary field area, where it is part of the floodplain facies association.

Caldes (1998) reported this facies in both the Upper Sego and the Iles formations. In the Sego Formation, where this facies is associated with hummocky cross-stratified sandstone and laminated mudstone, it is interpreted as a lower shoreface environment. In the Iles Formation, it is associated with carbonaceous shale, climbing ripples and current ripples and is interpreted as the distal toes of crevasse splays into floodplain lakes reworked by waves. Nelson (1984) stated that this facies is indicative of a tidal flat or estuarine environment.

The wave-rippled sandstone facies was most likely deposited in a shallow floodplain lake environment. Symmetrical ripples indicate the presence of two opposing currents of equal strength. The abundance of burrows suggests the presence of a permanent aqueous environment.

2.12 Bioturbated Sandstone Facies

The bioturbated sandstone facies (Table 2.1) consists of upper very fine sandstone with numerous vertical and horizontal burrows (Figure 2.13A). The bioturbation index

ranges from 3 to 4, based on the classification system in Bottjer and Droser (1994). This facies may show remnants of 5 cm thick trough cross-strata or exhibit convolute bedding (Figure 2.13B). Fragments of woody material are common. Beds are between 10 and 60 cm thick.

The bioturbated sandstone facies is observed overlying the coal facies and underlying the current-rippled sandstone facies. The base of the bioturbated sandstone is strongly mixed with the underlying coal. Units extend laterally for about 20 m before grading into the wave-rippled or trough cross-stratified sandstone facies. This facies is not present within the primary field area. It is only present in the floodplain facies association.

This facies was probably deposited in a floodplain lake. Original sedimentary structures were destroyed by subsequent burrowing. While Payne (1982), Nelson (1984), and Anderson (personal communication) report the presence of *Thalassanoides* and *Ophimorpha* burrows in the lower Iles Formation in the Rangely area, Nelson is the only author to describe a dominantly bioturbated facies. Burrows observed within the secondary field area could not be specifically identified.

2.13 Root-trace Dominated Sandstone Facies

The root-trace dominated sandstone (Table 2.1) facies consists of lower very fine to lower fine sandstone with no discernable sedimentary structures other than root traces which are very abundant (Figure 2.14). Randomly oriented mud clasts are also common. Beds are 15 cm to 1 m thick.

The root-trace dominated sandstone facies is most commonly surrounded by the undifferentiated mudstone facies. Beds tend to be lenticular, with a length of about 10 m,

pinching out into the undifferentiated mudstone facies. It is also observed overlain by the trough cross-stratified sandstone facies and truncated by the convolute sandstone facies. This facies is present in the floodplain facies association.

This facies likely represents small ephemeral channels. Original sedimentary structures were destroyed by subsequent rooting. Payne (1982), Nelson (1984) and Anderson (2005) observed root traces, but a root-trace dominated facies has not been previously described in the Rangely area.

2.14 Undifferentiated Mudstone Facies

The undifferentiated mudstone facies (Table 2.1) is volumetrically the most abundant facies in the field area. It consists of tan or gray clay to silt sized grains (Figure 2.15A). Two beds have a distinct green coloration (Figure 2.15B). This facies tends to outcrop poorly. Where better exposed, at the base of thick sand bodies, root traces and carbonized wood fragments are commonly observed. Permineralized wood and vertebrate bones are also common. Preserved logs may be several meters long (Figure 2.16). Two fossils were identified from photographs by Dr. Kenneth Carpenter: a rib bone from a dinosaur, probably from the hadrosaur genera, and a carapace from a baenid turtle, a terrestrial or fresh water group (personal communication, 2009). Continuous observed silt and clay thickness ranges from less than 1 cm to 16.5 m and may extend laterally for hundreds of meters. Because the focus of this project was on the sandstones, the finer grained sediments were not described in as much detail. A more detailed study of the mudstones would likely result in greater differentiation of this facies.

This facies is most commonly associated with the current-rippled sandstone facies. It is commonly associated with the structureless, planar tabular cross-stratified,

trough cross-stratified and convolute sandstone facies. It is rarely associated with the organic-rich mudstone and root-trace dominated sandstone facies and may underlie or overlie all of the previously mentioned facies. This facies rarely underlies the mud-clast conglomerate and climbing-rippled sandstone facies. In the broader field area, on the upper part of measured section F, it is also associated with the coal and wave-rippled sandstone facies. All observed basal contacts are sharp and non-incisive. It is also observed in sharp lateral contact with the structureless sandstone and root-trace dominated sandstone facies. This facies is present in both the channelbelt and the floodplain facies associations. In the channelbelt, thicknesses are less than 1 m while floodplain thicknesses are significantly greater.

The undifferentiated mudstone facies is common in previous work in the area (Payne, 1982; Nelson, 1984; Caldes, 1998; Anderson, 2005). In the floodplain facies association, this facies represents overbank deposits. Channelbelt-associated clays and silts were probably deposited in areas of stagnation.

2.15 Organic-rich Mudstone Facies

The organic-rich mudstone facies (Table 2.1) is poorly sorted consisting of clay to very fine sand sized grains with a visibly elevated percentage of organic matter (Figure 2.17A). Fragments of woody material and root traces are common. It has a distinct red-brown color. Beds are between 25 cm and 2 m thick, although most are less than 50 cm thick.

This facies is most commonly associated with the undifferentiated mudstone facies. It forms gradational contacts with the underlying and overlying undifferentiated mudstone facies. Beds also tend to extend around 30 m laterally before grading into the

undifferentiated mudstone facies. This facies also underlies the structureless sandstone and the current-rippled sandstone facies. The organic-rich mudstone facies is only present in the floodplain facies association.

Payne (1982), Nelson (1984), and Caldes (1998) have previously described similar facies. Caldes (1998) interprets it as a floodplain lake or pond deposit and Payne (1982) adds that the high preservation of organic matter suggests poor drainage. The presence of root traces suggests that deposition occurred in a very shallow fresh water environment. This facies most likely represents a poorly developed coal.

2.16 Coal Facies

The coal facies (Table 2.1) consists of black, fine grained material consisting of more than 75% organic matter (Figure 2.17B). Coal beds are between 10 cm and 2.3 m thick. Most of the beds are less than 50 cm thick. Coal beds may extend laterally for more than 100 m.

There is no coal present within the primary field area as defined from the top of Point Bar G in Anderson (2005) to the top of Sandbody D/E in this study (Figure 1.3). This lack of coal is somewhat surprising given that it is relatively common both below the field area, in the area described by Anderson, and in the secondary field area above Sandbody D/E (Above 52 m on Figure 1.4). Payne (1982) and Nelson (1984) also reported the presence of coal. In the secondary field area, the coal facies may underlie or overlie the undifferentiated mudstone facies and the current-rippled sandstone facies. A coal bed underlying Sandbody Z is loaded into by the wave-rippled sandstone facies (Figure 2.17B) and is also observed mixed into the bioturbated sandstone facies. This facies is only present in the floodplain facies association.

The organic matter is sourced from terrestrial plants that were deposited in an anoxic shallow water setting. The lack of coal within the primary field area likely represents an environmental or chemical change in the area during the time of deposition.

2.17 Paleocurrents

A total of 269 paleocurrent measurements were taken in the field area (Figure 2.18). Most measurements were taken from planar tabular cross-bedding, with lesser amounts from trough cross-bedding, ripple laminations, and sigmoidal cross-bedding. The mean resultant direction for all measurements is 123° . This southeast direction is consistent with previous work (Payne, 1982; Nelson, 1984; Caldes, 1998; Anderson, 2005). Accordingly, 41% of the measurements recorded were in the southeast quadrant. The northeast and southwest quadrants accounted for 21% of the measurements each and the remaining 18% were in the northwest quadrant (Figure 2.18A). Four of the eight major sandbodies in the field area exhibit bi-directionality, which is most commonly observed in the planar tabular cross-stratified sandstone facies. Paleocurrents for each sandbody will be discussed in greater detail in Chapter 3.

2.18 Summary of Floodplain Facies Association

The floodplain facies association consists of mostly fine grained sediment deposited outside of the area of active channel deposition. This facies association consists mostly of the undifferentiated mudstone facies. The other fine grained facies, the organic-rich mudstone facies, and the coal facies, are exclusively present in the floodplain facies association. The most common sand sized facies is the current-rippled sandstone facies. The planar tabular cross-stratified, trough cross-stratified, structureless, convolute, mud-

draped planar tabular cross-stratified, wave-rippled, root-trace dominated, and bioturbated sandstone facies are present in lesser quantities.

The floodplain facies association is interpreted as an environment of intermittent subaerial exposure with the majority of deposition occurring as overbank deposits in times of flood. The abundance of fine grained sediment suggests a very low energy environment. Root traces and wood fossils in a number of facies indicate subaerial exposure. Small sandbodies within this facies association are interpreted as minor crevasse splays or channels. The organic-rich mudstone, coal, wave-rippled sandstone, and bioturbated sandstone facies indicates the presence of floodplain lakes or marshes. However, only the organic-rich mudstone facies is present in the strictly defined field area and it is not abundant, indicating that standing water was uncommon when the rocks in the specific field area were deposited.

2.19 Summary of Channelbelt Facies Association

The channelbelt facies association was deposited in active channels and consists mostly of sand-sized sediment interbedded with lesser proportions of fine-grained mudstone. The most common facies in the channelbelt facies association is the planar tabular cross-stratified sandstone facies; however, the structureless, current-rippled, convolute, and trough cross-stratified sandstone facies are also common. Less common channelbelt facies are the mud-draped planar tabular cross-stratified sandstone, mud-clast conglomerate, climbing-rippled sandstone, mud-draped current-rippled sandstone, and sigmoidal cross-stratified sandstone facies.

Current velocities varied greatly within the channelbelt facies association. Mud drapes and the undifferentiated mudstone facies suggest that near zero current velocities

were periodically present, while pebble sized mud clasts in the mud-clast conglomerate facies indicate extremely high velocities. Larger clasts were observed within the mud-clast conglomerate facies, but these clasts likely represent collapse deposits and do not reflect current velocities. A typical, vertical facies succession of planar tabular cross-stratified sandstone to current-rippled sandstone, within this facies association, suggests decreasing energy over time is common. Sand units are typically 7 to 10 m thick with continuous sandstone up to 22 m thick. The abundance of dewatering structures and the presence of the climbing rippled sandstone facies indicate that deposition rates were typically high.

Tidal influence within the channelbelt facies association is indicated by the presence of the mud-draped planar tabular cross-stratified, mud-draped current-rippled, and sigmoidal cross-stratified sandstone facies, as well as, paleocurrent indicators. The amount of tidal influence varied over time and will be discussed further in subsequent chapters.

Table 2.1: Facies Identified in Field Area (Colors are used throughout thesis)

Color	Facies Name	Characteristics	Interpretation	Facies Association
Black	Coal	organic material from terrestrial plants	floodplain lake/marsh	Floodplain
Purple	Organic-rich mudstone	organic-rich mud, plant fragments and root traces	shallow floodplain lake/marsh	Floodplain
Grey	Undifferentiated mudstone	mud and silt sized grains, plant and vertebrate fossils common	overbank and abandonment deposits	Floodplain, Channelbelt
Green	Root-trace dominated sandstone	abundant root traces, lower very fine to lower fine sand	highly rooted, bioturbation index 5	Floodplain
Dark Green	Bioturbated sandstone	vertical and horizontal burrows, upper very fine sand	highly burrowed, bioturbation index 3-4	Floodplain
Yellow	Wave-rippled sandstone	symmetrical ripples, vertical burrows, medium very fine sand	wave ripples in floodplain lake	Floodplain
Light Yellow	Mud-draped current-rippled sandstone	mud-draped, sigmoid shape ripples, upper fine to lower medium sand	tidally modified low velocity traction flow	Channelbelt
Light Yellow	Current-rippled sandstone	current ripples, lower very fine to lower medium sand	low energy traction flow	Floodplain, Channelbelt
Light Green	Climbing-rippled sandstone	climbing ripples, upper very fine to upper fine sand	low energy traction flow with high deposition rate	Channelbelt
Orange	Mud-draped planar tabular cross-stratified sandstone	mud-draped, planar tabular cross-strata, lower fine to lower medium sand	moderately high velocity traction flow with periodic hiatuses	Floodplain, Channelbelt
Red	Sigmoidal cross-stratified sandstone	35 cm thick sigmoidal cross-sets, lower fine sand	moderately high velocity traction flow with subordinate current direction	Channelbelt
Light Blue	Convolute sandstone	convolute laminations, upper very fine to lower medium sand	post-depositional liquification	Floodplain, Channelbelt
Dark Blue	Structureless sandstone	no sedimentary structures, lower very fine to lower medium sand	post-depositional liquification	Floodplain, Channelbelt
Orange	Planar tabular cross-stratified sandstone	10 to 90 cm thick planar tabular cross-sets, lower very fine to lower medium sand	moderately high velocity traction flow	Floodplain, Channelbelt
Red	Trough cross-stratified sandstone	5 to 35 cm thick trough cross-sets, upper very fine to lower medium sand	high velocity traction flow	Floodplain, Channelbelt
Purple	Mud-clast conglomerate	pebble to lower boulder mud clasts in very fine to fine sand matrix	very high energy traction flow (units with boulder sized clasts- bank collapse)	Channelbelt



Figure 2.1 Photographs of mud-clast conglomerate facies A) Matrix supported conglomerate with boulder sized mud clasts in Sandbody G. Jacob staff is 1 m. B) Clast supported bed in Sandbody G. Hammer is 33 cm. C) permineralized vertebrate bones (outlined) in Sandbody D/E. Pencil is 15 cm. D) imbricated clasts in Sandbody G. Hammer is 33 cm.

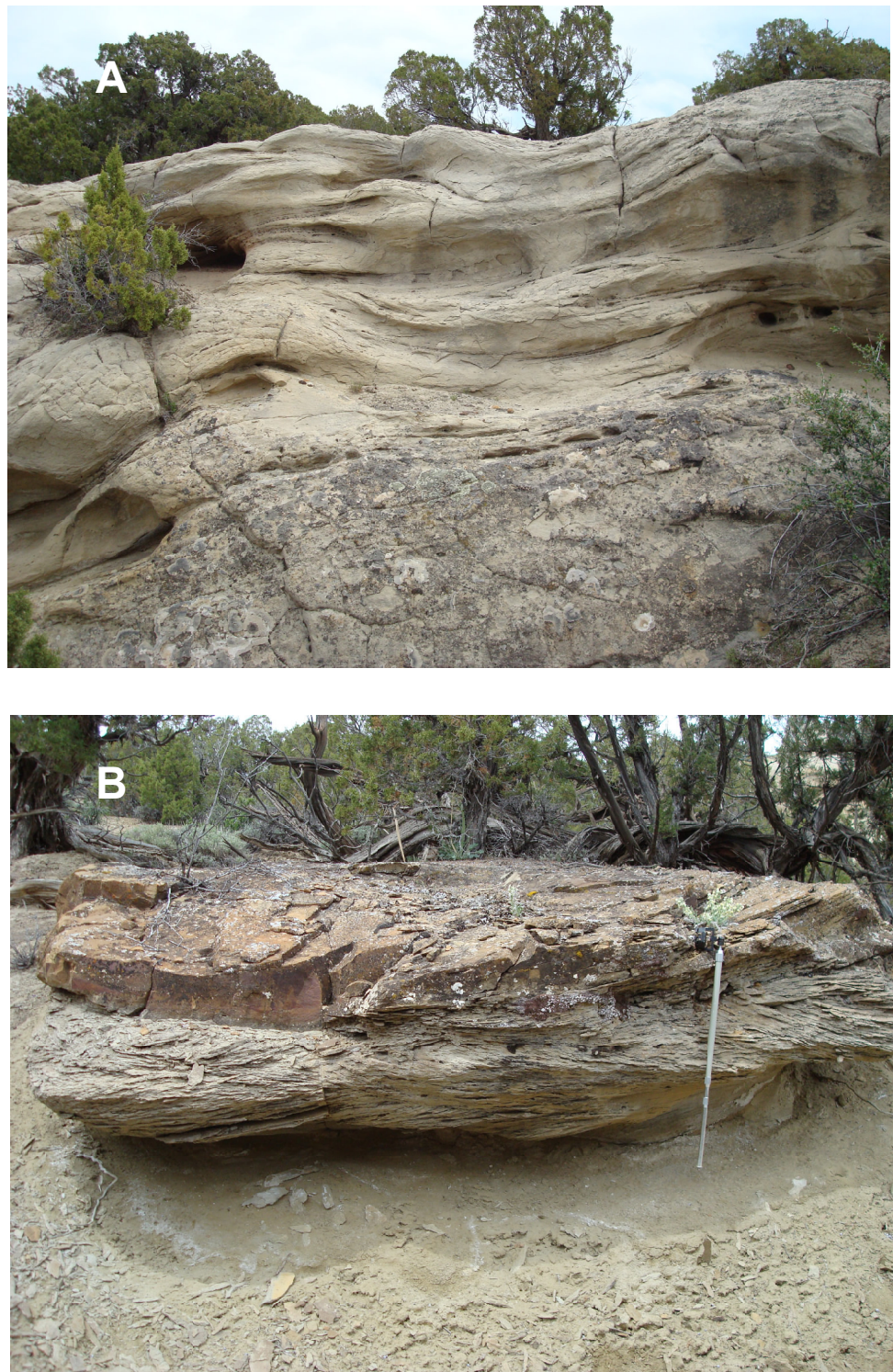


Figure 2.2 Photographs of trough cross-stratified sandstone facies with A) large trough cross-sets in Sandbody G. Tree on outcrop left is about 1 m. B) multiple current directions. Jacob staff is 1 m.



Figure 2.3 Photographs of planar tabular cross-stratified sandstone facies with A) large planar tabular cross-sets in Sandbody D/E. Jacob staff is 1 m.



Figure 2.4 Photographs of convolute sandstone facies with A) randomly oriented mud clasts in Sandbody D/E. Pencil is 15 cm. B) Large soft-sediment fold involving multiple beds. Jacob staff is 1 m.



Figure 2.5 Photographs of structureless sandstone facies A) thickly bedded in Sandbody G. Jacob staff is 1 m. B) containing ammonite fossil in Sandbody D/E. Pencil is 15 cm.



Figure 2.6 Photographs of sigmoidal cross-stratified sandstone facies in Sandbody I. A) showing rounded top-sets. Segments on Jacob staff are 10 cm. B) showing mounded shape. Highlighted by line. GPS unit is 17 cm.

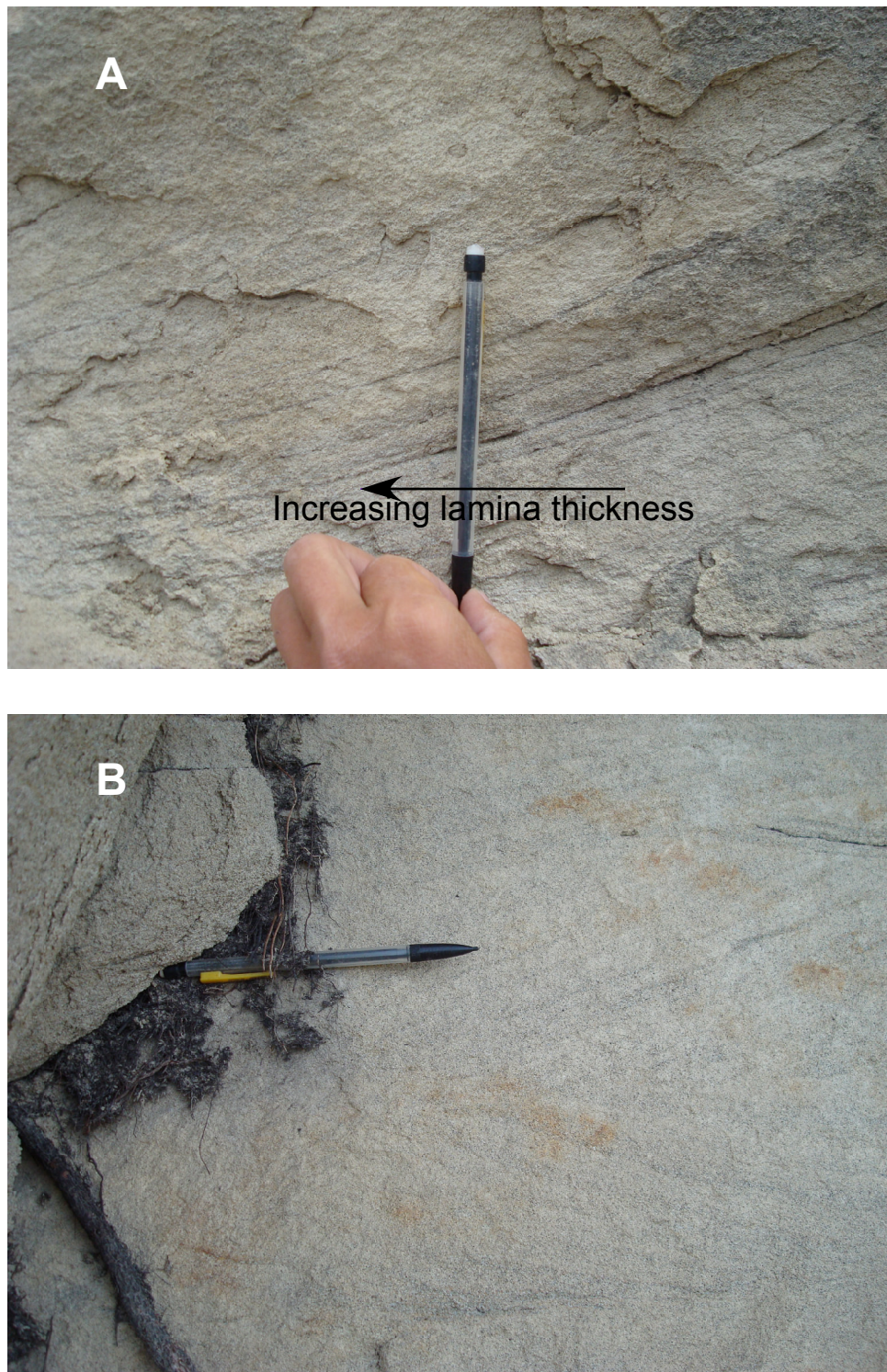


Figure 2.7 Photographs of mud-draped planar tabular cross-stratified sandstone facies with A) bundled pattern in Sandbody D/E. Pencil is 15 cm. B) with herring-bone cross-stratification in Sandbody D/E. Pencil is 15 cm.



Figure 2.8 Photograph of climbing-rippled sandstone facies with steep angle of climb and partial to nearly complete mud drapes in Sandbody A. Pencil is 15 cm.

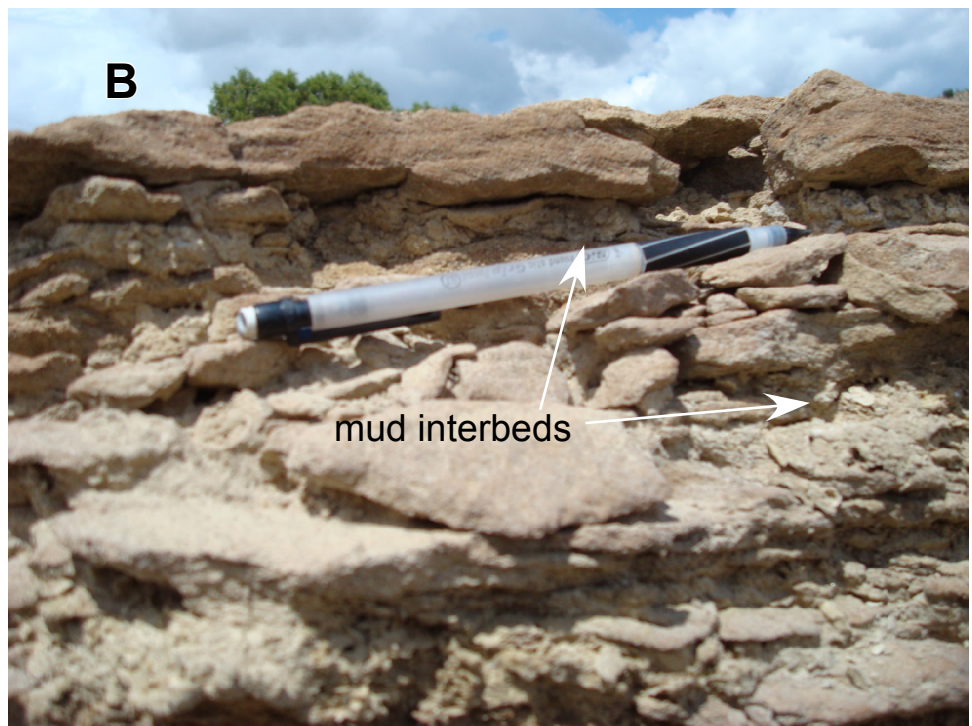


Figure 2.9 Photographs of current-rippled sandstone facies with A) asymmetrical ripples. B) thin mud interbeds. Pencil is 15 cm.

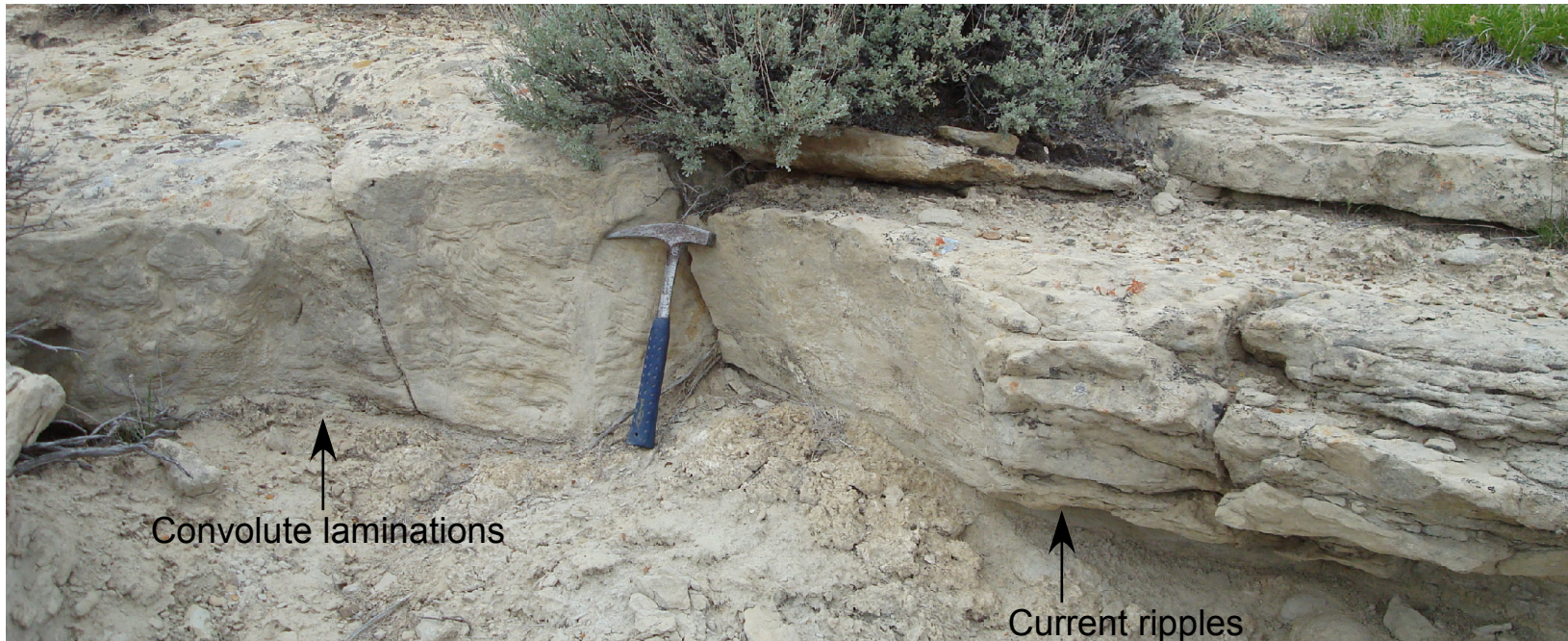


Figure 2.10 Photograph of current-rippled sandstone facies in lateral contact with convolute laminations. Hammer is 33 cm.



Figure 2.11 Photograph of mud-draped current-rippled sandstone facies with rounded top-sets in Sandbody I. Pencil is 15 cm.

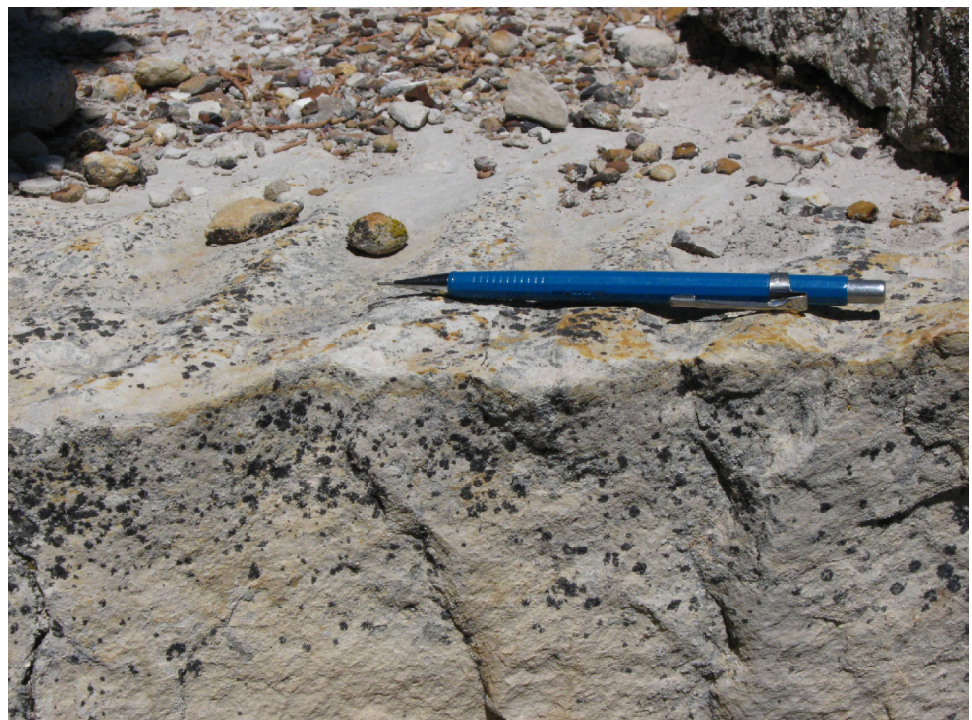


Figure 2.12 Photograph of wave-rippled sandstone facies showing symmetrical ripples and straight crests in Sandbody Z of secondary field area. Pencil is 15 cm.

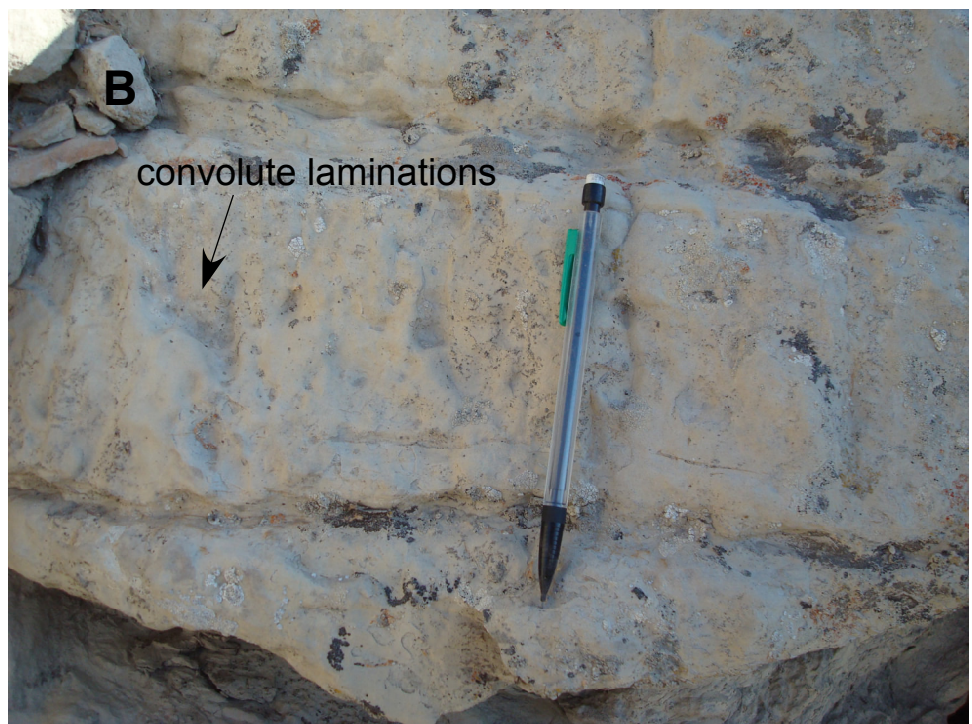


Figure 2.13 Photographs of bioturbated sandstone facies A) showing vertical and horizontal burrows. B) showing convolute laminations in Sandbody Z of secondary field area. Pencil is 15 cm.



Figure 2.14 Photograph of root-trace dominated sandstone facies showing numerous vertical root traces. Pencil is 15 cm.



Figure 2.15 Photographs of undifferentiated mudstone facies with A) knobby weathering B) green coloration. Pencil is 15 cm.



Figure 2.16 Photograph of undifferentiated mudstone facies with large permineralized log. The entire length of the log extends beyond photograph. Jacob staff is 1.5 m.

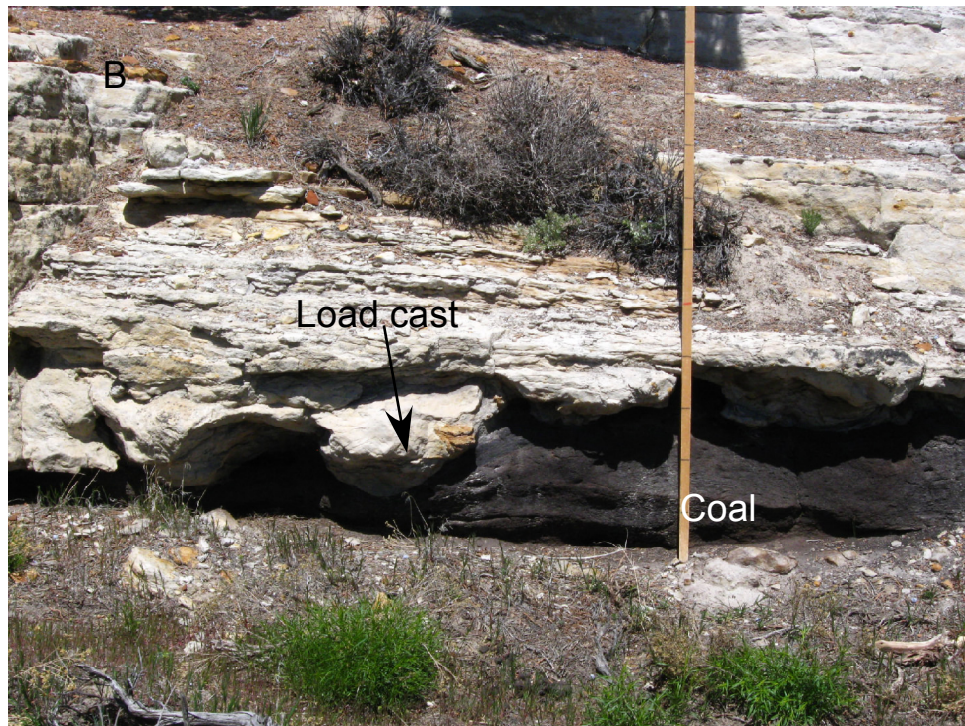


Figure 2.17 Photographs of A) organic-rich mudstone facies. Pencil is 15 cm. B) wave-rippled sandstone facies in Sandbody Z loaded onto underlying coal facies in secondary field area. Jacob staff is 1.5 m.

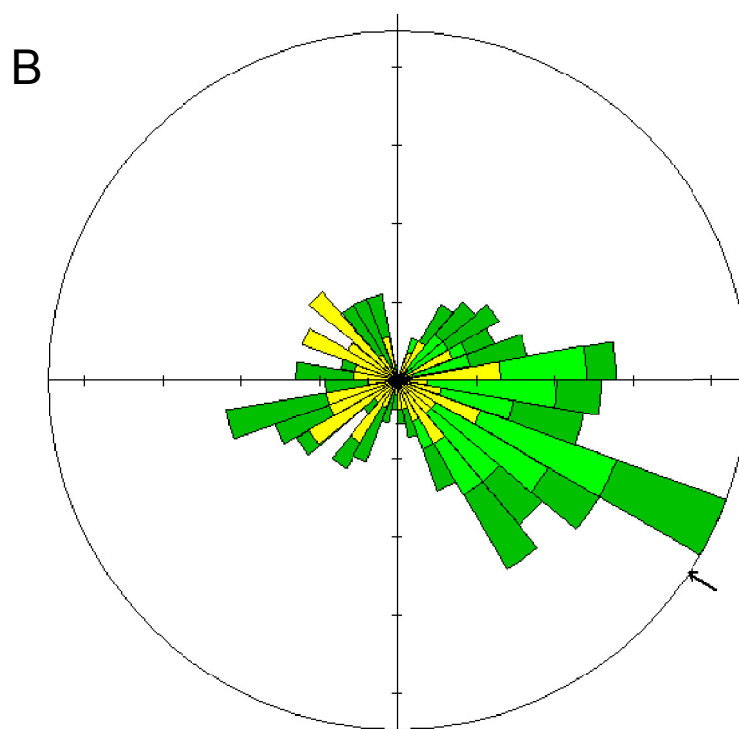
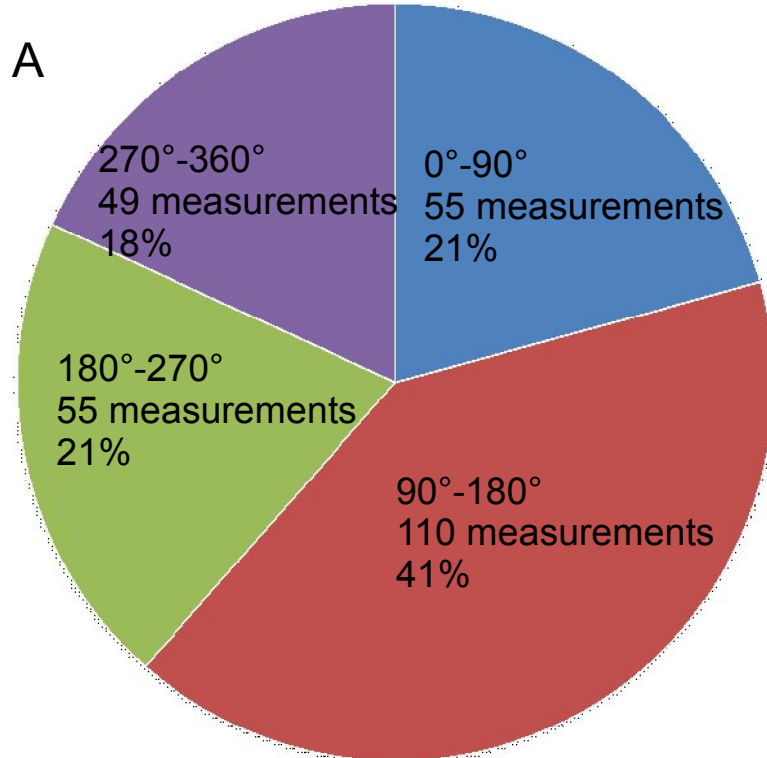


Figure 2.18 A) Proportion of paleocurrent measurements per compass quadrant. B) Current rose of all measurements. S1-Yellow, S2-Light green and S3-Dark green. The average of all 269 paleocurrent measurements 123°.

CHAPTER 3: MAJOR SANDBODIES

This chapter describes and interprets eight major sandbodies located within the primary field area and contains a general description of two sandbodies in the secondary field area. The major sandbodies are described in stratigraphic order. They are named Sandbody I, Sandbody J, Sandbody A, Sandbody H, Sandbody G, Sandbody B/C, Sandbody F and Sandbody D/E, in order from oldest to youngest (Figure 1.5). These major sandbodies are located with sandstone dominated intervals named S1, S2, and S3, in stratigraphic order. The S1 interval contains Sandbodies I, J, A, and H. The S2 interval contains Sandbodies G and B/C. The S3 interval contains Sandbodies F and D/E. Sandbodies within each of these intervals are partially or fully temporally concurrent. Each sandbody is composed of 2 to 4 subbodies, which are closely physically, stratigraphically, and depositionally related. Descriptions in this chapter include the shape, accretion and paleocurrent orientations of the sandbodies, facies distributions and abundance, and any other information relevant to a depositional interpretation. Facies percentages used in this chapter are measured as described in Chapter 1. Totals may not equal 100% due to rounding.

3.1 Sandbody I

Sandbody I is stratigraphically the lowest of the major sandstone bodies found within the field area. It is located within the S1 interval (Figure 1.5). The outcrop extends approximately 600 m northwest-southeast. The overall thickness of Sandbody I ranges from 0 to 10 m with an average of about 7 m. The base of the sandbody is erosive with the deepest erosion near the northwestern end.

Sandbody I is an elongate complex consisting of three subbodies: I1, I2, and I3 (Figure 3.1). Subbodies I1 and I2 are elongate to the northwest-southeast parallel to the outcrop, while Subbody I3 is V-shaped scouring into Subbody I1. Paleocurrents are in Subbody I1 are oriented to the northwest, while paleocurrents in Subbody I3 are to the southeast. The overall facies distribution is 42% planar tabular cross-stratified sandstone, 18% current-rippled sandstone, 14% convolute sandstone, 14% structureless sandstone, 7% undifferentiated mudstone, 1% mud-draped planar tabular cross-stratified sandstone, and less than 1% of mud-draped current-rippled sandstone, climbing-rippled sandstone, sigmoidal cross-stratified sandstone, and trough cross-stratified sandstone (Figure 3.2).

3.1.1 Subbody I1

Subbody I1 is the largest and oldest of the three subbodies. It outcrops over 520 m in the northwest-southeast direction. The undulatory base is deeply incised into the underlying mudstones with the depth of incision decreasing to the southeast (Figure 3.1). Comparing the base of Subbody I1 to the lower red-brown sandstone marker (Figure 3.3A) suggests a maximum depth of erosion about 4 m with the greatest depth of erosion near the northwestern end of the body. The orientation of accretion sets is between 107° and 167° with dips between 2° and 10°. Paleocurrents range from 210° to 346° with a mean of 300°. The southeast trending accretion is directly opposed to the dominant paleocurrent direction.

The facies distribution of Subbody I1 is indicative of decreasing energy to the southeast with a vertical decreasing energy pattern also apparent on the southeast end. These depositional energy patterns are indicated by the lateral and vertical transitions from mostly planar-tabular cross-stratified sandstone to mostly current-rippled sandstone

to undifferentiated mudstone. Planar-tabular cross-stratified sandstone is the most prevalent facies on the northwestern half of the subbody, accounting for almost 50% of the total facies distribution. The convolute, structureless, mud-draped planar-tabular cross-stratified, and less commonly trough cross-stratified sandstone facies transition laterally into the planar-tabular cross-stratified sandstone facies and are interpreted as roughly equivalent in depositional energy. These facies form an interfingering pinchout with the current-rippled sandstone facies in the vicinity of measured section HH (Figure 3.1). The mud-draped planar-tabular cross-stratified sandstone facies is most abundant on the northwest end of the subbody where it exhibits tidal bundling and grades laterally into the convolute sandstone facies. The most abundant facies on the southeast end of the subbody is current-rippled sandstone. This facies is in lateral contact with the mud-draped current-rippled and climbing rippled sandstone facies. The mud-draped current-rippled and climbing rippled sandstone facies indicate strong tidal influence and high deposition rates, respectively. A single dune of sigmoidal cross-stratified sandstone is observed in this ripple dominated portion of the subbody. The presence of the sigmoidal cross-stratified sandstone facies indicates a temporary increase in depositional energy with strong tidal influence. The southeast portion of the subbody between measured sections HH and BB is capped by a unit of undifferentiated mudstone. This unit represents a phase of very low depositional energy.

3.1.2 Subbody I2

Subbody I2 overlies the eastern portion of Subbody I1. It crops out for approximately 200 m in the northwest-southeast direction and is 0 to 3.5 m thick. The base of the subbody is scoured into the mudstone layer which caps Subbody I1 and is 2.1

m thick at measured section S and truncates in the vicinity of measured section BB (Figure 3.1). No measurable accretion sets or paleocurrents were observed in this subbody. However, the overall geometry appears similar to Subbody I1.

The facies distribution of Subbody I2 probably closely resembled Subbody I1 at the time of deposition, with a high energy northeastern end transitioning to a low energy southeastern end, but much of the information has been obscured by soft-sediment deformation. Subbody I2 is dominated by the convolute sandstone facies which accounts for 87% of the subbody and another 10% of the subbody consists of the structureless sandstone facies. Although undeformed facies are rare where they are present they have a similar distribution to Subbody I1 with planar-tabular cross-stratified sandstone on the northwest end and current-rippled sandstone to the southeast.

3.1.3 Subbody I3

Subbody I3 is roughly V-shaped and is scoured completely through the base of Subbody I1 (Figure 3.1). It has a maximum thickness of about 10 m and an outcrop length of around 160 m in the northwest-southeast direction. No accretion sets were observed in this subbody. Paleocurrents ranged from 111° to 149° with an average of 127°.

The facies distribution of Subbody I3 suggests high energy currents were prevalent throughout deposition with only a minor component of low energy facies near the end of deposition. Subbody I3 is comprised mostly of the planar tabular cross-stratified and structureless sandstone facies. The planar tabular cross-stratified sandstone facies is 55% of the subbody and grades laterally into both the structureless and convolute sandstone facies which account for 43% and 2% of the subbody, respectively.

Numerous internal scour surfaces exist in the structureless sandstone facies which dominates the deepest part of the subbody (Figure 3.3B). The mud-draped current-rippled sandstone facies accounts for less than 1% of the subbody and is present on the thin portion near the top of the northwestern side of the subbody. This may represent shallow water near the bank of a channel.

3.1.4 Interpretation

Subbody I1 is most likely a downstream accreting, tidal bar form. Previous work in the area has established that the regional transport direction is to the southeast (Payne, 1982; Anderson, 2005), so the oppositely directed northwest-trending paleocurrent direction suggests flood tidal dominance. The bar is accreting in the seaward (southeast) direction suggesting river deposition, but the dominance of northwest-trending paleocurrents indicates tidal reworking. This subbody contains a number of other tidal indicators including mud drapes, bundling, and sigmoidal cross-strata. The transition from mostly planar tabular cross-stratified sandstone to mostly current-rippled sandstone to undifferentiated mudstone indicates a general decrease in current energy to the southeast, indicating a waning flow pattern.

Subbody I2 formed as a compensatory body to Subbody I1 and likely formed in a similar manner. The dominance of the convolute sandstone facies in Subbody I2 makes this subbody more ambiguous as no original depositional relationships could be observed. However, its close physical and stratigraphic relationship to Subbody I1 and its similar geometry suggest a similar depositional history. A depositional relationship to Subbody I1 is also suggested by the compensating stacking pattern of the bodies. The thickest part of Subbody I2 occurs directly above the thinnest part of Subbody I1.

Subbody I3 had a different depositional history than the other I subbodies. While the age relationship with Subbody I2 cannot be definitively proven, Subbody I3 is most likely the youngest of the three subbodies. Subbody I3 incised through Subbody I1 and was backfilled. The lateral relationships between the planar-tabular cross-stratified, structureless, and convolute sandstone facies indicates a high depositional energy throughout the subbody followed by extensive dewatering. The structureless sandstone facies is concentrated at the deepest part of the subbody indicating a higher degree of liquification at the channel axis. The deep incision into Subbody I1, internal scour surfaces, and the high current energy indicates a channel deposit. Currents are to the southeast indicating fluvial dominance; however, tidal influence is indicated by the presence of the mud-draped current-rippled sandstone facies on the thin upper part of the channel suggesting a shallow, lower energy bank.

Sandbody I is a tidally to fluvially dominated unit. Subbody I1 is a downstream accreting tidal bar deposited in a fluvially cut channel and Subbody I2 is probably a smaller, compensatory unit with a similar depositional history. The mudstone layer at the top of Subbody I1 suggests an abandonment of the channel at this time. Subbody I3 indicates the cutting and subsequent fill of a later fluvially dominated channel with only a minor component of tidal influence.

3.2 Sandbody J

Sandbody J is within the S1 interval and is time equivalent to Sandbodies I and A (Figure 1.5). Although the outcrop is V-shaped (Figure 3.4), only the southeastern outcrop was studied in detail. The outcrop is elongated in the southwest-northeast direction for 200 m. The maximum thickness of the sandbody, including intervening

mudstones, is about 7 m and thins and pinches out to the northeast. The maximum sandstone thickness is 4.5 m.

Sandbody J consists of three subbodies: J1, J2 and J3 (Figure 3.4). Subbodies J1 and J3 consist of V-shaped forms with a laterally extensive capping unit. Subbody J2 consists of two offlapping accretionary packages. Paleocurrents are dominantly to the southwest with some southeast and northeast current indicators. The overall facies distribution is 44% current-rippled sandstone, 25% convolute sandstone, 19% undifferentiated mudstone, 5% trough cross-stratified sandstone, 4% structureless sandstone, 2% planar tabular sandstone, 1% mud-clast conglomerate, and less than 1% mud-draped planar tabular cross-stratified sandstone (Figure 3.5).

3.2.1 Subbody J1

Subbody J1 is the oldest of the three subbodies. It is about 125 m in the southwest-northeast direction. The outcrop of Subbody J1 is V-shaped with a thin upper unit which extends laterally in to the southwest and northeast of the thickest portion of the subbody (Figure 3.4). It is a maximum of 3 m thick and thins and pinches out to the southwest and northeast. The base of the subbody is incised about 2.5 m into the underlying mudstones. There are four fining upwards stories in this subbody (Figure 3.4). From the base upward, the first story is about 1 m thick, the second is about 35 cm thick, the third is about 75 cm thick and the fourth is about 85 cm thick. Paleocurrents range from 212° to 267° with an average of 237°.

Subbody J1 is a composite channel fill consisting of four fining upward stories. The facies distributions in each of these stories also indicate decreasing energy over time. The first story has a base of trough cross-stratified sandstone overlain by structureless

sandstone and capped by a thin layer of undifferentiated mudstone. The second story consists of mud-clast conglomerate overlain by through cross-stratified sandstone and the third story consists of trough cross-stratified sandstone overlain by current-rippled sandstone. The fourth story filled the channel and formed a splay to the southwest and northeast of the channel. It is composed of convolute sandstone along the channel axis grading to current-rippled sandstone to the northeast and a vertical sequence of trough cross-stratified sandstone to mud-draped planar-tabular cross-stratified sandstone to current-rippled sandstone to the southwest.

3.2.2 Subbody J2

Subbody J2 crops out over 65 m in the southwest-northeast direction. It consists of two fining upward, offlapping sandstone units which pinch out in the vicinity of measured section LL (Figure 3.4). Each is capped by a mudstone unit which extends an indeterminate distance to the northeast, as they become indistinguishable from the floodplain mudstones. Subbody J2 is thickest near measured section GG, where it is about 2.5 m thick, and thins to the northeast. The subbody terminates abruptly to the southwest, but this is an effect of modern erosion and the subbody was originally more extensive to the southwest. Both of the offlapping packages are a maximum of 1.25 m thick. The orientation of accretion sets is from 53° to 77° with dips from 1° to 8° . Paleocurrents range from 36° to 260° with a mean of 203° . Most of the paleocurrents are oriented to the southwest with a few oriented to the southeast and northeast.

The two offlapping packages of Subbody J2 exhibits both an upwards and lateral waning flow pattern shown by the facies distribution and the vertical grain size grading. The base of the lower fining upward package is composed of the planar-tabular cross-

stratified sandstone and the mud-clast conglomerate facies. These facies pinchout to the northeast and are overlain by the current-rippled sandstone facies which pinches out near measured section LL. The current-rippled sandstone is overlain by the undifferentiated mudstone facies which thickens to the northeast. The upper fining upward package consists of planar-tabular and trough cross-stratified sandstone which grades laterally into current-rippled sandstone. The current-rippled sandstone unit pinches out in the vicinity of measured section LL and is overlain by a layer of undifferentiated mudstone which thickens to the northeast.

3.2.3 Subbody J3

Subbody J3 is the youngest of the three subbodies. It crops out for 200 m in the southwest-northeast direction. This subbody is located 1.25 m above Subbody J1 and 0 to 0.25 m above Subbody J2 (Figure 3.4). It has a central V-shape with a maximum thickness of 2 m and a capping unit which thins to a pinch out to the southwest and northeast. No accretion sets or paleocurrents were observed on this subbody.

The facies distribution of Subbody J3 suggests consistently low energy deposition with an extensive overprint of soft-sediment deformation. Two-thirds of this subbody consists of convolute or structureless sandstone. These facies are observed grading laterally into the current-rippled sandstone facies.

3.2.4 Interpretation

Subbody J1 is probably a fill-and-spill channel. Each of the four fining upward stories in this subbody suggest a separate stage of channel fill and the mudstone layer between the first two fining upward units suggests a hiatus. Because the paleocurrents are directed to the southwest, this subbody may be a tidal creek. The multiple pulses of

channel fill suggests it was only active during strong spring tides. During the fourth stage of filling, the channel overflowed forming a splay and deposited the thin lower energy flanks.

Subbody J2 is likely two tidal bars. The primary accretion direction is to the northeast and the primary paleocurrent direction is to the southwest. This pattern suggests deposition by a northeast current and reworking by a southwest current. The presence of some northeast and southeast paleocurrents is further evidence for tidal influence. The facies patterns and upward fining cycles suggest decreasing current energy both vertically and to the northeast for both bar forms.

Subbody J3 has a similar geometry to Subbody J1 and is also likely a fill-and-spill channel. This subbody is characterized by low energy deposition with a strong overprint of soft-sediment deformation. The broad, low energy flanks suggests that the channel formed a splay in the late stage of deposition. Although no direct tidal indicators were observed, tidal influence is likely because of an association with the S1 interval where tidal influence is commonly observed.

Sandbody J represents a series of small, tidally dominated units which were subsidiary to the primary channel. Subbodies J1 and J3 represent fill-and-spill tidal creeks, while Subbody J2 consists of two tidal bars which formed in a small, tidally dominated channel.

3.3 Sandbody A

Sandbody A is present within the S1 interval (Figure 1.5). Subbody A1 is coeval to slightly younger than Sandbodies I and J and the younger subbodies of Sandbody A are coeval to slightly younger than Sandbody H. The outcrop is triangular in shape and

extends about 340 m in the northwest-southeast direction and about 440 m in the north-south direction (Figure 3.6A). The thickness ranges from 0 m to 9 m with an average of about 7 m. It is thin and narrow on its southern end, widening and thickening to the north and northeast.

Sandbody A consists of four subbodies: A1, A2, A3, and A4 (Figure 3.6A, B and C). In outcrop, Subbody A1 is a large, triangular form, Subbody A2 has a mounded geometry, and Subbodies A3 and A4 are V-shaped. Paleocurrent directions vary by subbody with Subbodies A1 exhibiting bi-directionality in the northeast-southwest direction, Subbody A2 exhibiting southerly paleocurrents, and Subbodies A3 and A4 exhibiting unidirectional paleocurrents to the east and southeast, respectively. The overall facies distribution is 22% planar tabular cross-stratified sandstone, 19 % convolute sandstone, 17% structureless sandstone, 17% trough cross-stratified sandstone, 12% mud-draped planar tabular cross-stratified sandstone, 11% current-rippled sandstone, 1% climbing-rippled sandstone, and less than 1% mud-clast conglomerate and undifferentiated mudstone (Figure 3.7).

3.3.1 Subbody A1

Subbody A1 is the largest and oldest of the subbodies. The outcrop has a triangular geometry with a thin, narrow southern end which widens and thickens to the north and northeast. It reaches a maximum width of around 340 m at its northern end with an observed length of 440 m in the north-south direction. The eastern side of the subbody thickens to the northeast to an abrupt, interfingering pinchout (Figure 3.6B). The western side of the subbody thickens to the north and is interpreted as continuing into the subsurface (Figure 3.6C). Accretion surfaces measured on the upper portion of the

western side of the outcrop ranged from 354° to 359° with dips between 7° and 12°. The apparent dips of accretion surfaces on the east side of the outcrop, but they are apparently slightly steeper and to the northeast (Figure 3.8). Fourteen easterly paleocurrent measurements were made ranging from 35° to 154° and a mean of 78°. Eleven westerly paleocurrent measurements were made ranging from 212° to 348° with a mean of 258°.

The facies distribution of Subbody A1 indicates decreasing energy to the north and northeast. On the eastern side of the outcrop, this decreasing energy pattern is indicated by the planar-tabular cross-stratified sandstone facies grading into the current-rippled sandstone facies and pinching out into the undifferentiated mudstone facies (Figure 3.6B). On the western side of the outcrop, this decreasing energy pattern is suggested by the trough cross-stratified sandstone facies grading into the mud-draped planar-tabular or the planar-tabular cross-stratified sandstone facies to the point where the outcrop ends due to modern topography.

There is also a significant change in the facies in the upper 1 to 4 m of the subbody which indicates a change from tidally to fluvially dominated. This transition is marked by several layers of mud-clast conglomerate alternating with structureless sandstone in the vicinity of measured section OO (Figure 3.6C). Below this interval, almost all of the planar-tabular cross-sets are mud draped and paleocurrents are dominantly to the southwest. Above the mud-clast conglomerate interval, planar-tabular cross-sets are not mud draped and paleocurrents are dominantly to the northeast. There is also a significant decrease in the abundance of the convolute and structureless sandstone facies.

3.3.2 Subbody A2

Subbody A2 occurs directly above the southern end of Subbody A1. At measured section R, there is a 0.6 m mudstone layer between the subbodies which pinches out in the vicinity of measured section PP. Subbody A2 crops out for about 50 m in the north-south direction. It forms concave-upward mounded shape with a maximum thickness of 2.25 m near measured section G and thins nearly symmetrically to an interfingering pinchout on both the north and south ends of the subbody (Figure 3.6C). This subbody has two accretion directions (Figure 3.9). Accretion surfaces in the basal unit are from 142° to 212° with dips from 2° to 23° . Dips become shallower upwards. In the upper portion of the subbody, accretion surfaces range from 346° to 17° with dips of 3° to 13° . Dips also become shallower upwards in this portion of the subbody. Paleocurrents range from 151° to 204° with an average of 177° .

The facies distribution pattern for Subbody A2 suggests significant variability to the deposition rates and current energy. The climbing-rippled sandstone facies forms a mounded shape in the basal, central portion of the subbody. The climbing ripples in this subbody are partially mud draped (Figure 2.8). This suggests a high deposition rate with low current energies. Subbody A2 is dominated by the current-rippled sandstone facies which accounts for 50% of the subbody. This facies is seen nearly surrounding the climbing-rippled sandstone unit and indicates a decrease in the deposition rate. A thin unit of undifferentiated mudstone is present between two layers of current-rippled sandstone suggesting a brief pause in sandstone deposition. Three layers of other sandstone facies indicate temporary increases in current energy. The first layer contains both planar-tabular and trough cross-stratified sandstone. The second of these higher energy layers consists of planar-tabular cross-stratified sandstone overlain by climbing-

rippled sandstone and these facies grade laterally into the current-rippled sandstone facies. The third high energy layer caps this subbody and consists of structureless and mud-draped planar-tabular cross-stratified sandstone.

3.3.3 Subbody A3

Subbody A3 is the smallest of the four subbodies. The outcrop is V-shaped with a maximum thickness of 0.75 m and sharp lateral margins (Figure 3.6C). There is a 0.25 m thick mudstone layer between this subbody and the top of Subbody A2. Subbody A3 is about 30 m long in the north-south direction. No accretion surfaces were observed on this subbody. Paleocurrents range from 24° to 122° with a mean of 87°.

The facies distribution of Subbody A3 suggests increasing current energy and soft-sediment deformation over time. The basal unit of the subbody is composed of current-rippled sandstone. The middle unit contains planar tabular cross-stratified sandstone and is overlain by convolute sandstone.

3.3.4 Subbody A4

Subbody A3 is located above the northern end of Subbody A2 with a 0.5 m mudstone layer between the two subbodies (Figure 3.6C). It is slightly younger than Subbody A3. The outcrop of Subbody A4 is V-shaped with a maximum thickness of 2.25 m and sharp lateral margins. It is about 60 m long in the north-south direction. No accretion surfaces were observed in this subbody. Paleocurrents ranged from 135° to 163°, averaging 149°.

The facies distribution of Subbody A4 indicates a low energy base signified by the current-rippled sandstone facies. Current energy then increased and before

establishing a waning flow pattern. This pattern is suggested by the vertical succession of trough cross-stratified to planar-tabular cross-stratified to current-rippled sandstone.

3.3.5 Interpretation

Subbody A1 is interpreted as a tidally influenced splay which transitions to fluvially dominated in the upper 1 to 4 m. The triangular geometry with two directions of radial accretion is indicative of splay type deposition. Splay deposition is further indicated by the decreasing paleocurrent energy to the north and northeast. Tidal influence in the subbody is suggested by southwestern paleocurrents and the presence of the mud-draped planar tabular sandstone facies. The presence of tidal indicators suggests that the splay remained in hydraulic contact with the primary channel and may indicate that it formed into a floodplain lake. The upper portion of the subbody does not exhibit mud drapes and paleocurrents are to the northeast indicating a fluvially dominated upper unit.

Subbody A2 is interpreted as a tidally influenced constructional barform. The lower southerly accreting unit resulted in a sloping upper surface and a compensatory northerly accreting upper unit. High sediment load at the base of this subbody are indicated by the prevalence of climbing ripples and steep accretion angles. Low current energies were typical in this subbody as suggested by the abundance of rippled sandstone, but brief increases in current energy are indicated by the presence of higher energy facies. Tidal influence is indicated by the abundance of mud drapes and the unusual southerly paleocurrent orientation.

Subbodies A3 and A4 are interpreted as fluvial channel backfill deposits. These subbodies are interpreted as deflecting around the central high formed by Subbody A2.

This interpretation is supported by the more easterly paleocurrents observed in Subbody A3 and the termination of this subbody against Subbody A2. Subbodies A3 and A4 are both V-shaped and incised into the underlying mudstones. Both subbodies have a low energy basal unit indicated by the current-rippled sandstone facies followed by a higher energy facies. The facies distribution of Subbody A4 indicates decreasing current energy over time in the upper part of the subbody. Subbody A3 may exhibit the same pattern, but liquefaction obscures the upper portion of this subbody.

Sandbody A is a succession of subbodies indicating decreasing tidal influence over time. Subbody A1 is a splay deposit with a tidally dominated base and a fluvially dominated upper unit. Subbody A2 is a small constructional bar which formed in tidally influenced channel. Subbodies A3 and A4 are small fluvially dominated channels which formed compensatory to the central high created by Subbody A2.

3.4 Sandbody H

Sandbody H is located within the S1 interval near the center of the field area (Figure 1.5). It was deposited concurrently with the latter stages of Sandbodies I and A. The outcrop is about 100 m in the north-south direction and is 0 to 6 m thick. A modern gully cuts through this sandbody between measured sections X and MM (Figure 3.10).

Sandbody H consists of two subbodies, Subbody H1 and Subbody H2, both of which have roughly U-shaped outcrops and are about 3 m thick (Figure 3.10). The dominant current direction is to the east. The overall facies distribution is 46% convolute sandstone, 36% trough cross-stratified sandstone, 11% structureless sandstone, and 7% current-rippled sandstone (Figure 3.11).

3.4.1 Subbody H1

Subbody H1 crops out for approximately 30 m in the north-south direction and has a maximum thickness of 3 m (Figure 3.10). It is U-shaped and incised into the underlying mudstones with sharp lateral contacts. The width to depth ratio is approximately 10:1. Trough cross-sets indicate the dominant paleocurrent direction is nearly perpendicular to the north-south trending outcrop surface and therefore east-west trending transport. No accretion sets were observed in this subbody and it consists of a single story of channel fill.

Subbody H1 exhibits a clear, upward waning-flow pattern. The lower 77% of the subbody consists of trough cross-stratified sandstone and the upper 23% consists of current-rippled sandstone. This trend continues into a mudstone layer which overlies the subbody.

3.4.2 Subbody H2

Subbody H2 crops out in a sinuous 3D pattern for about 100 m in the north-south direction with a maximum thickness of 3.5 m (Figure 3.10). It is U-shaped with an approximate 30:1 width to depth ratio and is sharply incised into the underlying mudstones. Accretion at the southern end of the subbody is oriented between 20° and 60° with dips from 3° to 13°, while accretion surfaces on the northern end of the subbody are oriented between 165° and 187° with dips from 7° to 18° (Figure 3.15). These represent two sides of a connected U-shaped accretion pattern. Paleocurrents are from 82° to 105° degrees averaging 95°.

The internal facies succession in Subbody H2 exhibits a waning-flow pattern which is partially obscured by soft-sediment deformation. The trough cross-stratified

sandstone facies constitutes about a quarter of the subbody and can be found near the base of the outcrop in the vicinity of measured section MM. A thin layer of current-rippled sandstone directly overlies the trough cross-stratified sandstone unit which is in turn overlain by the structureless sandstone facies. The structureless sandstone facies comprises about a quarter of the subbody on the upper southeast end and was most likely deposited as current-rippled sandstone. The convolute sandstone facies obscures the northwestern side of the subbody and grades laterally into the other facies present. The convolute sandstone unit is located in thickest portion of the subbody and may indicate greater fluidization in the channel axis.

3.4.3 Interpretation

Subbody H1 is a channel backfill deposit. It is U-shaped with a 10:1 width to depth ratio. As there are no indicators of tidal influence, the dominant current direction was easterly, somewhat consistent with the regional transport direction. The transition from trough cross-stratified to current-rippled sandstone indicates decreasing energy over time.

Subbody H2 is also a channel backfill deposit. The width to depth ratio is about 30:1 with a U-shape. The U-shaped accretion suggests a downstream channel filling. The east trending paleocurrent direction is consistent with the downstream accretion. Much of the original facies information has been obscured by soft-sediment deformation. However, this subbody appears to follow the same decreasing current energy pattern seen in Subbody H1, as evidenced by the base of trough cross-stratified sandstone capped by current-rippled sandstone.

Sandbody H consists of two small fluvial channels. Subbody H2 is slightly larger, wider, and younger than Subbody H1. If not for the high degree of soft-sediment deformation in Subbody H2, these subbodies would likely be nearly identical in facies proportions and distributions (Figure 3.11). The thickest portion of Subbody H2 is offset about 20 m from the thickest portion of Subbody H1 indicating a compensatory relationship.

3.5 Sandbody G

Sandbody G is located in the S2 interval (Figure 1.5). It crops out for about 500 m in the northwest-southeast direction and about 170 m in the northeast-southwest direction. The northwestern portion of the sandbody is covered by alluvium (Figure 1.3). It has a maximum thickness of about 16 m and averages about 8 m thick. Incision of about 3 m is observed on the northwest end of the body and decreases to the southeast.

Sandbody G is a sandstone complex consisting of four subbodies: G1, G2, G3, and G4 (Figure 3.13). Subbody G1 is lenticular and incised into the underlying mudstones. Subbodies G2, G3, and G4 are constructional concave-upward mounds with flat bases. Paleocurrents are consistently to the southeast in the entire body. The overall facies distribution is 37% structureless sandstone, 30% planar tabular sandstone, 19% trough cross-stratified sandstone, 10% mud-clast conglomerate, 2% of both convolute and current-rippled sandstone, and 1% undifferentiated mudstone (Figure 3.14).

3.5.1 Subbody G1

Subbody G1 is the oldest of the four subbodies. It crops out for 250 m in the northwest-southeast direction. The subbody is lenticular and incised about 3 m into the underlying mudstones (Figure 3.13). No accretion sets were observed in this subbody.

Paleocurrents range from 82° to 149°, averaging 122°. It is about 45 m wide perpendicular to the dominant paleocurrent direction, giving it a width to depth ratio around 15:1.

The facies distribution of Subbody G1 suggests consistently high energy for the majority of deposition followed by a brief phase of very low energy. Subbody G1 is dominated by the planar tabular cross-stratified sandstone facies. This facies composes 82% of the subbody. The planar tabular cross-stratified sandstone facies overlies and grades laterally into the convolute sandstone facies which constitutes 14% of the subbody. A unit of undifferentiated mudstone less than 0.25 m thick caps the southeastern portion of the subbody indicating a sudden decrease in current velocity to near zero values.

3.5.2 Subbody G2

Subbody G2 is the largest of the three subbodies and directly overlies Subbody G1 (Figure 3.13). Southeast of measured section J, the base of this subbody is incised less than 0.25 m into the mudstone layer that caps Subbody G1. Subbody G2 is a mounded shape with a thickness of between 7 and 8 m. Subbody G2 can be further divided into a basal unit, G2a, and an upper unit, G2b. It is about 300 m long in the northwest-southeast direction. Accretion sets oriented 122° and 130° were measured, both dipping 3°. Paleocurrents are between 84° and 158° with a mean of 116°, indicating seaward transport.

The facies distribution of Subbody G2 indicates high energy flow throughout subbody with very high depositional energy at the base. The G2a unit is the basal unit for most of the subbody. The G2a unit consists mostly of mud-clast conglomerate and structureless sandstone. A small pocket of trough cross-stratified sandstone is also

observed at the base. This unit reaches a maximum thickness of about 3 m in the vicinity of measured section J, where clast supported conglomerates (Figure 2.1B) and imbricated clasts are observed (Figure 2.1D). Clasts at the base of this unit are up to boulder size (Figure 2.1A). The G2a unit likely represents a bank collapse or a levee break which was followed by a very high energy flow. The mud-clast conglomerate facies pinches out laterally beneath the planar tabular cross-stratified sandstone facies to the northwest and grades both laterally and vertically into the structureless sandstone facies to the southeast. The G2b unit overlies the G2a unit and consists of planar-tabular cross-stratified and structureless sandstone. The planar-tabular cross-stratified sandstone facies composes the lower, northwest end of the subbody and grades laterally into the structureless sandstone facies.

3.5.3 Subbody G3

Subbody G3 is overlies the tail portion of and continues to the southeast of the pinch-out of Subbody G2 (Figure 3.13 and 3.15). Subbody G3 also forms a constructional mounded shape about 200 m long in the northwest-southeast direction. It reaches its maximum thickness of about 8 m near the northwest end of the subbody and tapers to an interfingering pinch-out to the southeast. This subbody averages about 6 m thick. Only one accretion plane could be measured on this subbody. It was oriented at 112° with a 3° dip. Paleocurrents were between 88° and 145° with an average of 113° .

The facies distribution of Subbody G3 suggests that paleocurrent energy was typically high in this subbody, but lower energy currents are also observed. These lower energy currents are represented by the current-rippled sandstone facies which is most prevalent near the interfingering pinch-out with the undifferentiated mudstone facies at

the southeast end of the subbody. This suggests decreasing energy to the edge of the subbody. This trend is further indicated by the pinch-out of the basal unit of mud-clast conglomerate under the structureless sandstone facies. This conglomeratic unit contains clasts up to boulder size which were likely deposited during a bank collapse or a levee break. Above the basal 3 m, this subbody is almost entirely composed of the structureless, planar-tabular cross-stratified, and trough cross-stratified sandstone facies suggesting fairly constant high energy flow dominated the upper portion of this subbody. Brief, possibly local, variations in current energy are indicated by small pockets of the current-rippled sandstone and mud-clast conglomerate facies, suggesting temporary decreased and increased velocities, respectively.

3.5.4 Subbody G4

Subbody G4 is offset to the northeast of Subbody G2. It crops out for about 100 m in the northwest-southeast direction and forms a constructional mounded shape (Figure 3.13). It is 5 m thick and entirely composed of trough cross-stratified sandstone suggesting consistent high energy deposition. No paleocurrents or accretion sets were observed on this subbody.

3.5.5 Interpretation

Subbody G1 is probably a channel backfill deposit. It forms a lenticular shape with a width to depth ratio of about 15:1. Southeast oriented paleocurrents suggest a fluvially dominated channel with no observed tidal indicators. Most of the subbody, 96%, consists of planar tabular cross-stratified sandstone or convolute sandstone suggesting a consistent high energy environment and an overprint of soft-sediment deformation. The

upper mudstone unit suggests a significant drop in current energy and channel abandonment at the end of the deposition of this subbody.

Subbody G2 is a large, constructional fluvial barform. Currents are consistently southeast and subparallel to the accretion direction. The mounded shape, which is thickest on the northwest end and tapers down to the southeast, is consistent with a southeasterly oriented current direction. The thickness of the subbody suggests an aggradational stacking pattern. The facies present indicate high energy deposition and the mud-clast conglomerate base indicates extremely high energy dominated the early stage of deposition. The G2a unit may represent a mass transport event, such as a debris flow.

Subbody G3 is also a large, constructional fluvial barform. Like Subbody G2, it has a mounded shape which tapers down to the southeast and southeast oriented paleocurrents nearly parallel to the primary accretion direction. Also like Subbody G2, the facies present indicate this subbody was dominated by high to very high depositional energy, but the presence of the current-rippled sandstone facies indicates parts of the subbody, especially the southeast end, were deposited under lower energy conditions. The smaller size of this subbody and the presence of low energy facies may be caused by the sheltering effect of the larger Subbody G2 upstream.

Subbody G4 is a smaller constructional fluvial barform. The mounded geometry is similar to Subbodies G2 and G3. Like Subbodies G2 and G3, it is dominated by high energy facies, but it is differentiated by not having a base of mud-clast conglomerate.

Sandbody G is a series of aggradational fluvial units. All four subbodies are dominated by high energy or soft-sediment deformed facies. Paleocurrents are oriented to the southeast and very consistent between Subbodies G1, G2, and G3. Subbody G1

represents the deepest part of a large fluvial channel. At the end of Subbody G1 deposition, there was a brief hiatus followed by a very high energy reactivation and the deposition of three constructional barforms, Subbodies G2, G3, and G4. These three subbodies are very similar and closely depositionally linked. The beginning of deposition of each of these subbodies represents a minor migration of the local depocenter, shifting southeast for Subbody G3 and back to the northwest for Subbody G4.

3.6 Sandbody B/C

Sandbody B/C is located within S2 and is slightly older than Sandbody G (Figure 1.5). It crops out across 120 m in the northwest-southeast direction and 60 m in the northeast-southwest direction. The overall thickness ranges from 0 to 5.5 m with an average thickness of about 5 m. This sandbody forms a triangular shape which widens to the northeast from about 30 to 120 m.

Sandbody B/C consists of two genetically related subbodies: B and C (Figure 3.16). Subbody B forms a triangular shape which widens and thins to the northeast. Subbody C is elongate in the northwest-southeast direction. Paleocurrents are consistently to the northeast. The overall facies distribution is 56% current-rippled sandstone, 16% trough cross-stratified sandstone, 11% structureless sandstone, 9% undifferentiated mudstone, 5% convolute sandstone, and 5% planar tabular cross-stratified sandstone (Figure 3.17).

3.6.1 Subbody B

Subbody B is the older of the two subbodies. It is observed on two outcrops separated by modern erosion and forms a triangular in shape increasing from about 30 m to 110 m wide in the southwest-northeast direction (Figure 3.16). It also thins to the

northeast from about 4 m to 2 m. This subbody pinches out laterally to the northwest and southeast and less than 2 m of scour was observed at its base. The orientation of accretion sets is between 31° and 53° with dips between 6° and 12° (Figure 3.18). Paleocurrents are from 28° to 79°, averaging 53°. With an average accretion orientation of 44°, there is a 9° difference between the dominant accretion and paleocurrent directions indicating downstream accretion.

The facies of Subbody B exhibit a general upward waning-flow pattern. The basal 1.5 m consists mostly of trough cross-stratified, planar-tabular cross-stratified, and structureless sandstone with minor components of convolute and current-rippled sandstone. The structureless sandstone facies grades laterally into the trough cross-stratified and planar-tabular cross-stratified sandstone facies and the trough cross-stratified sandstone facies also grades into the planar-tabular cross-stratified sandstone facies. The upper half of the subbody changes laterally from west to east from trough cross-stratified to current-rippled to structureless and convolute sandstone. The vertically decreasing energy pattern continues into a capping mudstone unit of 0 to 1 m thick and a clear upward-fining grain-size trend was observed in measured sections D and NN. Trough cross-stratification is more abundant to the western end of the subbody with planar-tabular cross-stratification more common to the east and the lower unit of the current-rippled sandstone facies is located on the eastern margin. This may indicate a slight decrease in energy to the eastern side of the subbody.

3.6.2 Subbody C

Subbody C has an elongate outcrop shape about 120 m long in the northwest-southeast direction with pinch-outs in both directions (Figure 3.18). The base of this

subbody is scoured into the upper mudstone unit of Subbody B. The top of the subbody around measured section EE is scoured with a V-shaped depression with a maximum depth of 0.5 m and a mudstone fill. The orientation of accretion is from 2° to 32° with dips of 6° to 30°. The average accretion orientation is 17°. Paleocurrents of 68° and 75° with a mean of 72° were measured. The primary accretion direction is about 55° from the dominant paleocurrent direction suggesting a lateral accretion.

The facies distribution of Subbody C indicates an early high energy phase of deposition followed by a lengthy low energy depositional phase. Subbody C is dominated by the current-rippled sandstone facies. This facies accounts for almost 80% of the subbody. About 10% of the subbody consists of trough cross-stratified sandstone which is present at the base of the subbody. The remainder of Subbody C consists of structureless sandstone which is observed grading into both of the previously mentioned facies.

3.6.3 Interpretation

Subbody B is interpreted as a downstream accreting fluvial barform. The orientation of accretion is roughly equal with the dominant paleocurrent direction suggesting that the subbody built out primarily in the downstream direction. The widening and thinning of the subbody to the northeast suggests a widening of the channel in that direction. The facies distribution and grain size trend implies a decrease in the paleocurrent energy over time. The facies distribution also indicates a slight decrease in energy to the east across the subbody, which is further supported by the average paleocurrent direction which is slightly more easterly than the average accretion direction as current velocities likely slowed down flowing over the subbody.

Subbody C is interpreted as an obliquely to laterally accreting fluvial barform. The averaged accretion orientation diverges about 55° from the average paleocurrent direction indicating a curve in the channel thalweg. This subbody may represent a point bar which did not fully develop or an alternate bar of a low sinuosity system. The abundance of the current-rippled sandstone facies indicates low current energies were common at the time of deposition with the presence of the trough cross-stratified sandstone facies at the base of the subbody indicating an early high energy phase. The primary accretion direction is into to plane of the outcrop, so the facies observed may represent the low energy flank of a higher energy sandbody. The V-shaped depression (Top of measured section EE, Figure 3.16) at the top of the subbody may be a remnant chute channel.

3.7 Sandbody F

Sandbody F is located in S3 and was deposited concurrently with the oldest beds of Sandbody D/E (Figure 1.5). It crops out about 240 m in the north-south direction. Sandbody F, including two floodplain-mudstone dominated intervals, has a maximum thickness of about 11 m and an average thickness of about 9 m. The maximum sandstone thickness is 9 m.

The three subbodies, F1, F2, and F3, on a northwest-southeast trending cross-section, are separated by mudstone layers (Figure 3.19). However, the lowest subbody, F1, and the highest subbody, F3, amalgamate in the third dimension to the northeast while the middle subbody, F2, pinches out. Sandbody F also amalgamates with Sandbody D/E in the third dimension. The outcrop of Subbody F1 forms a dumbbell shape, while Subbodies F2 and F3 have lenticular geometries. Paleocurrents are consistently to the

southeast. The overall facies distribution is 29% planar tabular cross-stratified sandstone, 21% structureless sandstone, 20% trough cross-stratified sandstone, 18% convolute sandstone, 10% current-rippled sandstone, 1% undifferentiated mudstone, and less than 1% of the mud-clast conglomerate (Figure 3.20).

3.7.1 Subbody F1

Subbody F1 crops out for about 200 m in the north-south direction. In 2-D cross-section, it has a dumbbell shape with the thickest portions on the ends and a thinner central portion. In 3-D, the base of the channel at measured section DD probably correlates to the base at measured section S (Figure 3.19). It is 4.5 m thick near the southeast end, 3 m thick near the northwest end and less than 2 m thick in the middle (Figure 3.19). The base of the body is incised into the underlying mudstones. Three stories were observed on this subbody. Paleocurrents are from 121° to 154° with an average of 141°.

The facies distribution of Subbody F1 suggests relatively constant high energy flow throughout the history of this subbody. More than 99% of the subbody consists of the planar-tabular cross-stratified, structureless, and trough cross-stratified sandstone facies. The trough cross-stratified sandstone facies is present in the upper units of the subbody which may indicate a slight increase in current energy over time. The structureless sandstone facies is concentrated in the thickest portions of the subbody and is observed grading laterally into the planar-tabular and trough cross-stratified sandstone facies. Two thin units of undifferentiated mudstone are observed in the northern part of the subbody indicating brief hiatuses in this part of the subbody.

3.7.2 Subbody F2

The outcrop of Subbody F2 is much smaller than that of the other two subbodies (Figure 3.19). It has a V-shaped geometry with a basal unit of containing a heterolithic mixture of mudstone and sandstone (Figure 3.21). This unit accounts for 13% of the subbody. The remaining 87% of the subbody consists of a single, lenticular bed of convolute sandstone about 1.5 m thick and 50 m long in the northwest-southeast direction. This subbody is located 1.25 m above the top of Subbody F1 with abundantly rooted sandstones and siltstones between the subbodies. No accretion sets or paleocurrents were observed.

3.7.3 Subbody F3

Subbody F3 is the youngest of the three subbodies. It crops out for about 240 m in the north-south direction (Figure 3.19). It has a thickness of 3 m near its southern end and thins consistently towards a pinch-out on the northern end. The subbody is thickest northeast of the cross-section line and it incises down to the top of Subbody F1. This subbody amalgamates with overlying Sandbody D/E in the third dimension to the northeast. It is located 1.25 m above Subbody F2. Between the two subbodies are mudstones with abundant root traces and carbonized wood fragments. Paleocurrents are from 106° to 116°, averaging 112°. No accretion sets were observed.

The facies distribution of Subbody F3 indicates decreasing current energy over time. The lower portion of this subbody consists mostly of the convolute, trough cross-stratified, planar-tabular cross-stratified sandstone facies, with the upper quarter consisting mostly of the current-rippled sandstone facies. The convolute sandstone unit, which is concentrated at the thickest portion of the subbody, is observed grading into the

trough cross-stratified sandstone facies, indicating they are likely depositionally equivalent. A thin unit of mud-clast conglomerate is present near the base of the subbody, suggesting a temporary increase in depositional energy, and a thin unit of undifferentiated mudstone near the top of the subbody likely indicates a brief hiatus.

3.7.4 Interpretation

Sandbody F is interpreted as a series of channel backfill deposits. Subbodies F2 and F3 both have lenticular shapes. The dumbbell shape of Subbody F1 is an outcrop effect and also represents a lenticular shape. The southeast oriented paleocurrents are consistent with the regional transport direction and indicate fluvially dominated seaward flow. The facies distribution in Subbody F1 indicates a slight increase in current energy over time, while Subbody F3 indicates decreasing current energies. The geometry and facies distribution of Subbody F2 suggests a high energy cutting phase when the heterolithic mixture of mud and sand was deposited followed by a lower energy phase when only sand was deposited. The presence of the undifferentiated mudstone facies in Subbodies F1 and F3 indicates brief hiatuses in deposition and the mud-clast conglomerate facies in Subbody F3 may indicate a reactivation of the channel. The distribution of convolute and structureless sandstone in all three subbodies indicates greater fluidization along the channel axes. The presence of the floodplain facies association, with intense plant activity, between the subbodies indicates significant time passed between deposition of the subbodies. The significantly smaller scale of these channels, compared to Sandbodies I, A, G, and D/E, and their close association with floodplain facies indicates that these channels were not within a major channelbelt.

3.8 Sandbody D/E

Sandbody D/E is located within the S3 interval and is the youngest sand body studied (Figure 1.5). It is the largest body observed in the field area and extends out of the primary field area to the southeast and also appears to crop out northwest of the primary field area. The sinuous outcrop in the field area is 1.18 km in the northwest-southeast direction. The thickness ranges from 0 m to 22 m, with an average thickness of 8 m.

Sandbody D/E consists of Subbodies D/E1 and D/E2 (Figure 3.22). The outcrop of Subbody D/E1 is an asymmetric V-shape scoured into the underlying mudstones. The outcrop of Subbody D/E2 is relatively sheet-like with a pinchout on the northwest end. Paleocurrents, observed on planar-tabular cross-sets, are bi-directional. The overall facies distribution is 44% planar tabular cross-stratified sandstone, 36% structureless sandstone, 13% convolute sandstone, 4% current-rippled sandstone, 1% trough and mud-draped planar tabular cross-stratified sandstone, and less than 1% mud-clast conglomerate and undifferentiated mudstone (Figure 3.23).

3.8.1 Subbody D/E1

Subbody D/E1 is the older of the two subbodies and is roughly coeval with Sandbody F (previous section). Subbody D/E1 has sharp lateral contacts with the surrounding mudstone and extends about 150 m in the north-south direction, which is perpendicular to the dominant paleocurrent directions (Figure 3.22). It reaches a maximum thickness of about 10 m near its northwest end and thins to a pinchout to the southeast, giving it a width to depth ratio around 15:1. Subbody D/E1 has an average thickness of about 5 m. It is incised through a thin sandstone unit, the Z marker bed

(Figures 1.5 and 3.24), 4 m above the base of this subbody at measured section F the maximum depth of incision is 10 m. Paleocurrents have a bi-directional orientation. Eight of twenty-one measurements were made recording an orientation ranging from 56° to 160°, averaging 88° and thirteen of twenty-one measurements were made recording orientations ranging from 244° to 284°, averaging 262°. The overall average paleocurrent orientation was 196°. No accretion surfaces were observed in this subbody.

The facies distribution of Subbody D/E1 indicates consistent, high energy flow for the majority of deposition followed by a late-stage, low-energy phase of fill less than 1 m thick and covered by a mudstone unit (Figure 3.22). Subbody D/E1 is comprised mostly of the structureless, planar-tabular cross-stratified, and convolute sandstone facies. Together these facies, which grade into one another and were likely depositionally equivalent, account for the lower 98% of subbody. The remaining 2% of the subbody is composed of current-rippled sandstone which is present at or near the top of the southeast end of the subbody. This unit represents a waning flow phase and abandonment at the end of deposition. The southeast end of the subbody is capped by a mudstone layer indicating a further decrease in depositional energy.

3.8.2 Subbody D/E2

Subbody D/E2 extends across and out of the primary field area. It consists of at least four stories. From oldest to youngest, the first story is up to 3 m thick, the second story is 2 to 6 m thick, the third story is up to 2 m thick, and the fourth story is up to 5 m thick (Figure 3.22). The base of this subbody amalgamates with Subbody D/E1 in the vicinity of measured section F and Sandbody F to the northeast of measured section S. A mudstone layer between the two subbodies increases in thickness to the southeast with a

maximum thickness of 2.75 m. A preserved tree trunk in life position at the base of Subbody D/E2 indicates a hiatus between the subbodies possibly for several hundred years (Figure 3.24). The axis thickness of this subbody reconstructed in Figure 3.26 is relatively constant between 7 m and 10 m. It thins to a pinchout on the northeast end. It also thins slightly in the vicinity of measured section S and thickens to 12 m in the vicinity of measured section F.

Paleocurrents are clearly bi-directional. Thirty-nine paleocurrent measurements record orientations ranging from 32° to 173° with a mean of 105°. Thirty-one paleocurrent measurements record orientations from 182° to 358° and an average of 270°. Easterly paleocurrents are more common in the lower half of the subbody, while westerly paleocurrents are more common in the upper half.

Although the overall geometry is sheet-like, the stories contain numerous small, constructional barforms (Figure 3.25A). Most of these barforms have been obscured or destroyed by subsequent soft-sediment deformation; however, some of them have been preserved (Figures 3.22 and 3.25). Beds overlapping a few of the constructional features exhibit an onlapping geometry (Figure 3.25B). The orientation of barform accretion surfaces were largely unidirectional ranging from 122° to 147° with dips between 5° and 11°. The accretion surfaces are contained within individual barforms. Preserved barforms consist primarily of planar-tabular cross-stratified sandstone and some are capped by a thin layer of current-rippled sandstone. However, two preserved barforms consist of trough cross-stratified sandstone and one consists of current-rippled sandstone. Mud-clast conglomerate layers are present at the base of several barforms. Other types of

architecture in this subbody include several small channel forms, such as those near measured sections II and RR (Figure 3.22).

The facies not in barforms consist mostly of planar-tabular cross-stratified, structureless, and convolute sandstone. These three facies commonly grade laterally into one another with the structureless and convolute sandstone facies most abundant in the thickest portions of the subbody. The planar-tabular cross-stratified sandstone facies is observed grading into the current-rippled sandstone facies in the first story as it thins to the southeast. The mud-draped planar-tabular cross-stratified sandstone facies rarely replaces the planar-tabular cross-stratified sandstone facies. The mud-draped planar-tabular cross-stratified sandstone facies is most common in the third story, including small pockets which exhibit tidal bundling (Figure 2.7A) and herring-bone cross-stratification (Figure 2.7B). The third story has a basal unit of mud-clast conglomerate near measured section SS and a thin mudstone unit is present at the top of the story near measured section RR. The current-rippled sandstone facies is most common at or near the top of the fourth story.

3.8.3 Interpretation

Subbody D/E1 is interpreted as a tidally influenced channel fill. The deeply incised V-shaped geometry with sharp lateral contacts and approximate 15:1 width to depth ratio implies that it is a channel. Tidal influence is suggested by the presence of two opposing paleocurrent directions. As the structureless and convolute sandstone facies were most likely deposited as planar tabular cross-stratified sandstone, it is interpreted that most of this subbody was deposited under high energy conditions with a thin low energy cap represented by the current-rippled sandstone facies.

Subbody D/E2 is interpreted as tidally influenced, multi-story braided river system. The wide, sheet-like geometry comprised of small, constructional barforms is suggestive of a braided channel. Accretion is oriented downstream and contained within individual barforms. The lack of large scale, lateral accretion surfaces and small preserved channel forms indicates flow was not organized into a single channel, as in a meandering channel. Multiple stories of channel fill suggest an aggradational stacking pattern. Thinning to the northwest and southeast likely indicates the edges of the channelbelt (Figure 3.26). The north-south distance from the pinchout on the northeast end to the thickest part of the subbody, at measured section F, is about 450 m. Assuming that this thick represents the center of the channelbelt, gives an estimated channelbelt width of approximately 900 m, similar to the width estimated in Figure 3.26. Assuming this width represents the bank-full stage, this formula:

$$\text{Bank-full channel width (in feet)} = 13.5 (\text{Drainage area (in sq. miles)})^{0.449}$$

(Westergard et al., 2005) gives a drainage area of about 420,500 sq. km, similar in scale to the Arkansas River (Kammerer, 1990). A minimum width of 450 m gives a drainage area of 89,800 sq. km, similar in scale to the Tennessee River (Kammerer, 1990). Tidal influence is indicated by bi-directional paleocurrents throughout the subbody. Tidal influence is further suggested by the presence of the mud-draped planar tabular cross-stratified facies, which includes rare herring-bone cross-stratification. Westerly paleocurrents are more abundant higher up on the subbody suggesting increasing flood tidal dominance over time. At least two ammonites were observed in the structureless sandstone facies near the top of the second story in the vicinity of measured section F (Figure 2.5A). The presence of ammonites may indicate salinities high enough to support

marine life, but these fossils may have been transported post-mortem. The correlation between the thickness of the subbody and the presence of the structureless and convolute sandstone facies suggests a higher degree of fluidization along the channel axis. High energy and soft-sediment deformed facies comprise more than 95% of the subbody with low energy facies more abundant in the upper portion of the subbody indicating the dominance of strong currents with a decrease in current energy near the end of deposition.

Both subbodies have similar ratios of high energy and soft-sediment deformed to low energy facies. Tidal and fluvial influence is also sub-equal in both subbodies. Despite these similarities, the contact between Subbodies D/E1 and D/E2 represents a significant increase in scale between the two subbodies. This may indicate the capture of a tributary, the migration of a larger river into the area, or an increase in carrying capacity due to climatic or structural causes. The change to a braided river system indicates that sediment supply exceeded discharge during the deposition of Subbody D/E2.

3.9 Sandbodies in Secondary Field Area

Sandbody Z is a thin, sheet-like sandbody observed in the secondary field area (Figures 1.5, 3.27, and 3.28). It is between 1 and 3 m thick with a lateral extent of more than 500 m. Facies consist mostly of wave-rippled sandstone, with a lesser amount of bioturbated sandstone. Sandbody Z is typically underlain by the coal facies and is observed loading (Figure 2.17B) and mixed by biological action into the underlying coal unit. It is interpreted as a floodplain lake based on the broad sheet-like geometry, abundance of symmetrical ripples, strong evidence of biological activity, and the close association with the coal facies.

Sandbody Y is a thick lenticular unit observed in the secondary field area (Figure 1.5). It crops out for about 400 m in the northwest-southeast direction with a maximum thickness of 15 m. It is slightly younger and incises through Sandbody Z (Figure 3.29). Observed facies include planar-tabular cross-stratified, trough cross-stratified, convolute, structureless, and current-rippled sandstone. Sandbody Y is most likely a channel fill unit based on the lenticular geometry, deep incision, and abundance of high energy and soft-sediment deformed facies.

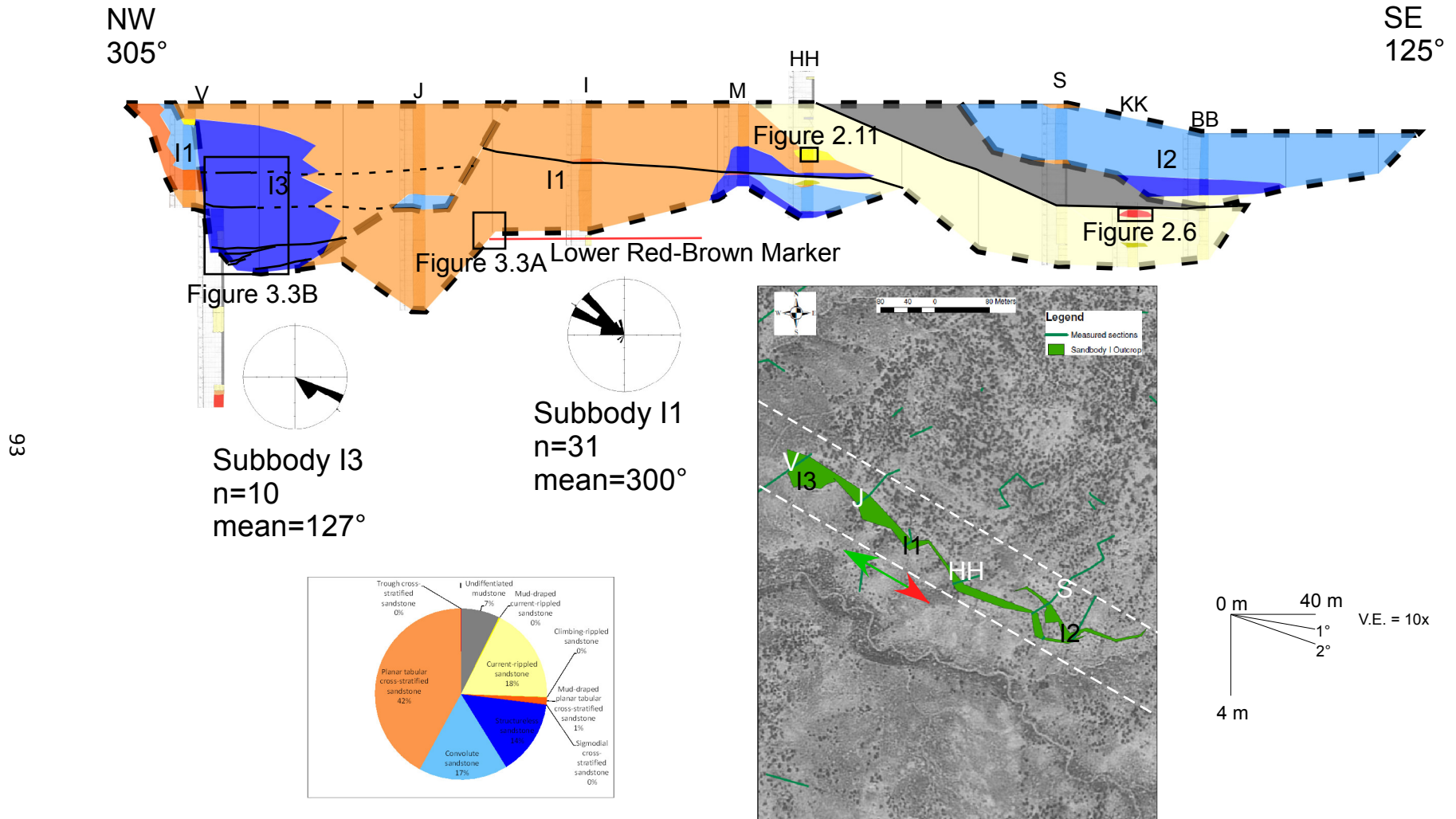


Figure 3.1 Cross-section of Sandbody I facies distribution. Inset map showing outcrop area of subbodies and measured sections. Air photo shown in background. White dashed lines indicates estimated channel margins for Subbody I1. Green arrow indicates dominant tidal paleocurrent direction. Red arrow indicates dominant fluvial paleocurrent direction.

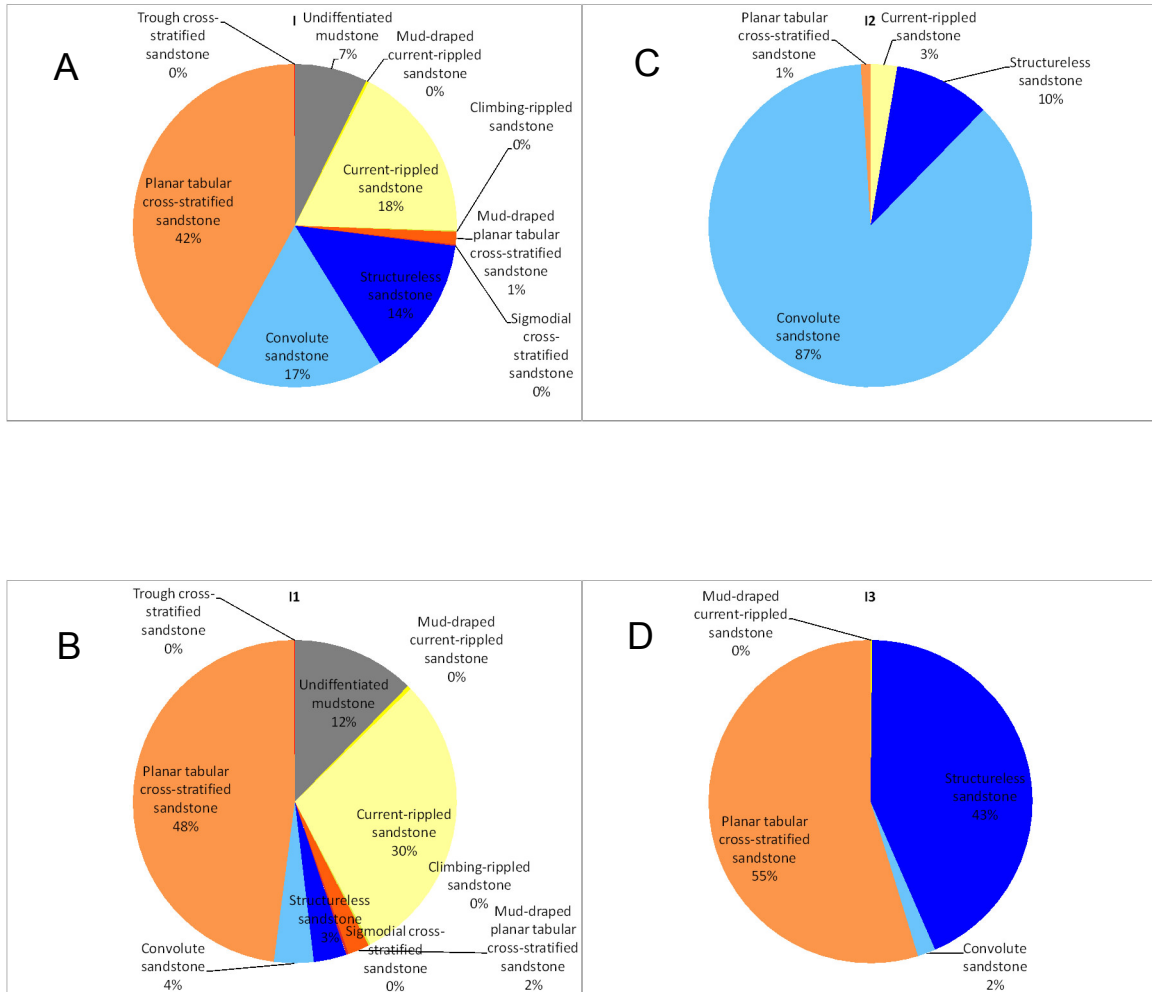


Figure 3.2 Relative abundance of facies in Sandbody I for A) overall sandbody B) Subbody I1 C) Subbody I2 D) Subbody I3.

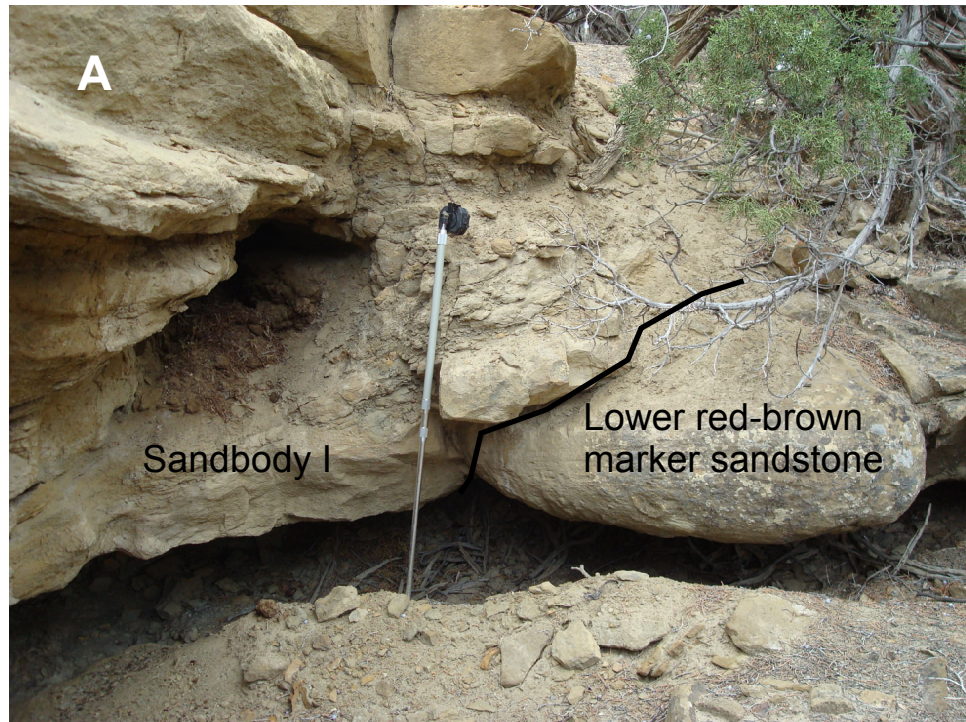


Figure 3.3 A) The base of Subbody I1 incising through the lower red-brown marker sandstone. Jacob staff is 1 m. B) Internal scour surfaces in Subbody I3. Facies consist of structureless sandstone.

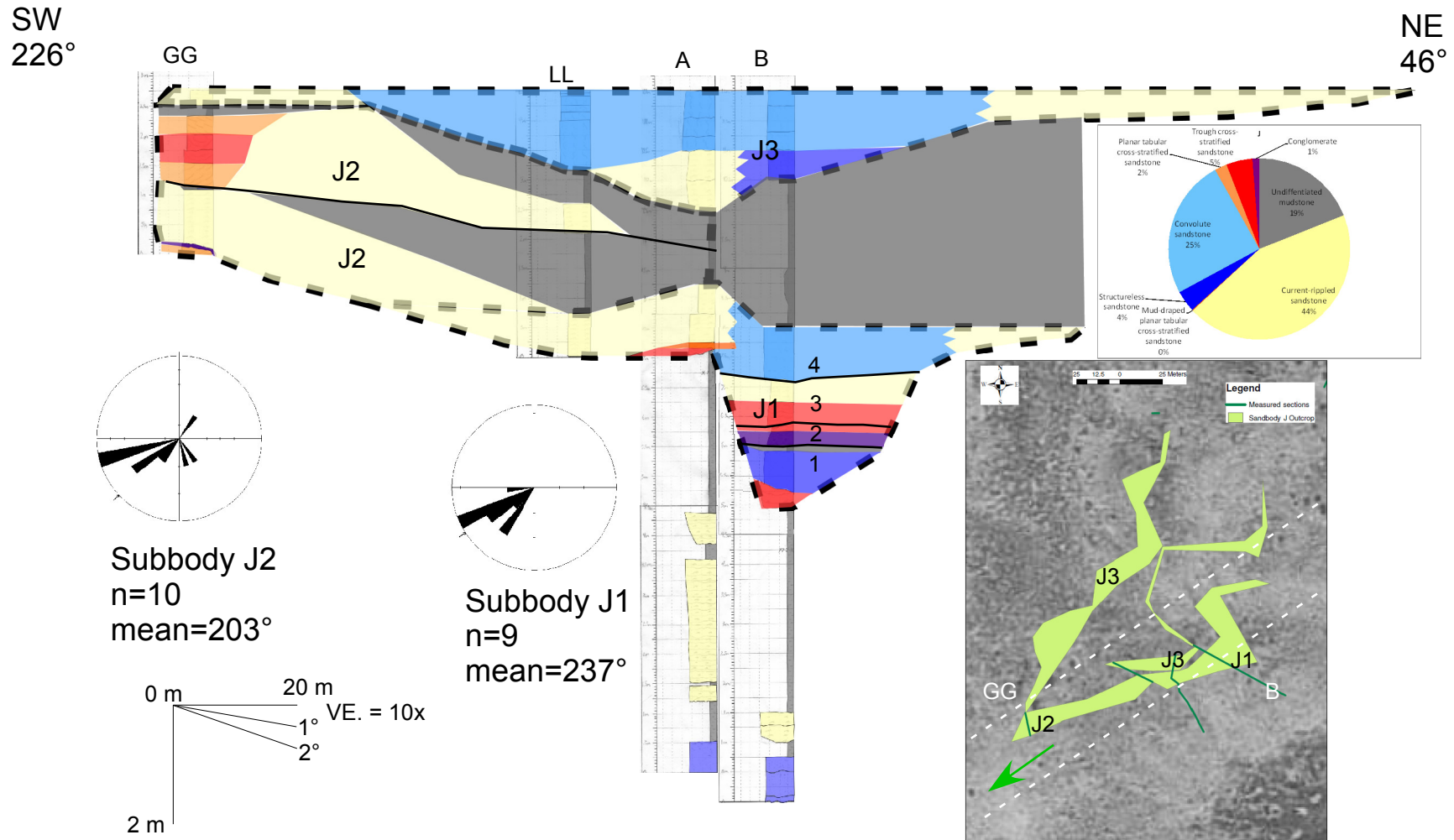


Figure 3.4 Cross-section showing facies distribution for Sandbody J. Projected on 226°-46° section line. Inset map showing outcrop area of subbodies and measured sections. Air photo shown in background. White dashed lines indicates estimated channel margins for Subbody J2. Green arrow indicates dominant tidal paleocurrent direction.

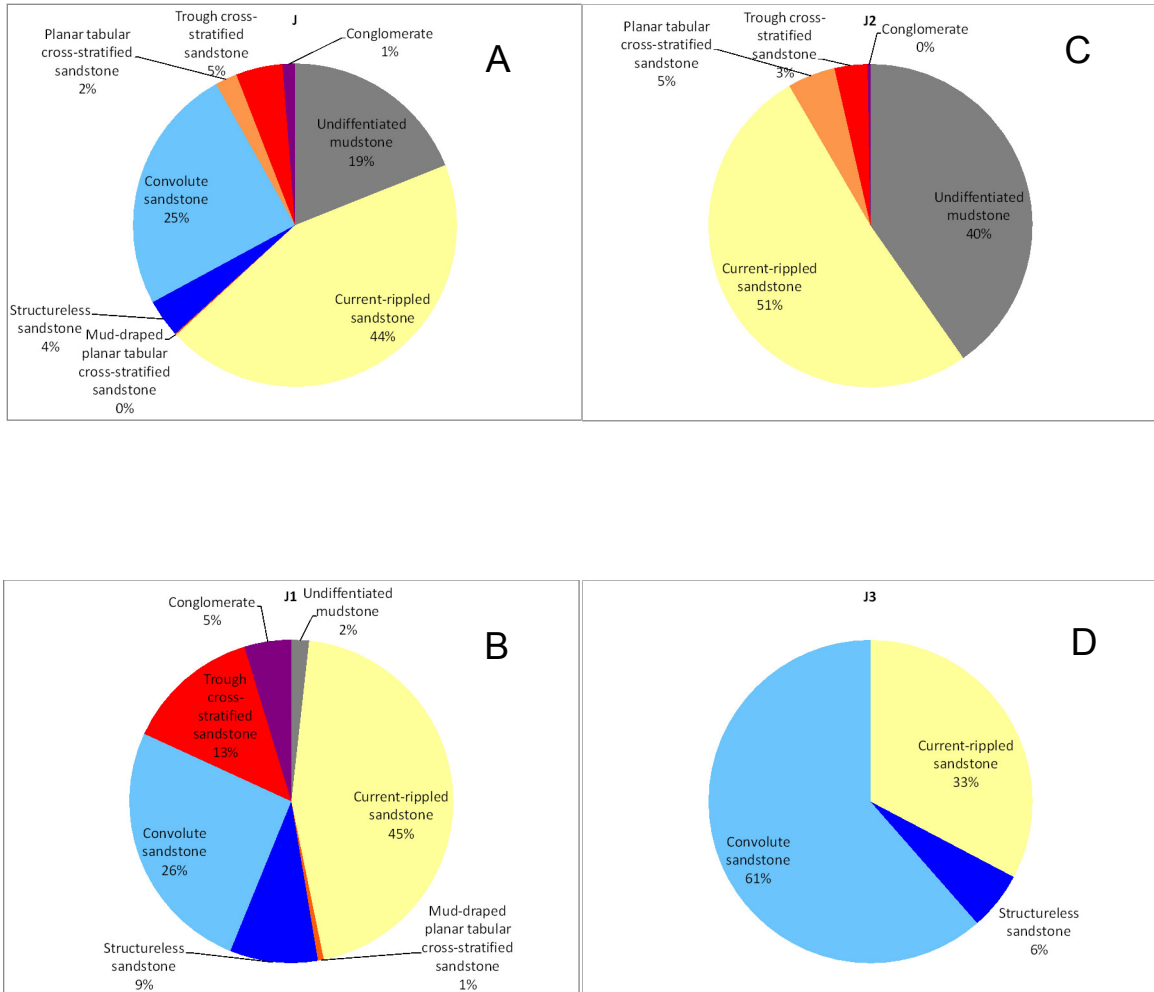


Figure 3.5 Relative abundance of facies in Sandbody J for A) overall sandbody B) Subbody J1
C) Subbody J2 D) Subbody J3.

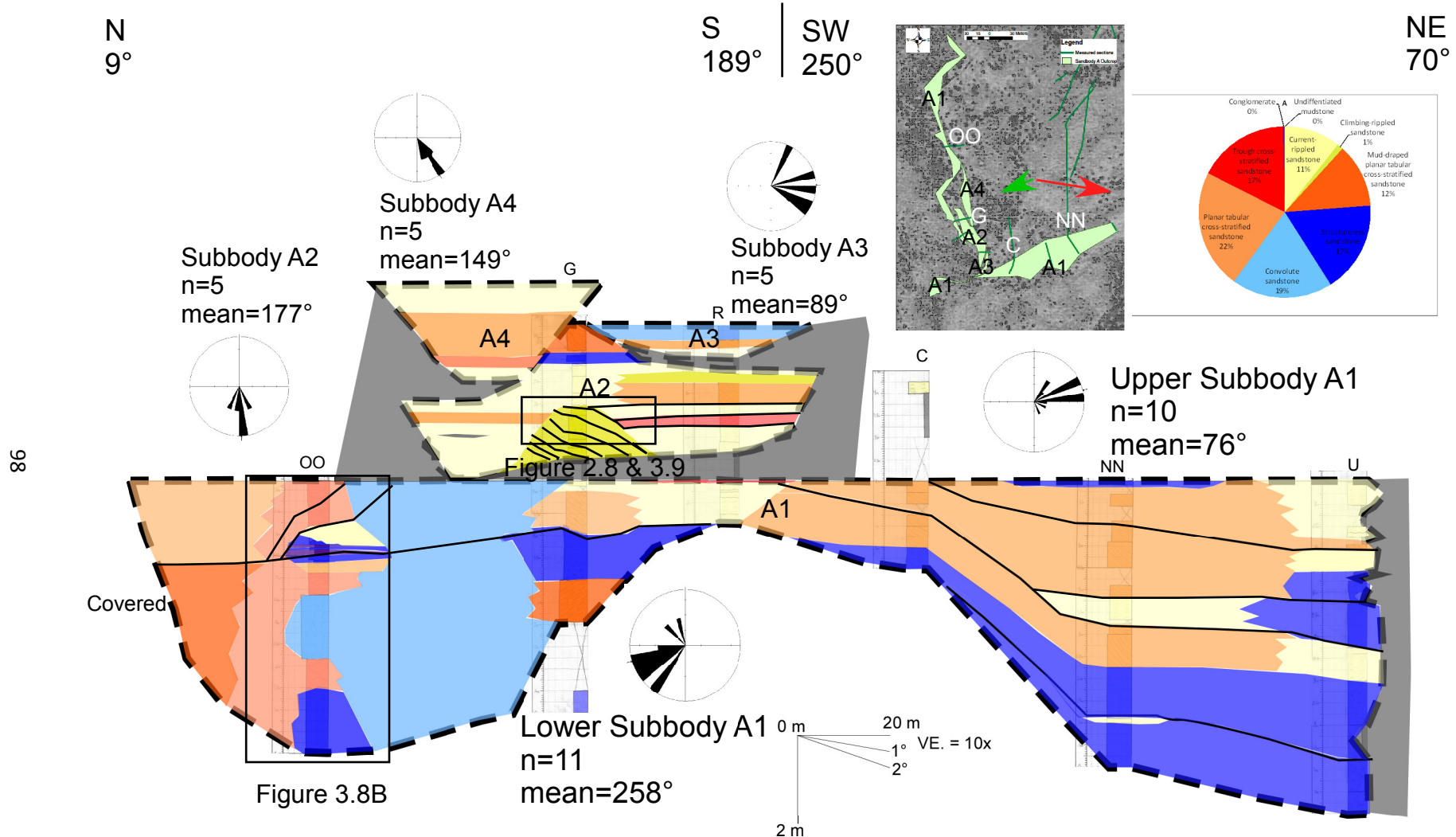


Figure 3.6A Cross-section of facies distribution of Sandbody A. Projected on 305°-125° section line. Inset map showing outcrop area of subbodies and measured sections. Air photo shown in background. Green arrow indicates dominant tidal paleocurrent direction. Red arrow indicates dominant fluvial paleocurrent direction.

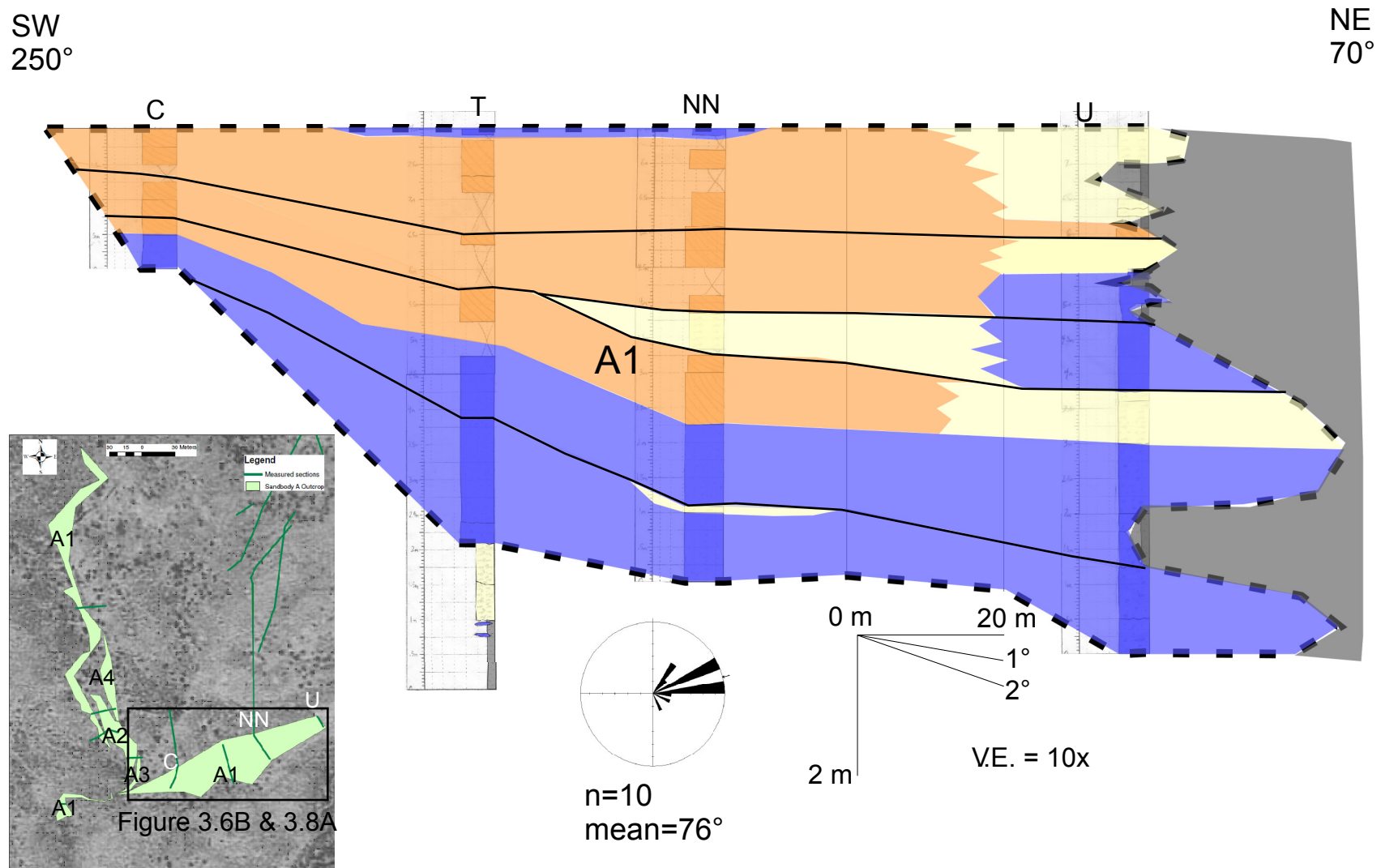


Figure 3.6B Cross-section of facies distribution of the eastern side of Subbody A1. Inset map showing outcrop area of subbodies and measured sections. Air photo shown in background.

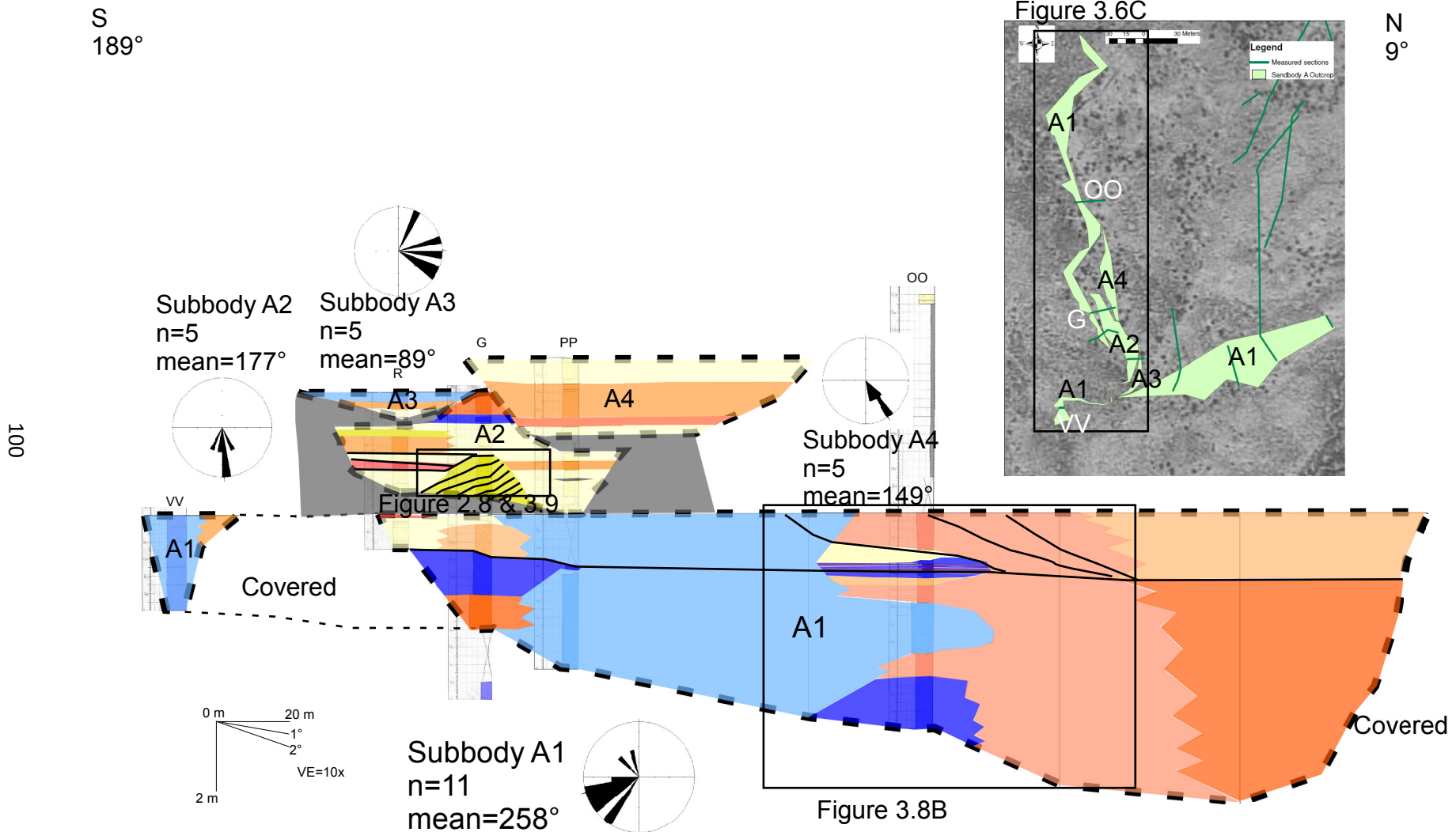


Figure 3.6C Cross-section of facies distribution of the western side of Sandbody A. Inset map showing outcrop area of subbodies and measured sections. Air photo shown in background.

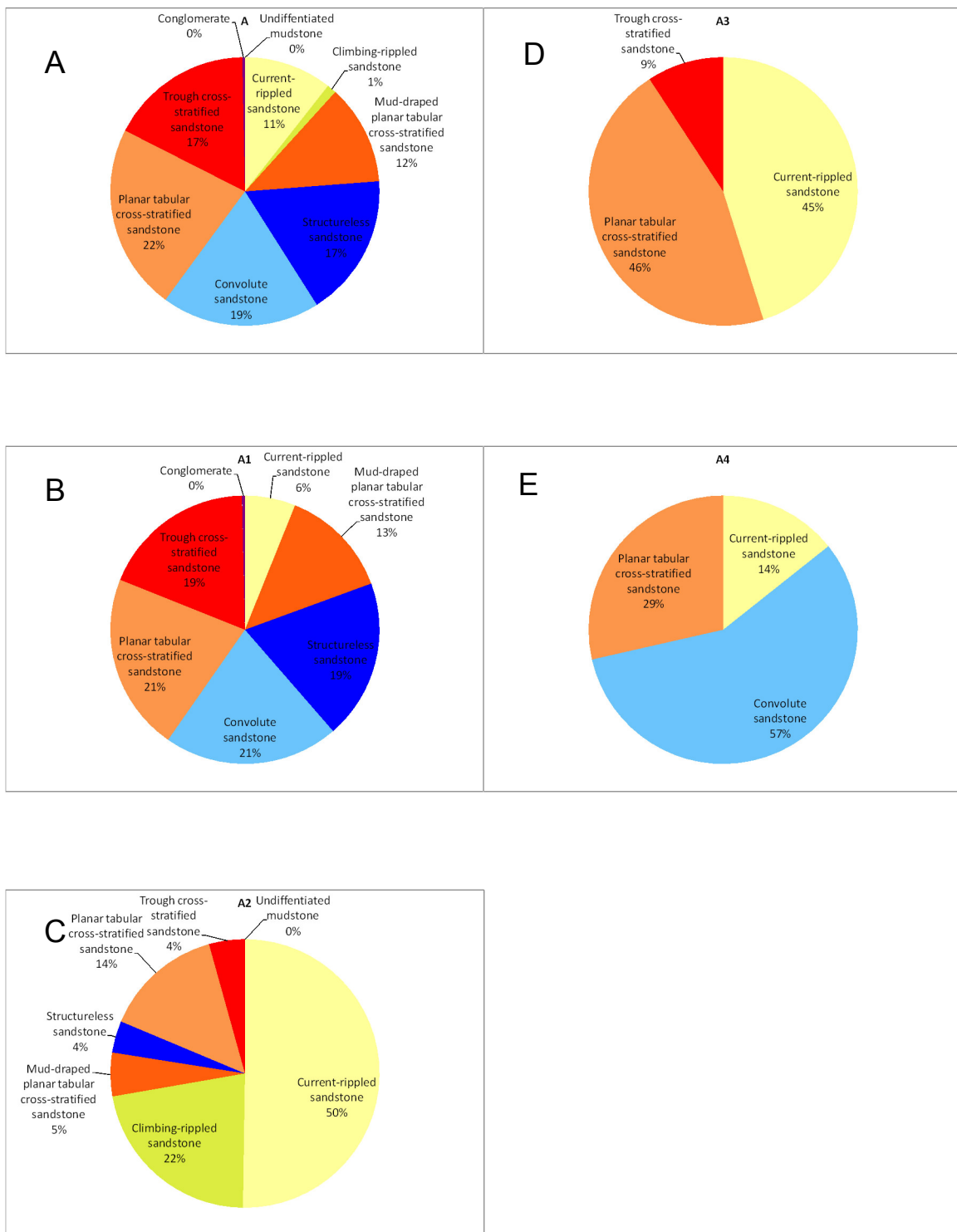


Figure 3.7 Relative abundance of facies in Sandbody A for A) overall sandbody B) Subbody A1 C) Subbody A2 D) Subbody A3 E) Subbody A4.

SW

NE

A



102

N

S

B

OO



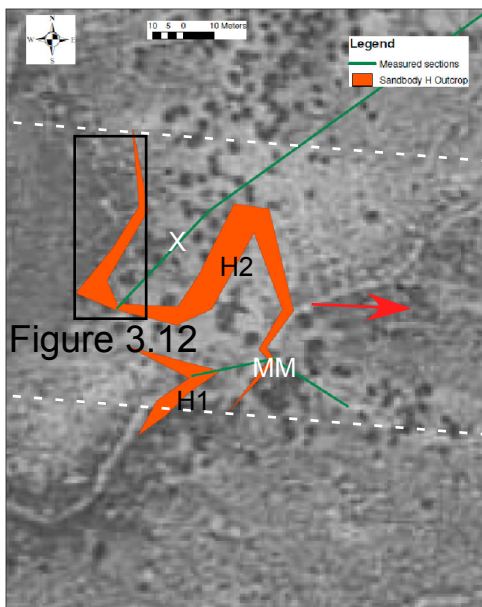
Figure 3.8 A) Accretion surfaces on the eastern side of Subbody A1 dipping to northeast. B) Accretion surfaces on the western side of Subbody A1 dipping to north. Approximate measured section locations labeled in white.

103



Figure 3.9 Accretion surfaces on Subbody A2. Lower accretion surfaces dip to south. Upper accretion surface dips to north.

104

NE
35°

0 m 20 m

1°
2°

V.E. = 10x

SW
215° | NW
291° | SE
111° | W
261° | E
81° | NE
27°SW
207°

Figure 3.12

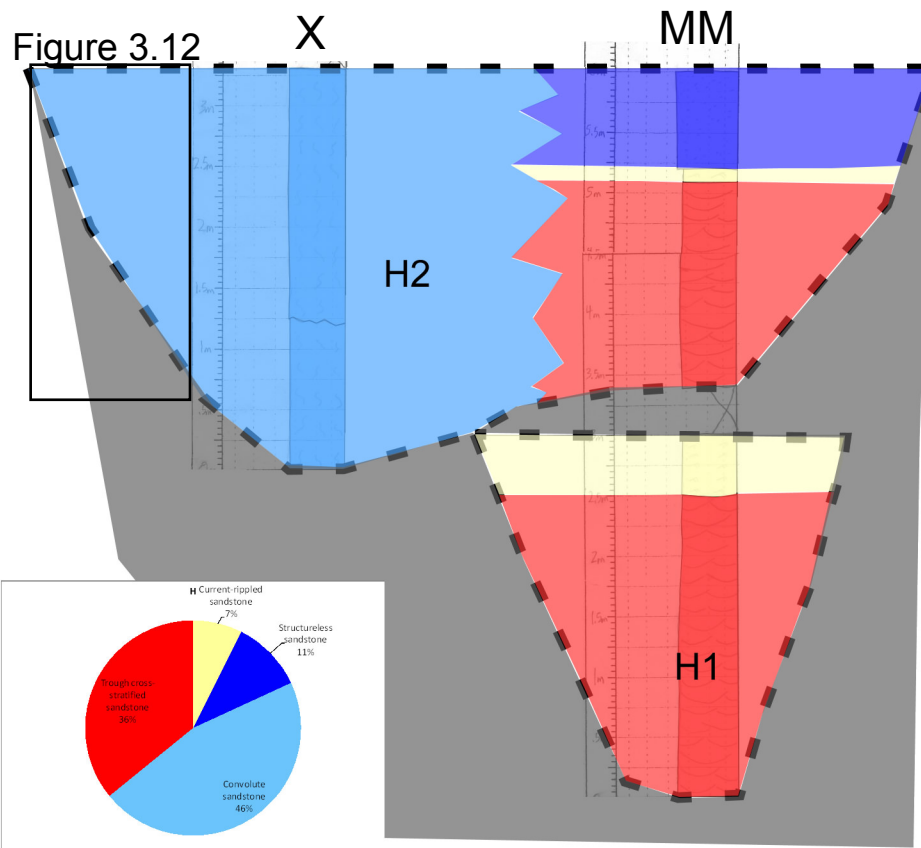


Figure 3.10 Cross-section of facies distribution for Sandbody H. Projected on a 305°-125° section line. Inset map showing outcrop area of subbodies and measured sections. Air photo shown in background. White dashed lines indicate estimated channel margins for Subbody H2. Red arrow indicates dominant fluvial paleocurrent direction.

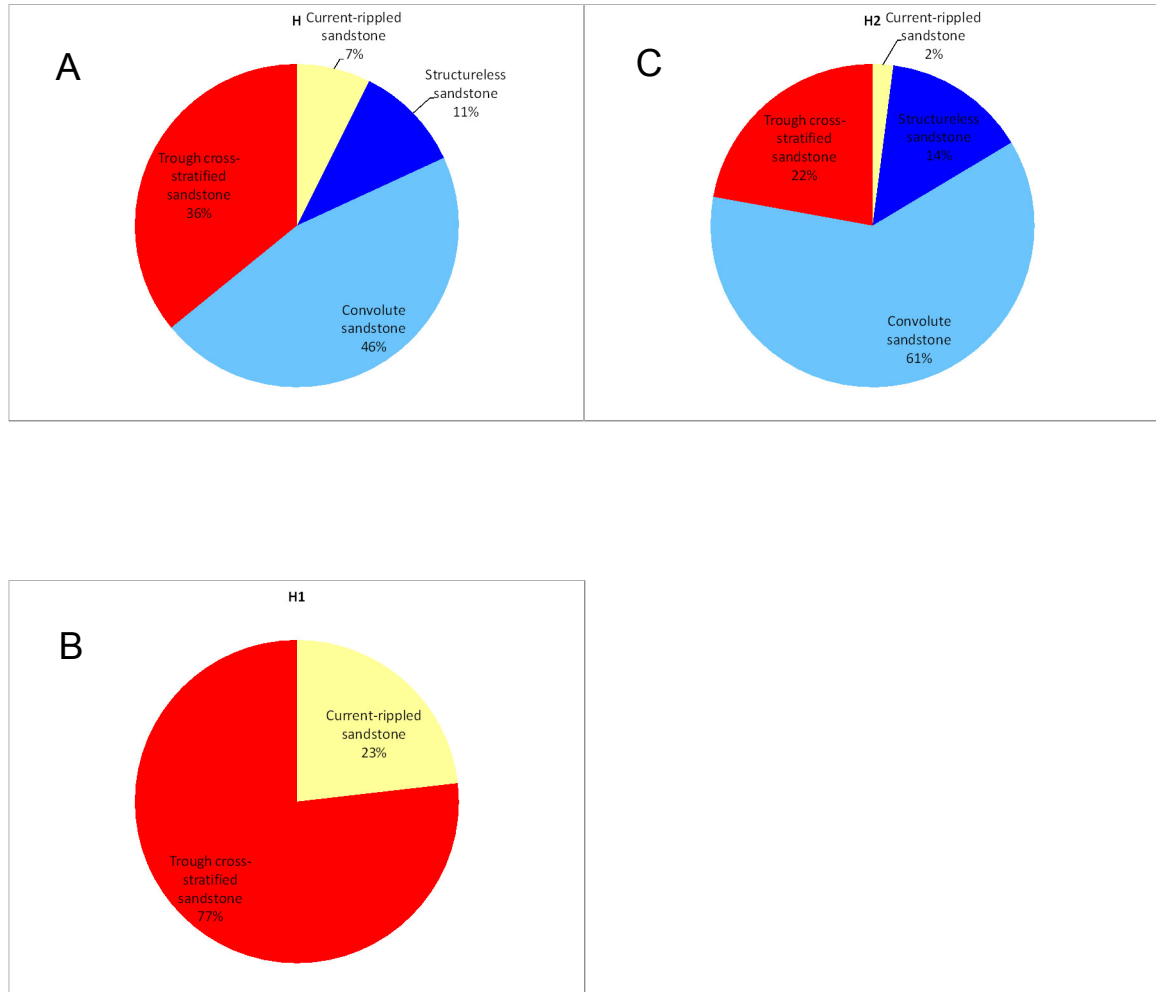


Figure 3.11 Relative abundance of facies in Sandbody H for A) overall sandbody B) Subbody H1 C) Subbody H2.



Figure 3.12 U-shaped accretion surfaces dipping into the page on the western side of Subbody H2.

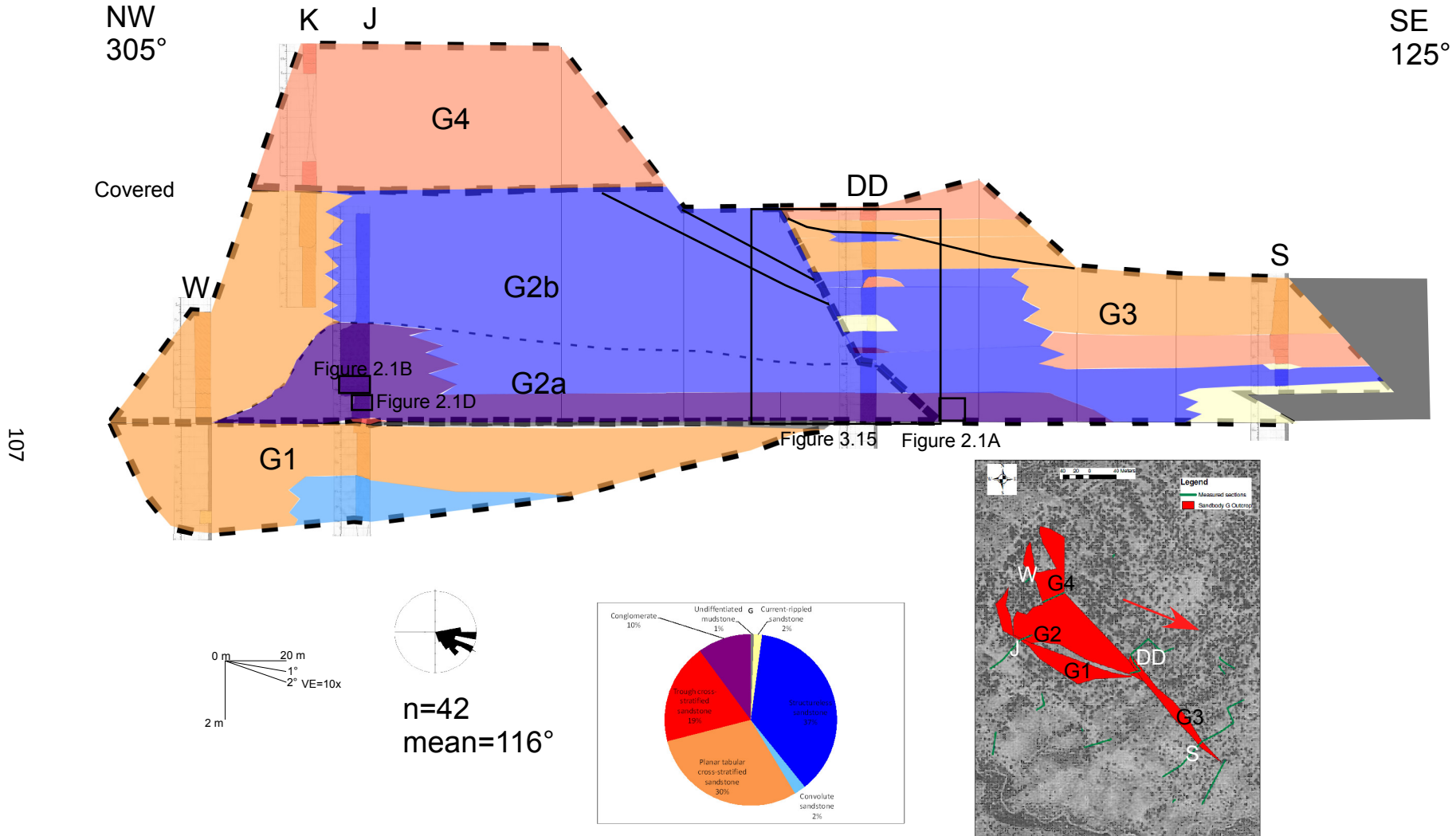


Figure 3.13 Cross-section of facies distribution for Sandbody G. Inset map showing outcrop area of subbodies and measured sections. Air photo shown in background. Red arrow indicates dominant fluvial paleocurrent direction.

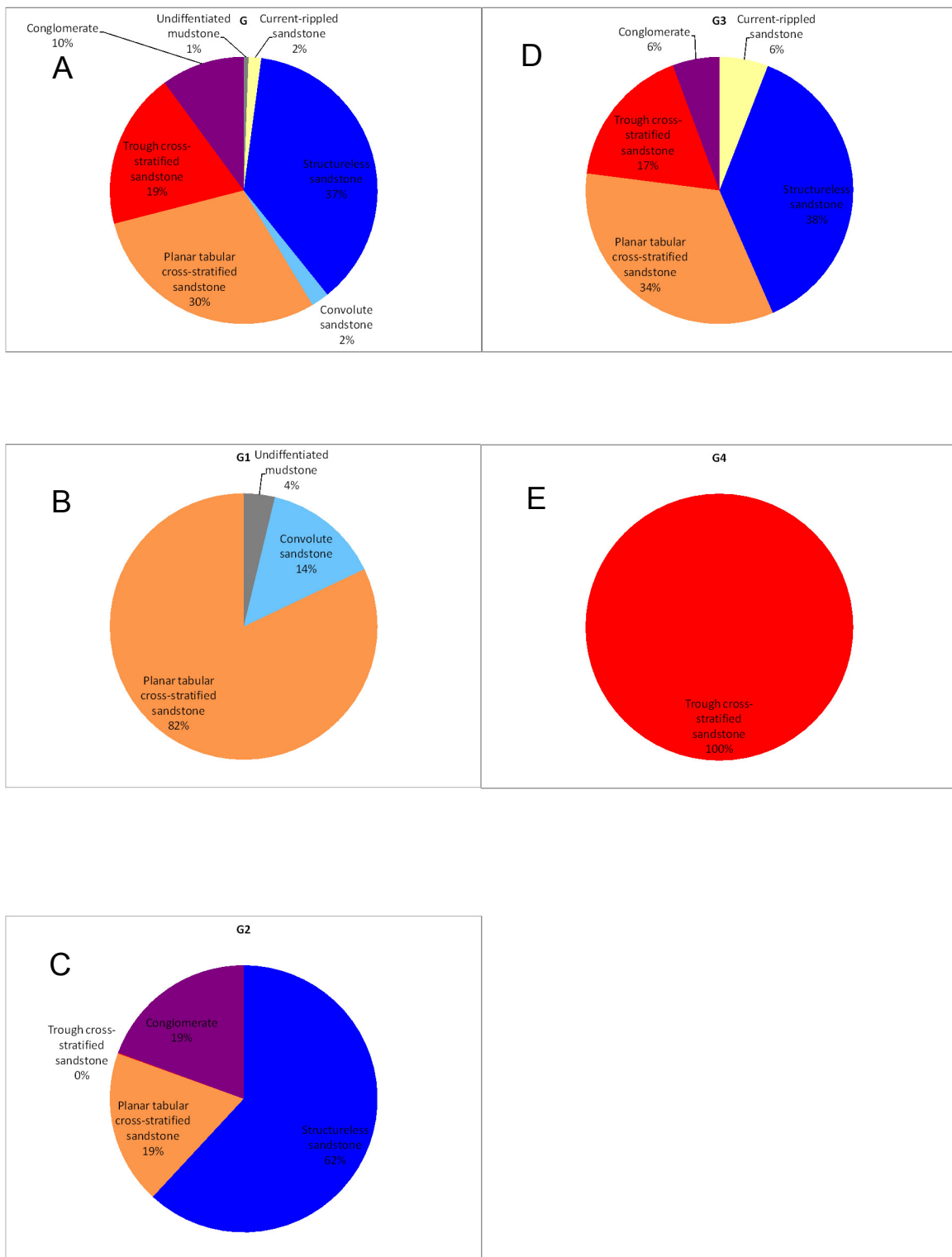


Figure 3.14 Relative abundance of facies in Sandbody G for A) overall sandbody B) Subbody G1 C) Subbody G2 D) Subbody G3 E) Subbody G4.

NW

SE

109

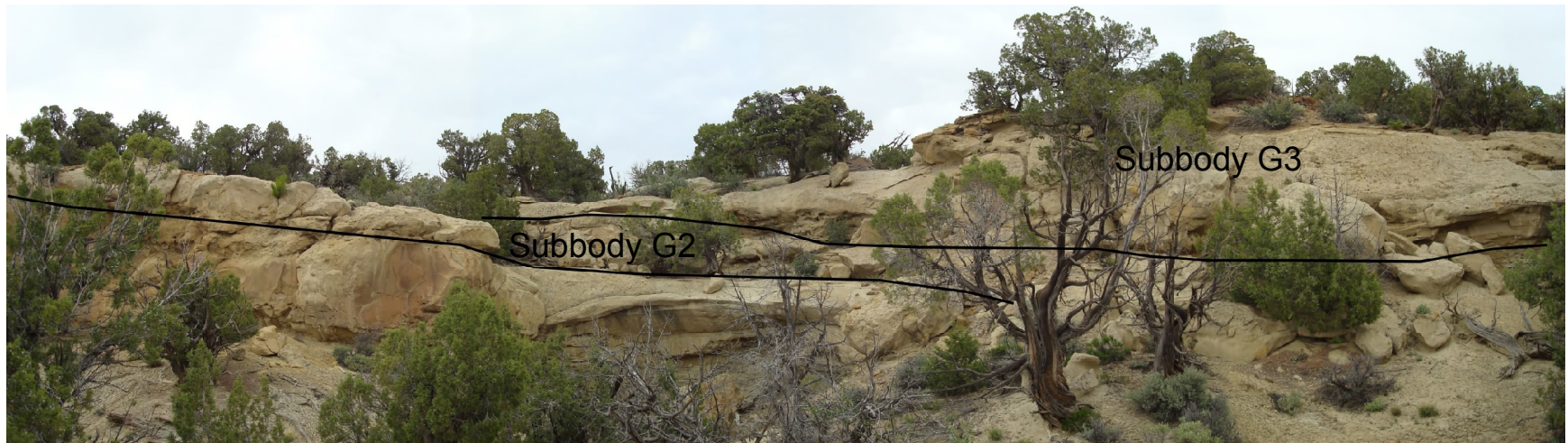


Figure 3.15 Contact between Subbodies G2 and G3

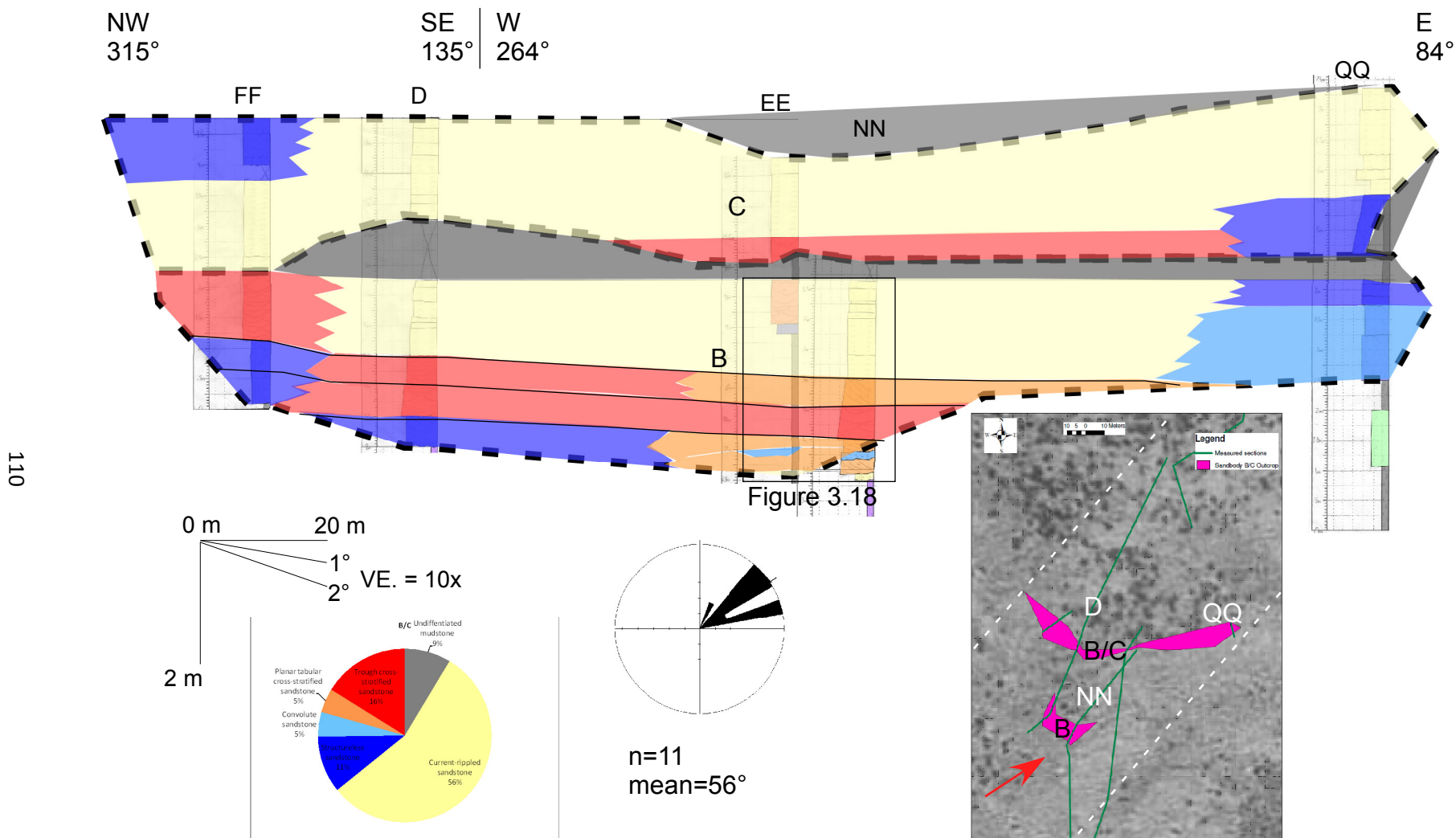


Figure 3.16 Cross-section of facies distribution for Sandbody B/C. Projected on section line of 305°-125°. Measured section NN has been transposed about 10 m southeast. Inset map showing outcrop area of subbodies and measured sections. Air photo shown in background. White dashed lines indicates estimated channel margins for Subbody B. Red arrow indicates dominant fluvial paleocurrent direction.

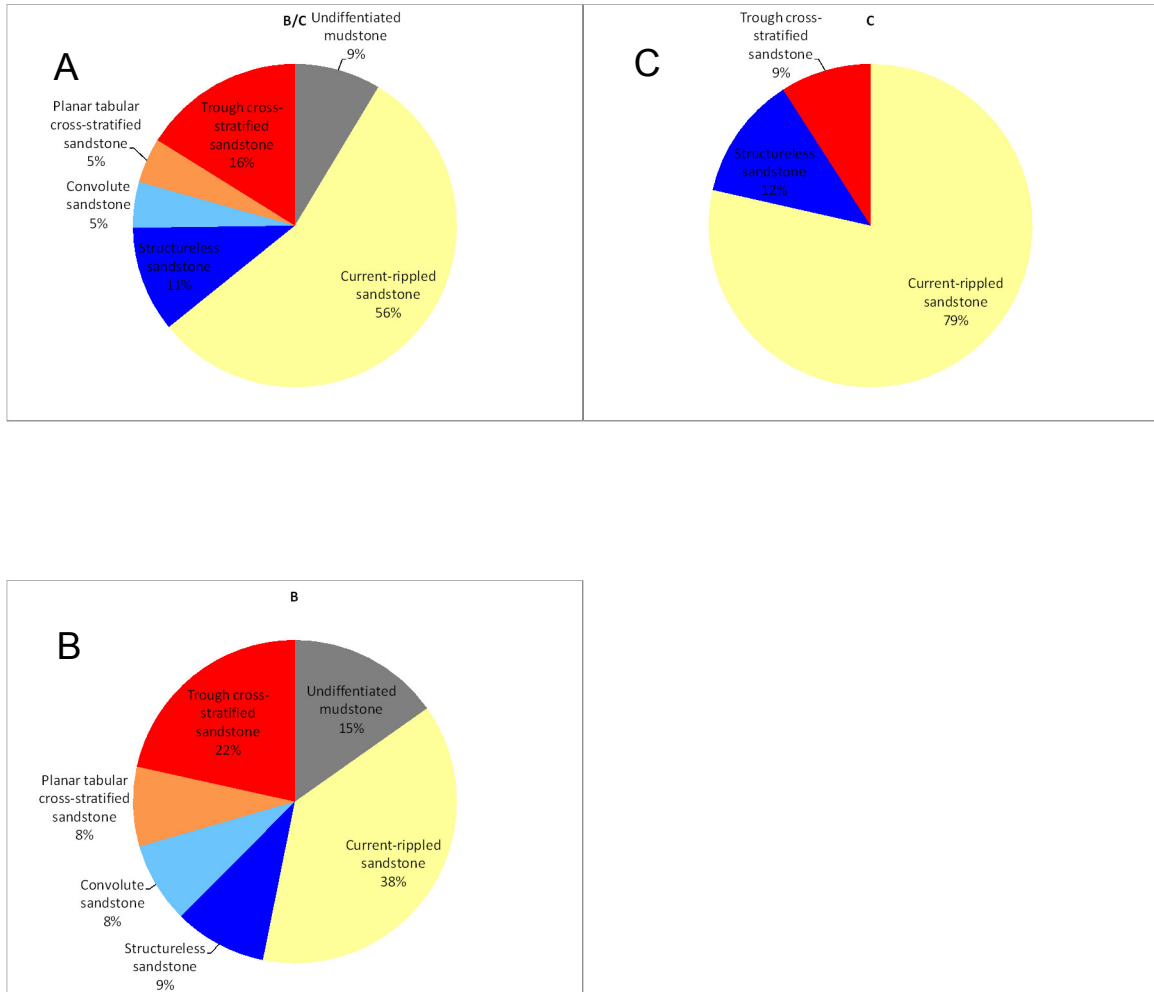


Figure 3.17 Relative abundance of facies in Sandbody B/C for A) overall sandbody B) Subbody B C) Subbody C.

112

SW

NE



Figure 3.18 Accretion surfaces on the eastern side of Subbody B. Colors correspond to facies in Table 2.1.

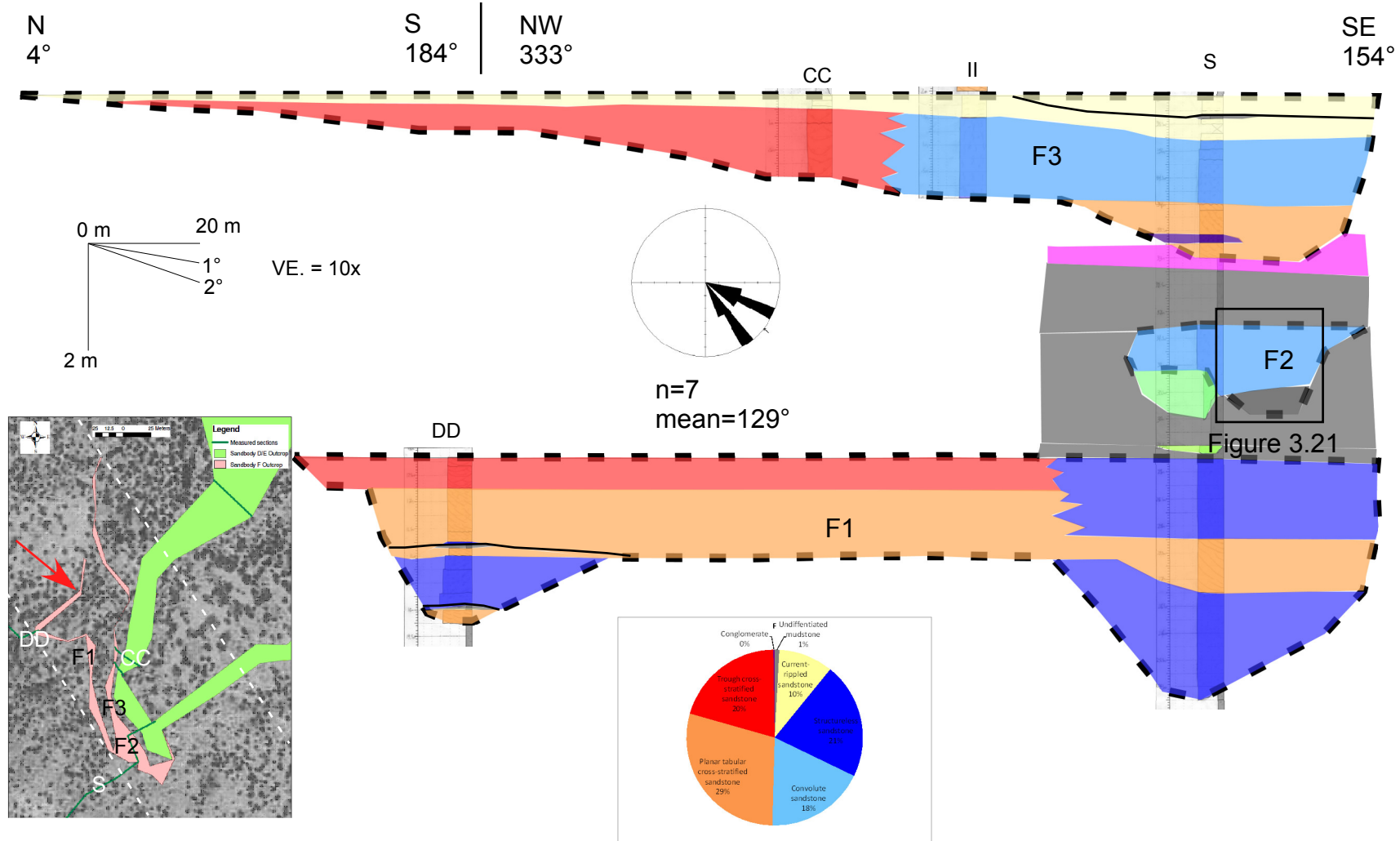


Figure 3.19 Cross-section of facies distribution of Sandbody F. Projected on 305°-125° section line. Inset map showing outcrop area of subbodies and measured sections. Air photo shown in background. White dashed lines indicates estimated channel margins for Subbody F3. Red arrow indicates dominant fluvial paleocurrent direction.

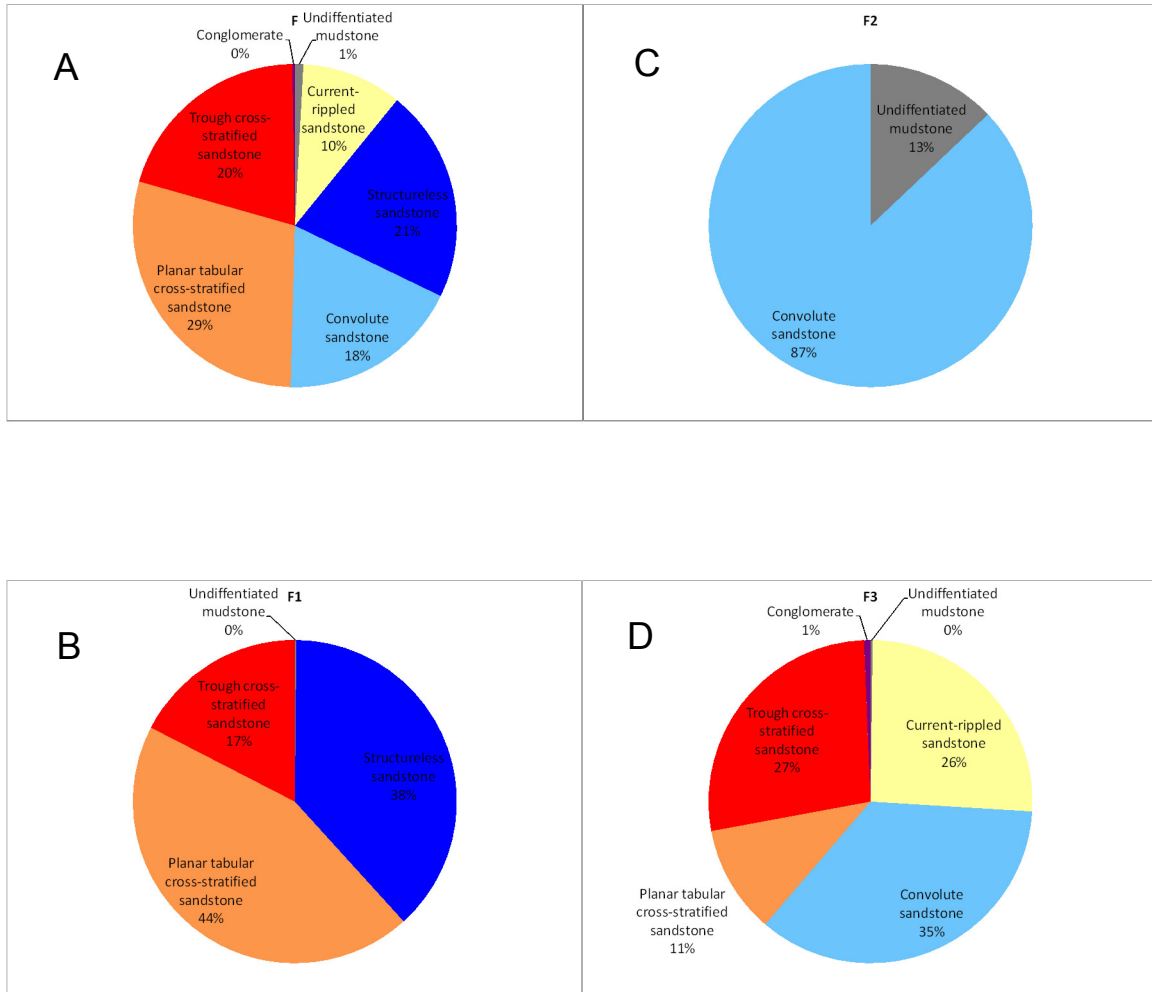


Figure 3.20 Relative abundance of facies in Sandbody F for A) overall sandbody B) Subbody F1
C) Subbody F2 D) Subbody F3.

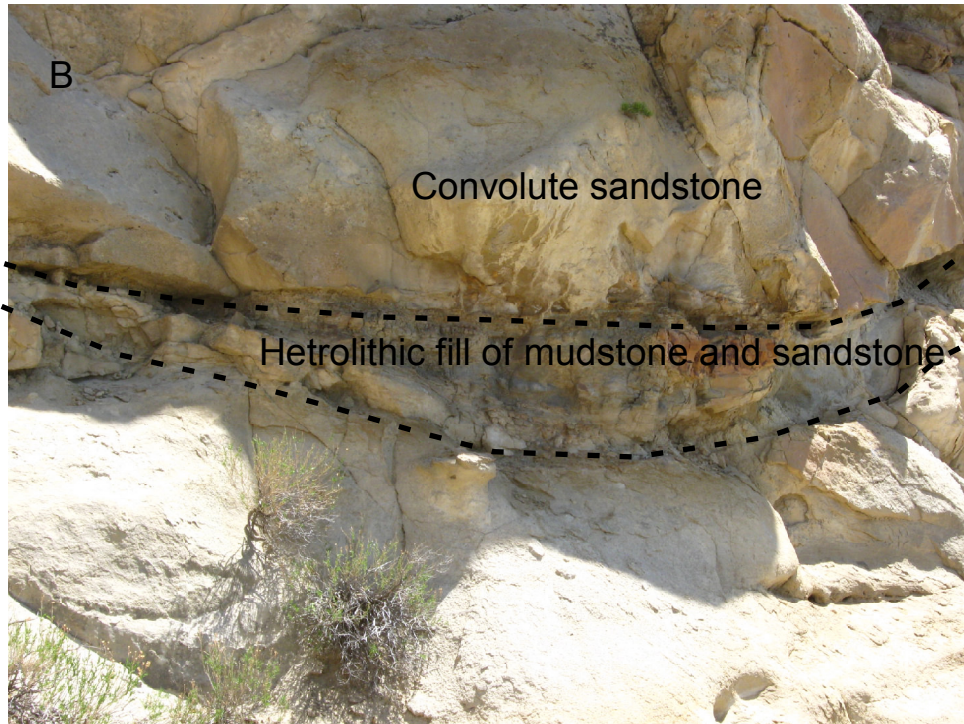
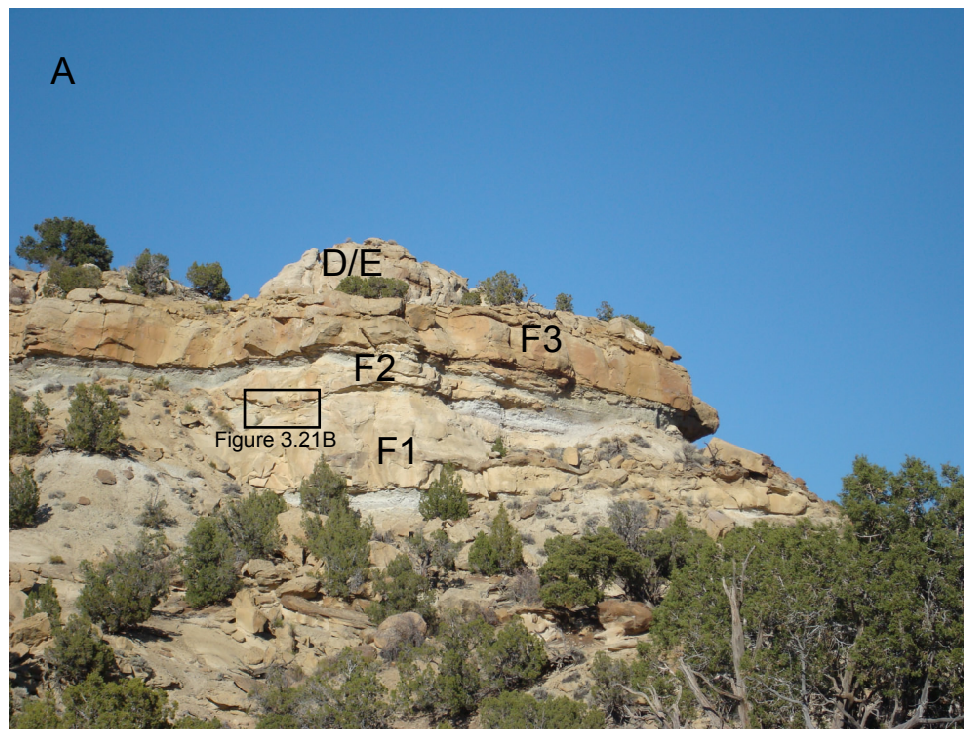


Figure 3.21 A) Photograph of Sandbody F. B) Basal unit of Subbody F2 consisting of a heterolithic mixture of mudstone and sandstone.

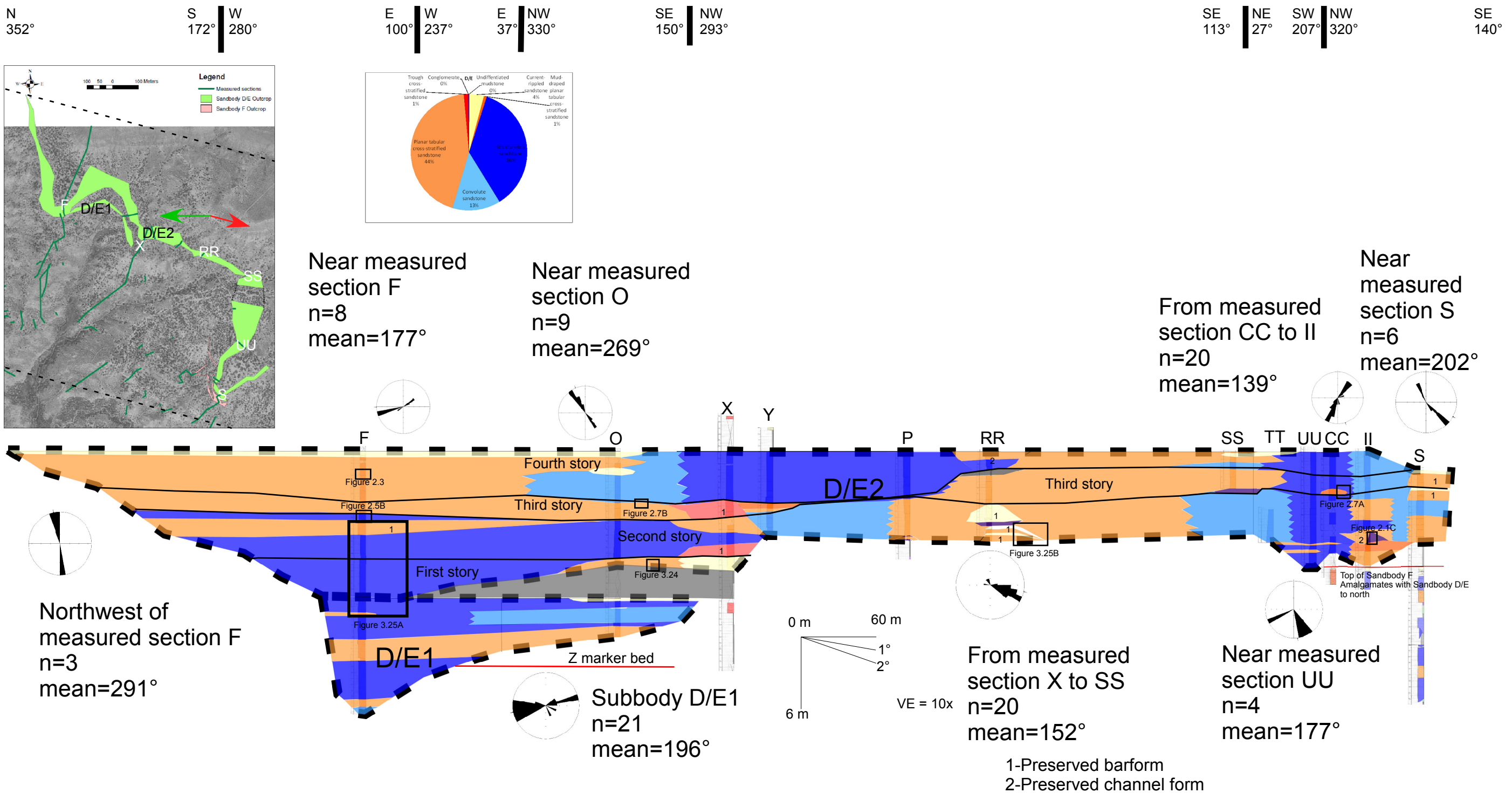


Figure 3.22 Cross-section of facies distribution of Sandbody D/E. Projected on 305°-125° section line. Inset map showing outcrop areas of subbodies and measured sections. Air photo in background. Black dashed lines indicates estimated channel margins for Subbody D/E2. Green arrow indicates dominant tidal paleocurrent direction. Red arrow indicates dominant fluvial paleocurrent direction.

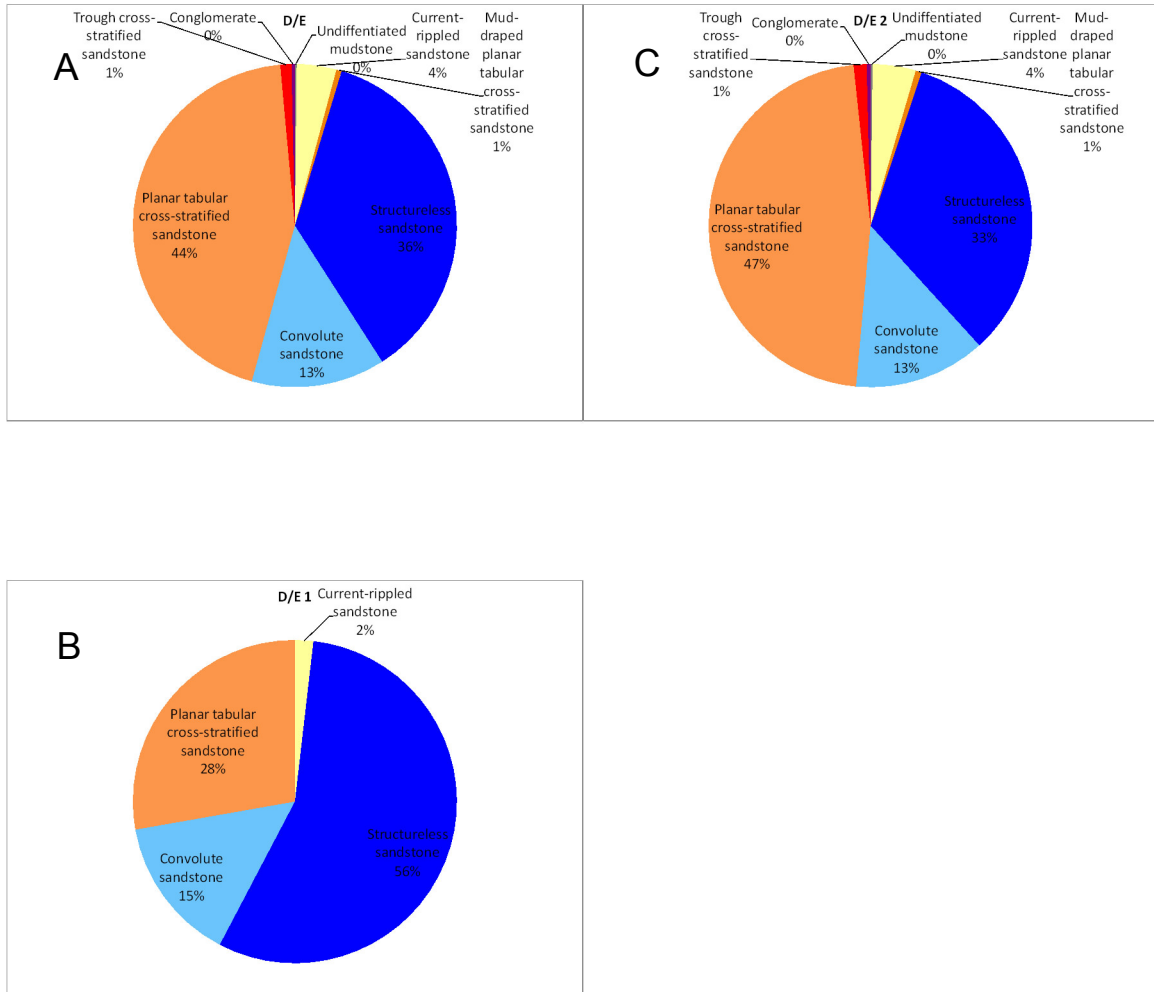


Figure 3.23 Relative abundance of facies in Sandbody D/E for A) overall sandbody B) Subbody D/E1 C) Subbody D/E2.



Figure 3.24 Life position tree stump at base of Subbody D/E2. Jacob Staff is 1.5 m.

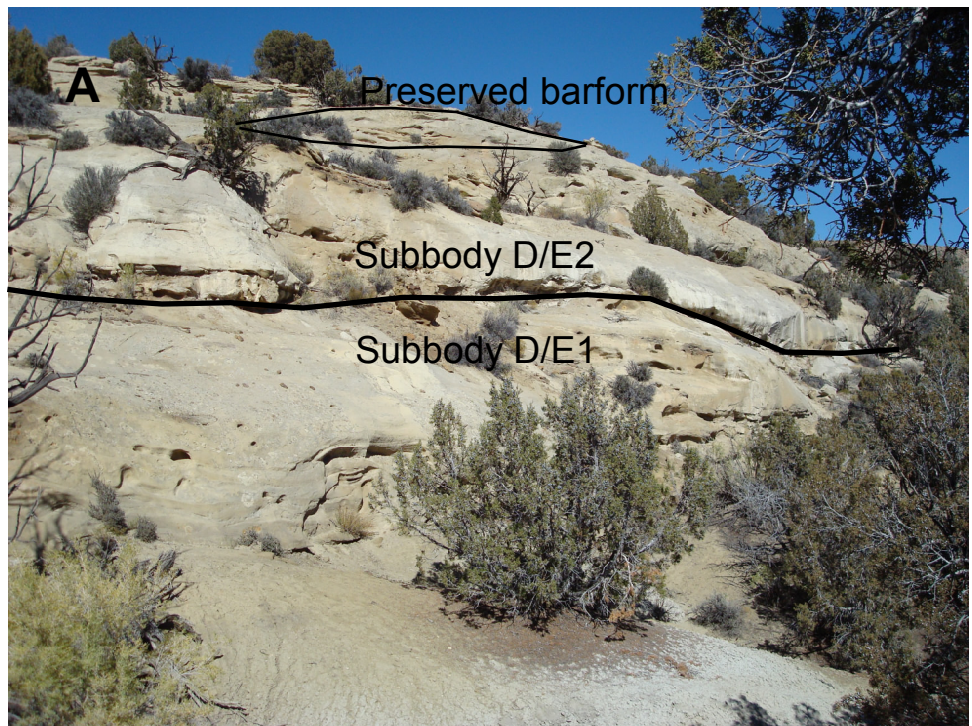


Figure 3.25 A) Contact between Subbodies D/E1 and D/E2 and preserved barform in Subbody D/E2. B) Preserved barform in Subbody D/E2 with overlying onlapping beds. Jacob Staff is 1 m.

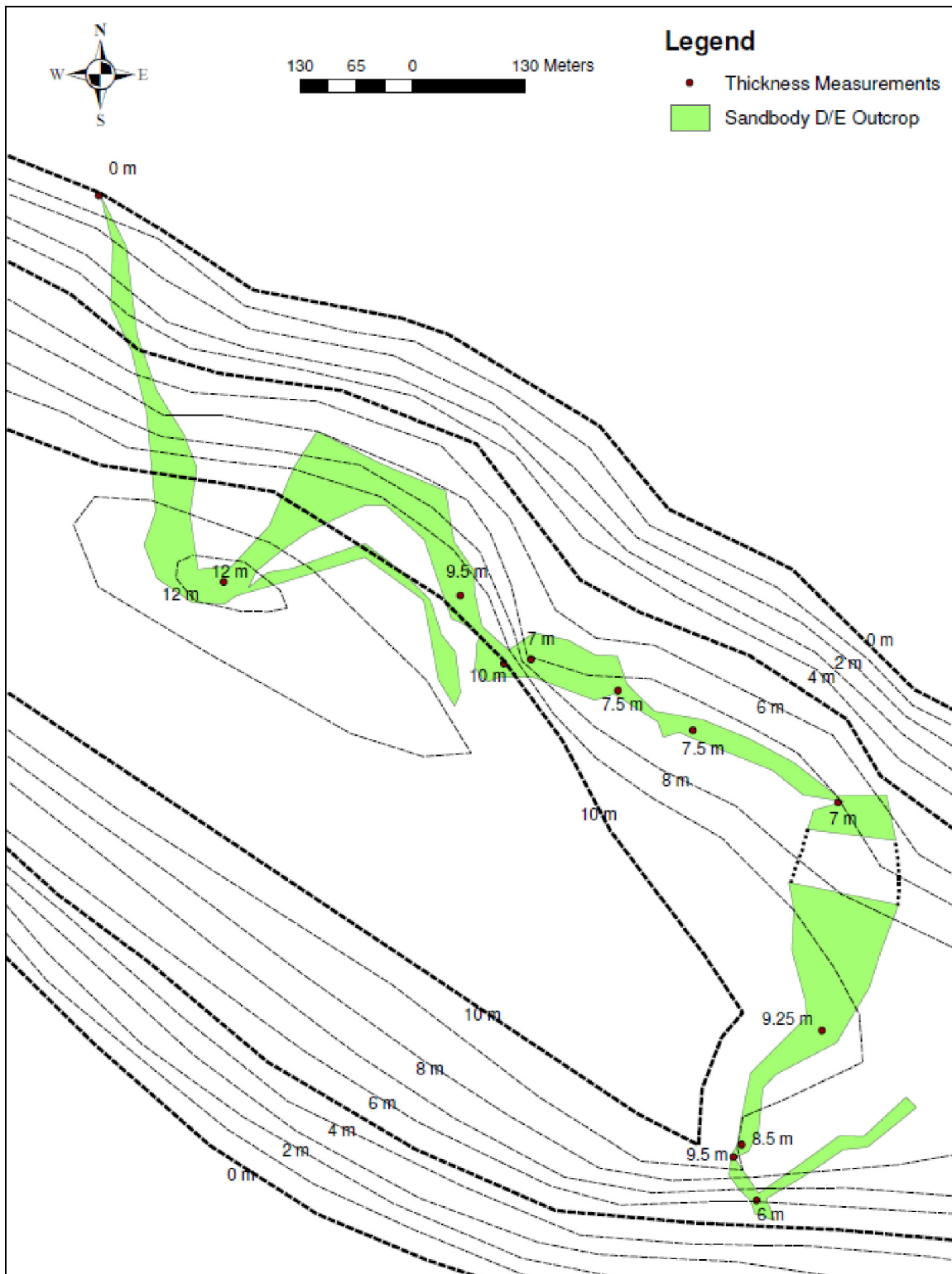


Figure 3.26 Isopach map for Subbody D/E2.



Figure 3.27 Thin wave-rippled sandstone beds in Sandbody Z. Jacob staff is 1.5 m.

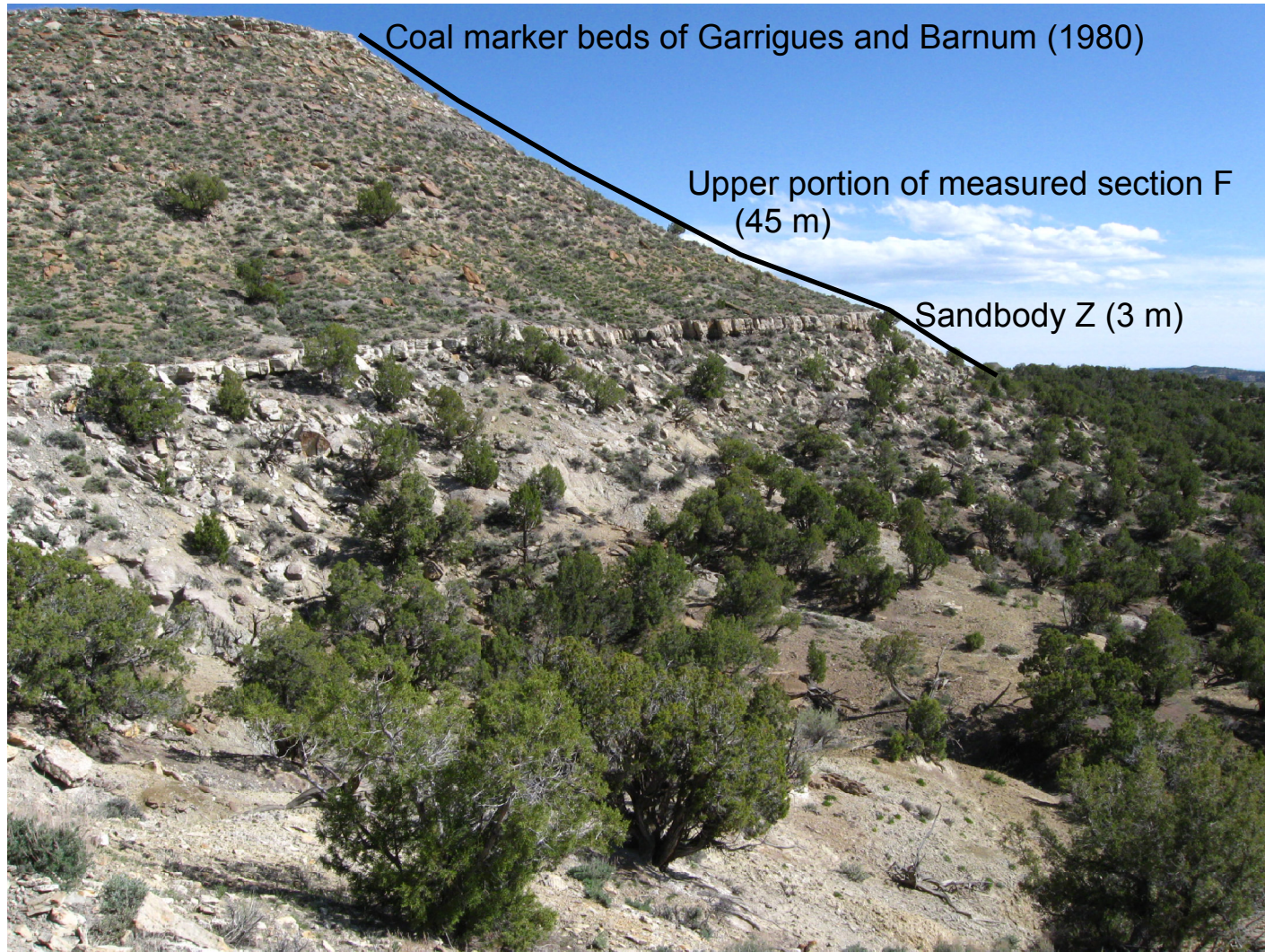


Figure 3.28 Photograph of hillside in secondary field area.



Figure 3.29 Sandbody Y incised through Sandbody Z.

CHAPTER 4: DISCUSSION AND CONCLUSIONS

This chapter groups the sandbodies in this study into 10 sandbody types and compares them to those in similar studies of non-marine strata of the upper Mesaverde Group. The second half of this chapter discusses the implications of this study on local and regional stratigraphy, including the cyclical patterns observed in the field area.

4.1 Sandbody Types within Primary Field Area

This study reports six types of tidally influenced sandbodies in the detailed field area including tidal bars (Subbodies I1, I2, and J2), tidally influenced channels (Subbodies I3 and D/E1), fill and spill channels (Subbodies J1 and J3), tidal influenced splays (Subbody A1), tidal constructional bars (Subbody A2), and tidally influenced braided complexes (Subbody D/E2) (Figure 4.1). The tidal bar sandbody type (Figure 4.2) is characterized by seaward accretion with paleocurrents oriented primarily in the landward direction. Subbodies I1 and J2 also exhibit a clear upward and seaward decreasing energy pattern. This pattern cannot be verified in Subbody I2 due to abundant soft-sediment deformation. Tidally influenced channels (Figure 4.2) are characterized by lenticular geometries with incisive lateral contacts. Subbody D/E1 consists of a single story of channel fill, while internal scour surfaces in Subbody I3 indicate multiple stories. The fill and spill channel sandbody type (Figure 4.2) is a type of tidally influenced channel where a thin splay unit formed at the top of the sandbody. One tidally influenced splay unit (Figure 4.2) was observed in the primary field area. It is characterized by radial accretion with a decreasing energy pattern towards the wide end of the sandbody. The tidal constructional bar sandbody type (Figure 4.2) is characterized by a mounded shape with bi-directional accretion. The tidally influenced braided complex (Figure 4.2) is

characterized by broad, sheet-like deposition with multiple stages of fill containing numerous relatively small barforms.

There are four types of fluvially dominated sandbodies in the primary field area including fluvial channel fills (Subbodies A3, A4, H1, H2, G1, F1, F2, and F3), fluvial constructional bars (Subbodies G2, G3, G4, and B), point bars (Subbody C), and minor crevasse splays and channels (minor sandbodies) (Figure 4.1). Fluvial channel fill sandbody types (Figure 4.2) are characterized by lenticular geometries with incisive lateral contacts. Subbodies F1 and F3 have thin mudstone units which indicate multiple stories of channel fill, while the other subbodies of this type consist of a single story of channel fill. Fluvial constructional bars (Figure 4.2) exhibit a mounded geometry with downstream accretion roughly parallel to the dominant paleocurrent direction and tend to be abundant in high energy facies. The point bar (Figure 4.2) in this study is characterized by accretion that is oblique to perpendicular to the dominant paleocurrent direction and exhibits a decreasing energy pattern. The minor crevasse splays and channels sandbody type (Figure 4.2) is characterized by thin, sheet-like geometries typically less than 1 m thick and is dominated by low energy facies.

4.2 Comparison to Similar Studies

This section compares the subbodies in this study to similar studies of non-marine strata in the Iles, Williams Fork, Farrer, Tusher, and Neslen formations of the Piceance and Uinta basins. The studies used for this comparison are Payne (1982), Nelson (1984), Caldes (1998), and Anderson (2005) from the Iles Formation, Cole and Cumella (2005) and Pranter et al. (2009) from the Williams Fork Formation, White et al. (2008) from the Farrer and Tusher formations, and Cole (2008) from the Neslen and Farrer formations

(Table 4.1). Of these studies, only Nelson (1984) and Cole (2008) reported tidal influence. The slack water macroform of Caldes (1998) appears to describe a tidally influenced deposit; however, he does not make this interpretation. Most of the tidal sandbody types have a close fluvial comparison sandbody in two or more of the comparison studies and only the tidal bar sandbody type in this study could not have developed its architecture in an entirely fluvial environment. The terminology between these studies is not standardized making direct comparisons difficult.

4.2.1 Splay Sandbody Types

The tidally influenced splay sandbody type in this study (Subbody A1) can be reasonably compared to the Gilbert delta type in Payne (1982) and Nelson (1984), the crevasse splay type in Caldes (1998), Anderson (2005), and Pranter et al. (2009), the splay sand body type in Cole (2008) and White et al. (2008), and Type E in Cole and Cumella (2005) (Table 4.1). These sandbodies are characterized by broad radial forms which exhibit decreasing energy towards the flanks. Subbody A1 is distinguished from the sandbodies described in these other studies by tidal influence. Payne (1982) and Nelson (1984) indicate that these sandbodies were forming in a floodplain lake. The tidal influence observed in this study implies that Subbody A1 maintained hydraulic contact with the ocean. The thickness range of 0.15 to 4.5 m of crevasse splays in Caldes (1998) and Pranter et al. (2009) and splay sand bodies in Cole (2008) and White et al. (2008) includes sandbodies described in this study as minor crevasse splays and channels (minor sandbodies) (Table 4.1). However, those described by Anderson (2005) are larger composite features with thicknesses up to 11 m. The size distinction in this study is important because the larger sandbodies indicate recurring events unlike the smaller

sandbodies and the smaller sandbodies would not make useful petroleum reservoirs.

Payne (1982) makes a similar distinction calling these smaller sandbodies crepe splays.

4.2.2 Bar Sandbody Types

The fluvial constructional bar type (Subbodies G2, G3, G4, and B) in this study is directly comparable to the downstream accreting bar macroform of Caldes (1998) (Table 4.1). These sandbodies represent mid-channel bars. They are dominated by high energy facies and exhibit downstream accretion. This study also includes two types of mid-channel bars which are not directly comparable to sandbodies in the other studies: the tidal bar type (Subbodies I1, I2, and J2) and the tidal constructional bar type (Subbody A2) (Table 4.1). These types are differentiated from the downstream accreting bar macroform in Caldes (1998) by the tidal influence in both types, the abundance of lower energy facies in the seaward direction of the tidal bar type and throughout in the tidal constructional bar type, the accretion in opposition to the dominant paleocurrent direction in the tidal bar type, and the bi-directional accretion of the tidal constructional bar type. None of the other studies describes any type of mid-channel bar.

The point bar sandbody type (Subbody C) is described in each of the comparison studies (Table 4.1). Point bars are sandbodies with lateral accretion sets and the highest energy near the toes of these sets. Caldes (1998) and Anderson (2005) simply refer to these sandbody types as point bars. Nelson (1984) calls them lenticular sandstones with lateral accretion surfaces and interprets them as tidal creek point bars based on the abundance mud drapes and the bi-modal paleocurrent distribution. Payne (1982) uses the term Type 2 which he interpreted as point bars in low sinuosity system. Cole and Cumella (2005), Cole (2008), White et al. (2008), and Pranter et al. (2009) do not

separate point bars from channel deposits. Cole and Cumella (2005) uses the term Type B, Cole (2008) and White et al. (2008) use the term single-story sand bodies and Pranter et al. (2009) uses the term single-story channel fill.

4.2.3 Channel Sandbody Types

This study describes four types of channel fill sandbodies. Channel fill sandbodies are described as incised lenticular units. The fluvial channel fill type (Subbodies A3, A4, H1, H2, G1, F1, F2, and F3) is the most common in this study. This type is comparable to Type 3 in Payne (1982), multi-story lenticular sandstone in Nelson (1984), the cut and fill macroform in Caldes (1998), Types B and C in Cole and Cumella (2005), single-story and multi-story sand bodies in Cole (2008) and White et al. (2008), and single-story and multi-story channel fills in Pranter et al. (2009) (Table 4.1). Subbodies F1 and F3 are multi-story channel fills in the terminology of Pranter et al. (2009) or multi-story sand bodies in the terminology of Cole (2008) and White et al. (2008), while the other subbodies are single-story channel fills or single story sand bodies, respectively. Type B units in Cole and Cumella (2005) are interpreted as simple sinuous channel systems and Type C units are interpreted as robust sinuous channel systems. They are equivalent to the Pranter et al. (2009) terms of single-story and multi-story channel fills, respectively. Payne (1982) and Nelson (1984) describe only multi-story channel fills and interpret them as anastomosing channels.

Cole (2008) notes one tidally influenced multi-story sand body in the Neslen Formation. Other than this sand body, there are no direct comparisons for the three tidally influenced channel types described in this study. However, they may be reasonably compared to their fluvial equivalents. Subbodies I3 and D/E1 of the tidally influenced

channel fill sandbody type are respectively comparable to the multi-story and single-story channel fills of Pranter et al. (2009) (Table 4.1). The fill and spill channel type (Subbodies J1 and J3) is additionally distinguished by the presence of a capping splay unit, similar to the Type A, narrow channel units, of Cole and Cumella (2005) (Table 4.1). Some of the single-story channel fills in Pranter et al. (2009) also had this geometry. The tidally influenced braided system (Subbody D/E2) in this study is similar to the amalgamated sand body of White et al. (2008) and the amalgamated channel complex of Pranter et al. (2009) (Table 4.1). These are described as thick, laterally extensive units composed of numerous channel form elements.

4.2.4 Discussion

Despite the prevalence of tidal influence in this study, tidal indicators were rarely reported in the comparison studies. It is possible that Anderson (2005), Cole and Cumella (2005), White et al. (2008), and Pranter et al. (2009) worked in entirely fluvially dominated areas. However, subtle tidal indicators could have been overlooked in the earlier studies. The field area in Payne (1982) and the stratigraphic interval in Caldes (1998) partially overlap that of this study, so the lack of tidal influence must be regarded as an oversight.

In this study, eight of the 23 subbodies were mid-channel bars, while only one was a point bar. Only Caldes (1998) reported the presence of mid-channel bars, while all of the comparison studies report the presence of point bars. This leads to the possibility that many point bars in the geologic literature are misinterpreted mid-channel bars. In this study, Subbody B bears a number of similarities to a point bar and in an outcrop view such as in Figure 3.18 could have been easily misinterpreted as such. These barform

types can only be reliably differentiated by comparing the paleocurrent and accretion directions.

This comparison also indicates the need for a standardization of the terminology in non-marine units. There is little agreement in terminology in these studies, even when they have a common author. Admittedly, this study does little to ease the confusion, using a number of terms which are not used in any of the comparison studies, but it does use standard barform terms as discussed in Chapter 1.

4.3 Local Stratigraphy

There are at least three complete cycles of floodplain to channelbelt dominated units represented within the field area. Each of these cycles represent thousands to tens of thousands of years. The first cycle contains the M1 and S1 intervals, the second cycle contains the M2 and S2 intervals, and the third cycle contains the M3 and S3 intervals (Figure 4.3). There is at least one more partial cycle represented by the M4 interval. Each of the mudstone intervals, M1, M2, M3, and M4, are strongly dominated by the floodplain facies association. Sandstone units in the mudstone dominated intervals are thin, often less than 1 m thick, but may be laterally extensive. These units most likely represent minor splay or channel deposits. These thin sandbodies are most abundant in the S2 interval (Figure 1.5). This suggests that proximity to an active channelbelt is an important factor in the deposition of these thin sandstone units. The mudstone dominated intervals most likely represent periods when the main channelbelt migrated out of the field area, with the sandstone dominated intervals representing times when the channelbelt was in the area.

There is one large scale cycle of tidal influence in the field area (Figure 4.3) which represents about 100,000 years. Tidal influence is strongest within the S1 interval with tidal dominance observed in the lower portions of Sandbodies I and A and throughout Sandbody J. With a net landward transport direction, the lower portion of the S1 interval is best described as a tidally dominated estuary. Tidal influence decreases in the upper portions of the S1 interval with lesser tidal influence observed in the upper portions of Sandbodies I and A and no tidal influence observed in Sandbody H. This trend continues into the S2 interval which is fluvially dominated with no signs of tidal influence and Sandbody F in the lower S3 interval also shows no sign of tidal influence. The tidal influence recurs in Sandbody D/E with the strength of tidal influence increasing throughout the time of deposition of Subbody D/E2. The overall pattern of tidal influence in the field area is probably related to the position of relative sea-level, with the strong tidal influence at the base of the S1 interval indicating high relative sea-level, decreasing tidal influence to complete fluvial dominance in the upper S1 to lower S3 intervals suggesting a lower relative sea-level, and the return of tidal influence in Sandbody D/E indicating a rise in relative sea-level.

4.4 Implications for Regional Stratigraphy

The Iles Formation consists of three members: the Corcoran, Cozzette, and Rollins, in stratigraphic order. Each of these members are separated by thin tongues of Mancos shale which represent transgressive phases. Another tongue of Mancos shale is present near the middle of the Cozzette member. In the southern Piceance basin, the Corcoran member is about 30 m thick, the Cozzette member has a maximum thickness of about 70 m, and the Rollins member is between 0 and 60 m thick (Hettinger and

Kirschbaum, 2002). This study records almost 100 m of Iles thickness and directly overlies about 60 m of Iles thickness from Anderson (2005). Analysis of well log data and the stratigraphic column from Payne (1982) suggests about 10 m of Iles thickness below the base of Anderson's study area. This gives a total Iles thickness of about 170 m in the Rangely area, similar to the maximum 160 m thickness in the southern Piceance basin (Hettinger and Kirschbaum, 2002).

There are two possible fourth order (~100,000 year) sequence boundaries in the primary field area. The S3 interval is highly amalgamated with up to 22 m of continuous sandstone thickness. Thick amalgamation of sandstone units is often used an indicator of sequence boundaries in non-marine settings (Shanley and McCabe, 1994; Plint et al., 2001; Atchely et al., 2004; Amorosi and Colalongo, 2005; Cleveland et al., 2010; Fanti and Catuneanu, 2010). Subbody D/E2 also represents the largest river in the field area and was probably deposited in a low-sinuosity, high-gradient system. Two green mudstone layers with abundant root traces and carbonized plant fragments observed in the lower S3 interval likely represent paleosol units, indicating a lengthy period of non-deposition. Permineralized wood and vertebrate bones are common within the field area. Permineralized wood within the field area is concentrated near Sandbodies I, A and D/E with the greatest concentrations at the base of these sandbodies (Figure 4.4). The locations of vertebrate fossils have been withheld in accordance with federal law, but show a similar pattern. The concentration of terrestrial fossils and the possible development of paleosol units suggest a long period of subaerial exposure. A sequence boundary is placed in the lower S3 interval based on the amalgamation of the sandbodies

and evidence of lengthy subaerial exposure. Another sequence boundary is tentatively placed at the base of the S1 interval based on the concentration of terrestrial fossils.

There are two transgressive intervals in the primary field area represented by the tidally influenced units in the S1 and S3 intervals. The use of tidal indicators to correlate to transgressive intervals has been well documented in the geologic literature (Shanley et al., 1992; Rodgers, 1998; Plint et al., 2001; Gomez-Veroiza and Steel, 2010). Maximum tidal influence is observed at the base of the S1 interval suggesting a maximum flooding surface near the base of this interval, immediately above the proposed sequence boundary at the base (postulated above). Tidal influence is observed increasing upward in the S3 interval suggesting the presence of a maximum flooding surface near the top of Sandbody D/E or alternately, in accordance with studies such as Fanti and Catuneanu (2010) which correlate marine maximum flooding surfaces with the landward extent of regional coal units, a coal bed within the overlying M4 interval.

Some tentative correlations can be made to the members of the Iles Formation. The coal marker beds at the top of the M4 interval have been previously correlated to the base of the Williams Fork Formation (Brownfield et al., 2000). This places all or most of the M4 interval, down to the maximum flooding surface, in the Rollins member. The interval between the sequence boundary in the lower S3 interval and the maximum flooding surface at or immediately above Subbody D/E2 likely correlates to the tongue of Mancos shale between the Cozzette and Rollins members. The sequence boundary in the lower S3 interval correlates to the top of the Cozzette member and the merged sequence boundary and flooding surface (or zone) in the lower S1 interval likely correlates to the

middle of the Cozzette member. This places the majority of the primary field area in the upper Cozzette member.

Despite the small size of the field area, this study has several implications for the regional geology of western Colorado during the Late Campanian. The thickness of the Iles Formation from this study is slightly greater than the maximum thickness in the southern Piceance basin as reported in Hettinger and Kirschbaum (2002). This implies that the available accommodation space may have been slightly greater in the Rangely area. The additional accommodation space appears to be taken up in the Corcoran and Cozzette members. The prevalence of tidal indicators more than 60 km from the shoreline would only be possible on a low-gradient coastal plain. The development of a large, braided river system in the S3 interval suggests a substantial increase in sediment supply. The typical grain size of sand in S3 interval is upper fine to lower medium compared to lower fine to upper fine in the rest of the primary field area. This indicates a significant change in the depositional system. Aschoff (personal communication) reports the presence of Campanian age growth strata in the Uinta Mountain area. Uplift in this area may have contributed to this increase in sediment supply and grain size.

4.5 Conclusions

A subsurface reservoir model based entirely on point bars would not accurately describe the primary field area. Of the 23 subbodies within the primary field area, organized into the eight major sandbodies, only one (Subbody C) is interpreted as a point bar. In addition to point bars this study reports three other types of fluvial sandbodies, including fluvial channel fills (Subbodies A3, A4, H1, H2, G1, F1, F2 and F3), fluvial constructional bars (Subbodies G2, G3, G4 and B), and minor crevasse splays and

channels (minor sandbodies), and six types of tidal sandbodies, including tidal bars (Subbodies I1, I2 and J2), tidally influenced channel fills (Subbodies I3 and D/E1), fill and spill channels (Subbodies J1 and J3), tidally influenced splays (Subbody A1), tidal constructional bars (Subbody A2), and tidally influenced braided complexes (Subbody D/E2). An accurate subsurface reservoir model must consider more types of sandbodies than just point bars and the possibility of tidal influence on the system.

Tidal influence is strong within the primary field area, despite its location 60 to 70 km from the closest transgression of the Iles shoreline (Johnson, 1989; Cumella and Ostby, 2003; Gomez-Veroiza and Steel, 2010; Schwendeman, in press). The S1 and S3 intervals are both tidally influenced. The dominant transport direction in the lower portion of the S1 interval is landward indicating the development of a tide-dominated estuary. The strength and abundance of tidal influence in the primary field area indicates tidal currents may penetrate significant upstream distances in low-gradient fluvial systems.

Strata within the field area cannot be definitively correlated to the members of the Iles Formation; however, some tentative correlations can be made. The coal marker beds correlate to the base of the Williams Fork Formation (Brownfield et al., 2000), so all or most of the M4 interval correlates to the Rollins member. There is a possible sequence boundary in the lower S3 interval indicated by the high degree amalgamation of the sandstone units, the concentration of terrestrial fossils, and possible paleosol development. This sequence boundary is likely located at the top of the Cozzette member. Tidal influence increases vertically within Sandbody D/E suggesting the initiation of a transgressive phase with a maximum flooding surface at the base of the

Rollins member likely indicated by a coal unit within the M4 interval or the upper part of Sandbody D/E. Tidal units in the S1 interval likely represent the transgression in the middle of the Cozzette member.

Table 4.1: Comparison of Sandbody Types in This Study to Similar Studies

	This Study		Most Reasonable Equivalent in Comparison Study							
	Sandbody Types	Subbodies	Payne 1982	Nelson 1984	Caldes 1998	Anderson 2005	Cole and Cumella 2005	Cole 2008	White et al. 2008	Pranter et al. 2009
Tidal	Tidal bar	I1, I2, J2	-	-	-	-	-	-	-	-
	Tidally influenced channel	I3, D/E1	Type 3 (anastomosing channel)	Multi-story lenticular sandstone (anastomosing channel)	Cut and fill macroform	-	Type B and C (simple and robust sinuous channel systems)	Single-story/multi-story sand body*	Single-story/multi-story sand body	Single-story/multi-story channel fill
	Fill and spill channel	J1, J3	-	-	-	-	Type A (narrow channel system)	-	-	Single-story channel fill
	Tidally influenced splay	A1	Gilbert delta	Gilbert delta	Crevasse splay	Crevasse splay	Type E (crevasse splays)	Splay sand body	Splay sand body	Crevasse splay
	Tidal constructional bar	A2	-	-	-	-	-	-	-	-
	Tidally influenced braided complex	D/E2	-	-	-	-	-	-	Amalgamated sand body	Amalgamated channel complex
Fluvial	Fluvial channel fill	A3, A4, H1, H2, G1, F1, F2, F3	Type 3 (anastomosing channel)	Multi-story lenticular sandstone (anastomosing channel)	Cut and fill macroform	-	Types B and C (simple and robust sinuous channel systems)	Single-story/multi-story sand body	Single-story/multi-story sand body	Single-story/multi-story channel fill
	Fluvial constructional bar	G2, G3, G4, B	-	-	Downstream accreting bar macroform	-	-	-	-	-
	Point bar	C	Type 2 (low sinuosity point bar)	Lenticular sandstones with lateral accretion surfaces (point bar)*	Point bar	Point bar	Type B (simple sinuous channel systems)	Single-story sand body	Single-story sand body	Single-story channel fill
	Minor crevasse splays and channels	minor sandbodies	Crepe splay	-	Crevasse splay	-	Type E (crevasse splays)	Splay sand body	Splay sand body	Crevasse splay

* denotes tidally influenced sandbody in comparison study

- denotes no apparent equivalent in comparison study

138

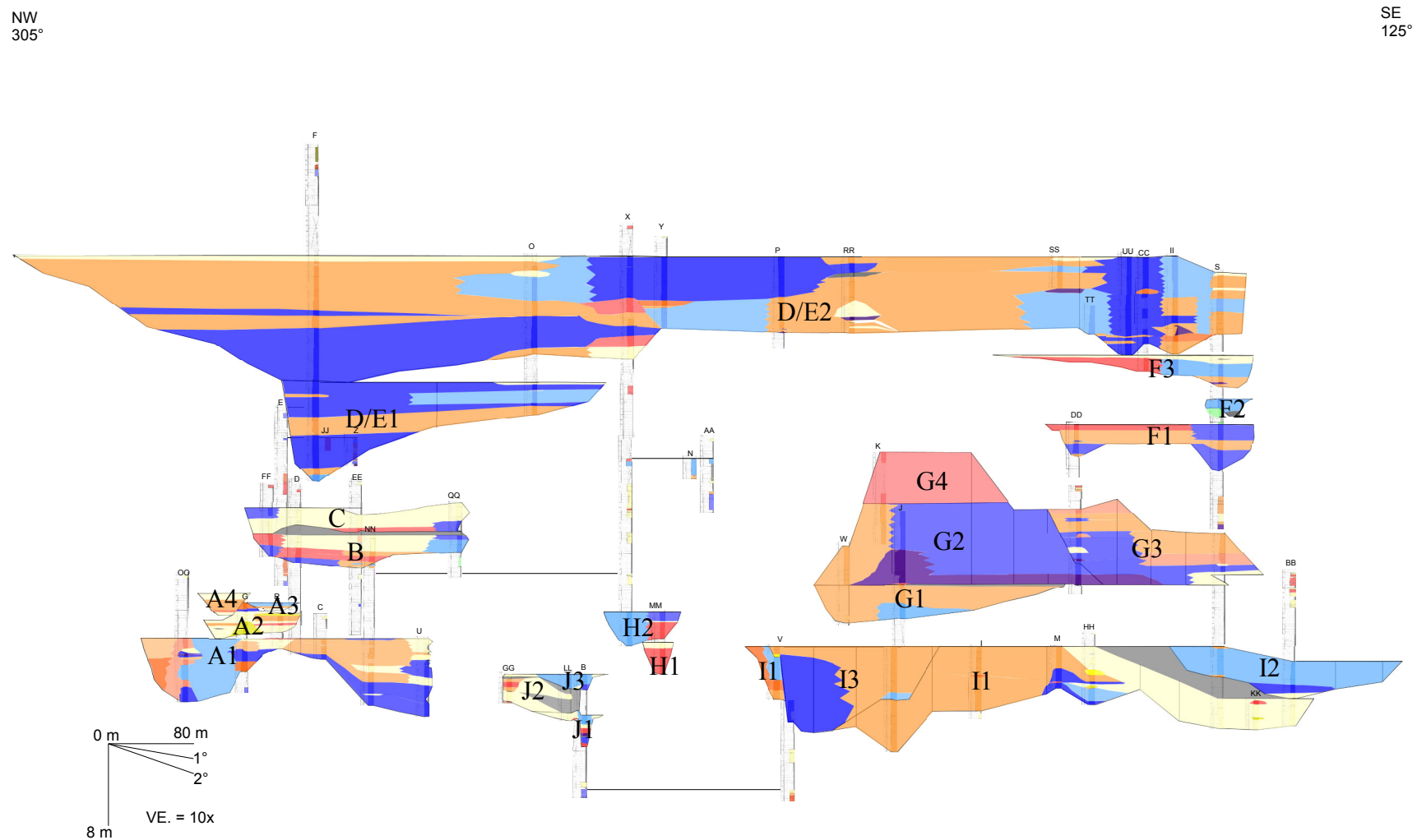


Figure 4.1 Composite cross-section of major sandbodies within the primary field area. For details, see cross-sections in Chapter 3.

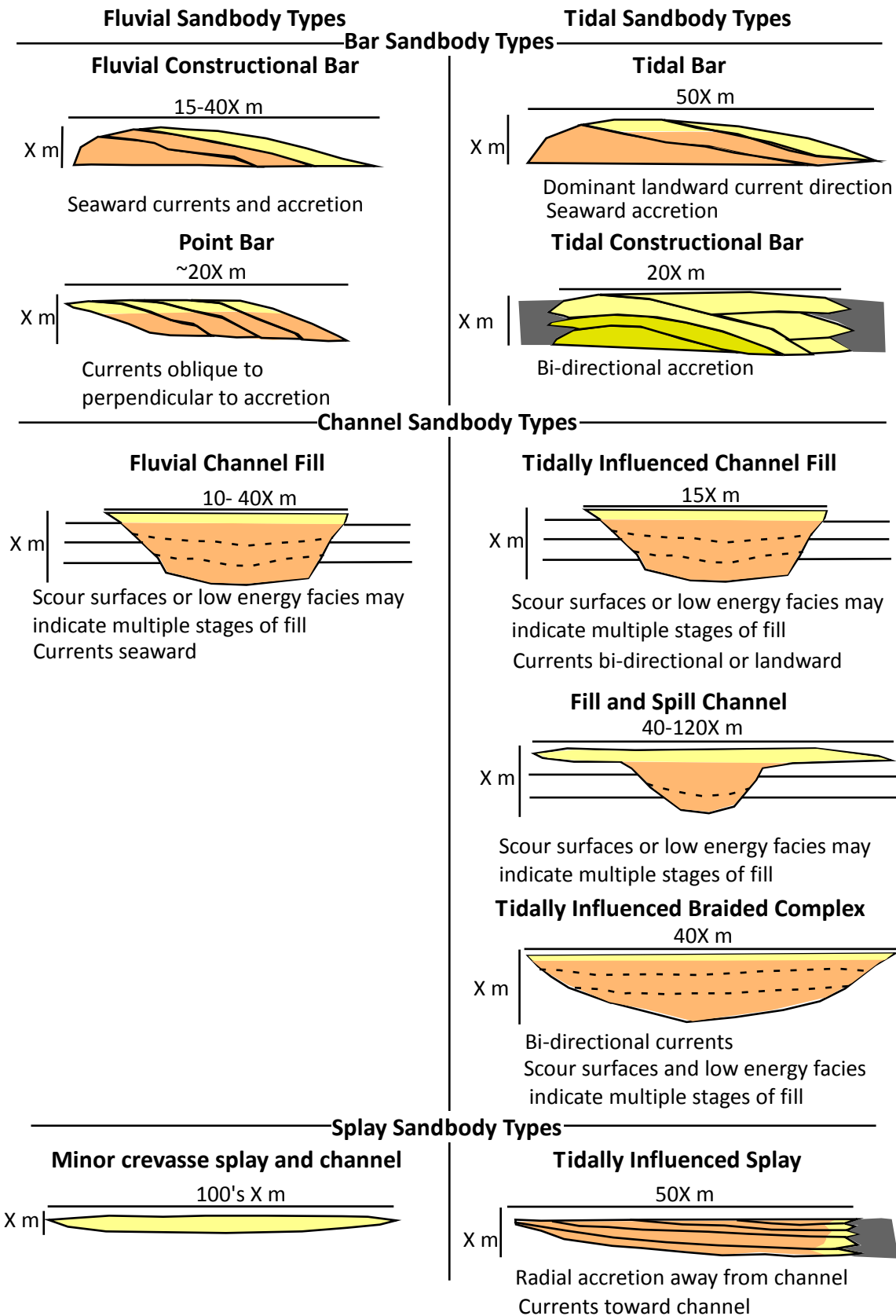


Figure 4.2 Generalized cross-sections of sandbody types observed in the primary field area.

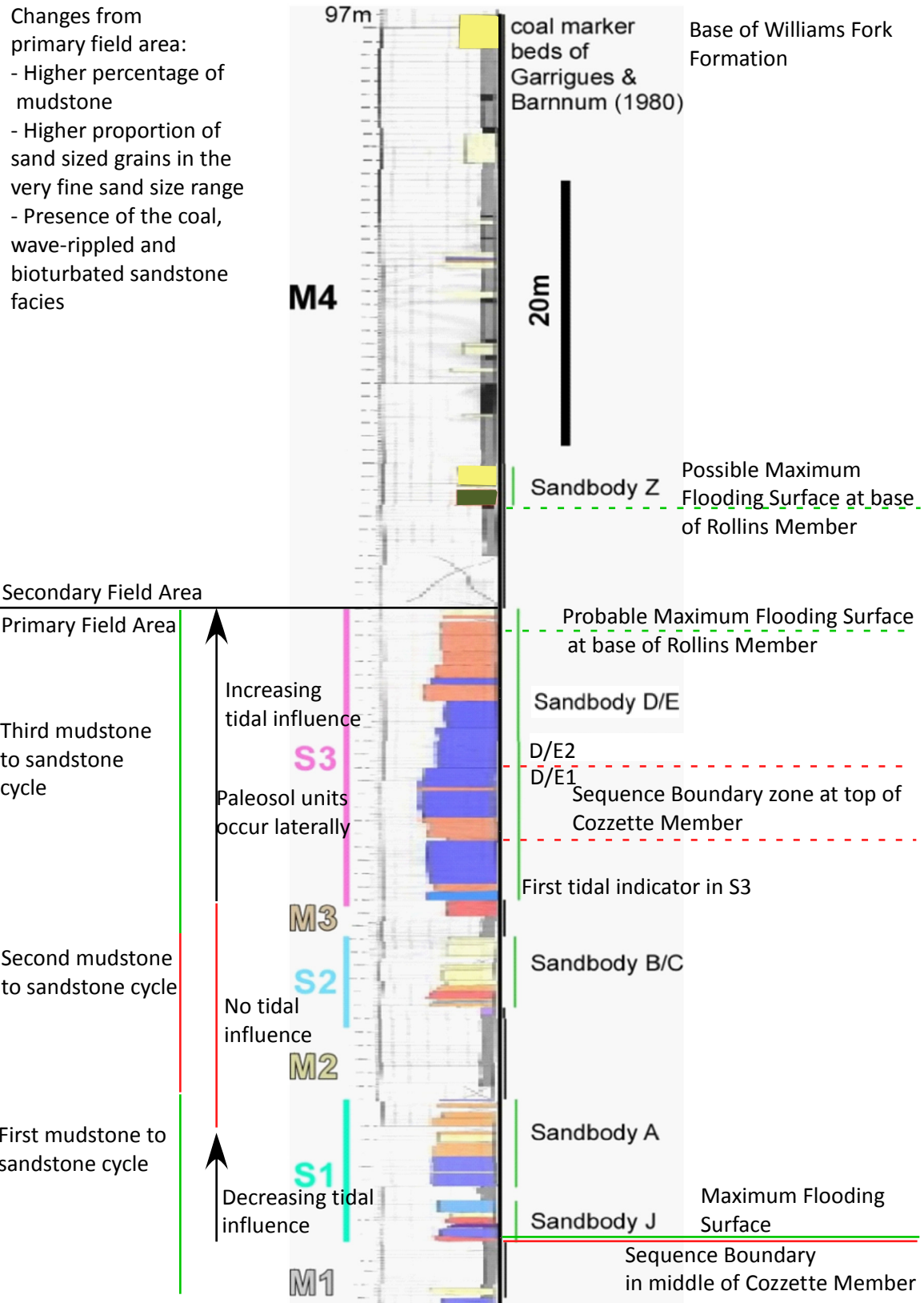


Figure 4.3 Composite stratigraphic column showing key stratigraphic surfaces and cycles interpreted within the field area.

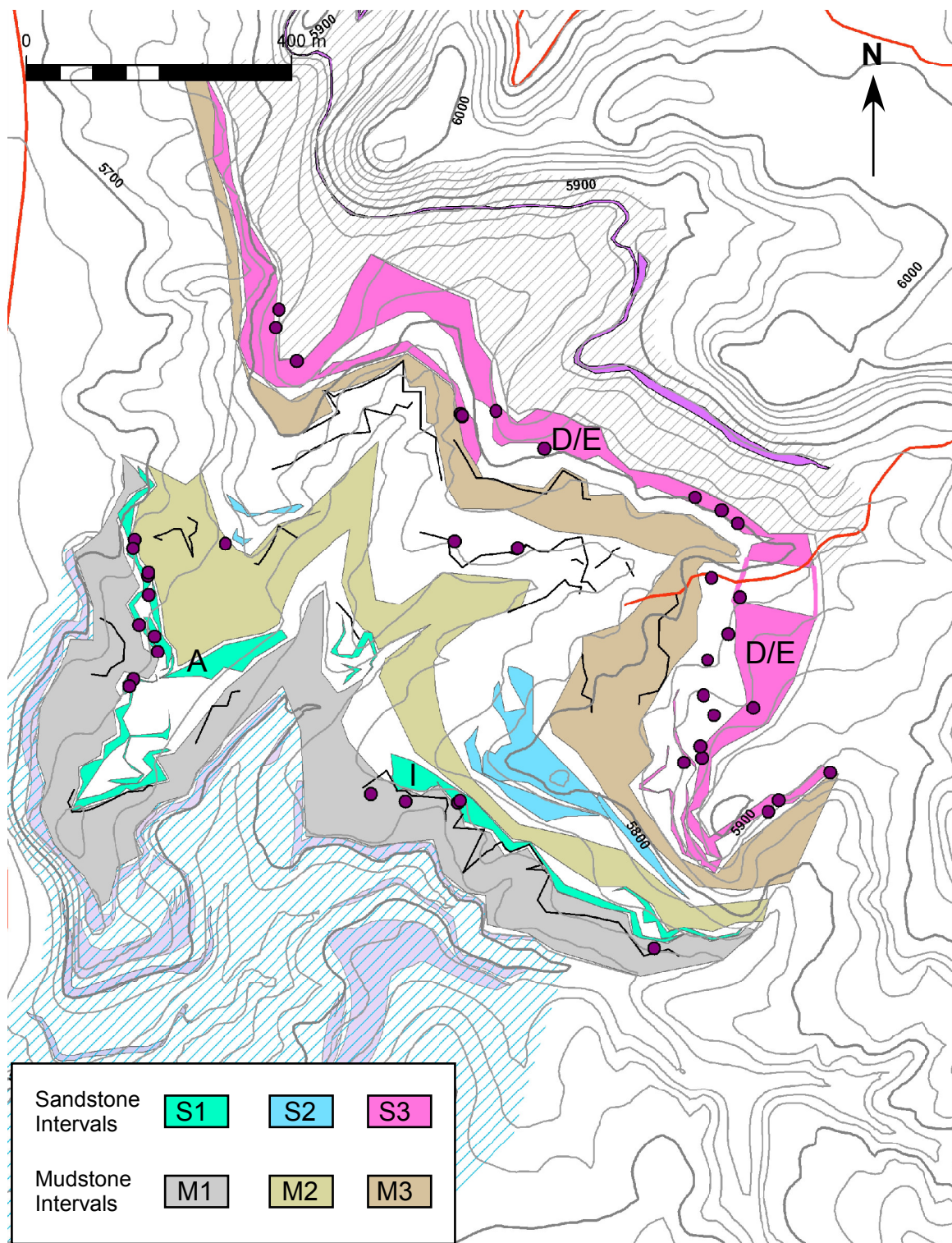


Figure 4.4 Map of field area showing location of permineralized wood fossils. Most points are near Sandbodies I, A and D/E.

REFERENCES CITED

- Amorosi, A., and Colalongo, M. L., 2005, The linkage between alluvial and coeval nearshore marine successions: Evidence from the late Quaternary record of the Po River Plain, Italy. *in* Blum, M. D., Marriott, S. B., and Leclair, S. F. *eds.* Fluvial sedimentology VII: Special Publication Number 35 of the International Association of Sedimentologists, p. 257-275.
- Anderson, D. S., 2005, Architecture of crevasse splay and point bar bodies of the nonmarine Iles Formation north of Rangely, Colorado: Implications for reservoir description: *The Mountain Geologist*, v. 42, No. 3, p. 109-122.
- Aschoff, J. L., and Steel, R., In press, Anatomy and development of a low-accommodation clastic wedge, Upper Cretaceous, Cordilleran Foreland Basin, USA: *Sedimentary Geology*.
- Aschoff, J. L., and Steel, R., In press, Anomalous clastic wedge development during the Sevier-Laramide transition: *GSA Bulletin*.
- Atchley, S. C., Nordt, L. C., and Dwarkin, S. I., 2004, Eustatic control on alluvial sequence stratigraphy: A possible example from the Cretaceous-Tertiary transition of the Tornillo basin, Big Bend National Park, west Texas, U.S.A.: *Journal of Sedimentary Research*, v. 74, No. 3, p. 391-404.
- Bader, J. W., 2009, Structural and tectonic evolution of the Douglas Creek Arch, the Douglas Creek Fault Zone, and environs, northwestern Colorado and northeastern Utah: Implications for petroleum accumulation in the Piceance and Unita basins: *Rocky Mountain Geology*, v. 44, No. 2, p. 121-145.
- Best, J. L., Ashworth, P. J., Bristow, C. S., and Roden, J., 2003, Three-dimensional sedimentary architecture of a large, mid-channel sand braid bar, Jamuna River, Bangladesh: *Journal of Sedimentary Research*, v. 73, No. 4, p. 516-530.
- Bottjer, D. J., and Droser, M. L., 1994, The history of Phanerozoic bioturbation. *in* Donovan, S. K. *ed.* *The paleobiology of trace fossils*: Wiley, p. 155-176.
- Bridge, J. S., and Tye, R. S., 2000, Interpreting the dimensions of ancient fluvial channel bars, channels, and channel belts from wireline-logs and cores: *AAPG Bulletin*, v. 84, No. 8, p. 1205-1228.
- Brownfield, M. E., Roberts, L. N. R., Johnson, E. A., and Mercier, T. J., 2000, Chapter N: Assessment of the distribution and resources in the Deserado Coal Area, Lower White River Coal Field, northwest Colorado. *in* Kirschbaum, M. A., Roberts, L. N. R., and Biewick, L. R. H. *eds.* *Geologic Assessment of Coal in the Colorado Plateau: Arizona, Colorado, New Mexico, and Utah*: U.S. Geological Survey Professional Paper 1625-B. 25 p.

- Caldes, B., 1998, Genetic stratigraphic interpretation of Upper Cretaceous continental strata, Mesaverde Formation, Rio Blanco County, northwest Colorado: M.S. Thesis. Colorado School of Mines. 148 p.
- Caldes, B. A., 2005, Attribute variation within fluvial sand bodies of the Iles Formation east of Rangely, Colorado: The Mountain Geologist, v. 42, No. 3, p. 123-139.
- Cant, D. J., 1978, Bedforms and bar types in the South Saskatchewan River: Journal of Sedimentary Petrology, v. 48, No. 4, p. 1321-1330.
- Cleveland, D. M., Achley, S. C., and Nordt, L. C., 2007, Continental sequence stratigraphy of the Upper Triassic (Norian-Rhaetian) Chinle strata, northern New Mexico, U.S.A.: Allocyclic and autocyclic origins of paleosol-bearing alluvial successions: Journal of Sedimentary Research, v. 77, p. 909-924.
- Cole, R., 2008, Characterization of fluvial sand bodies in the Neslen and Lower Farrer Formations (Upper Cretaceous), Lower Sego Canyon, Utah. *in* Longman, M. W., and Morgan, C. D. *eds.* Hydrocarbon systems and production in the Uinta basin, Utah: Rocky Mountain Association of Geologists and Utah Geological Association Publication 37, p. 81-100.
- Cole, R. D., and Cumella, S. P., 2005, Sand body architecture in the Lower Williams Fork Formation (Upper Cretaceous), Coal Canyon, Colorado, with comparison to the Piceance basin subsurface: The Mountain Geologist, v. 42, No. 3, p. 85-107.
- Cross, T. A., 1986, Tectonic controls of foreland basin subsidence and Laramide style deformation, western United States. *in* Allen, P. A., and Homewood, P. *eds.* Foreland basins: Special Publication No. 8 of the International Association of Sedimentologists, p. 15-39.
- Cullins, H. L., 1968, Geologic map of the Bantz Point Quadrangle, Rio Blanco County, Colorado: U.S. Geological Survey geologic quadrangle map GQ-703, Scale 1:24,000.
- Cumella, S. P., and Ostby, D. B., 2003, Geology of basin-centered gas accumulation, Piceance basin, Colorado. *in* Peterson, K. M., Olson, T. M., and Anderson, D. S. *eds.* Piceance basin 2003 guidebook: The Rocky Mountain Association of Geologists, p. 171-193.
- Fanti, F., and Catuneau, O., 2010, Fluvial sequence stratigraphy: The Wapiti Formation, west-central Alberta, Canada: Journal of Sedimentary Research, v. 80, p. 320-338.
- Fielding C. R., 1984, Upper delta plain lacustrine and fluviolacustrine facies from the Westphalian of the Durham Coalfield, NE England: Sedimentology, v. 31, p. 547-567.

Franczyk, K. J., Fouch, T. D., Johnson, R. C., Molenaar, C. M., and Cobban, W. A., 1992, Cretaceous and Tertiary paleogeographic reconstructions for the Uinta-Piceance basin study area, Colorado and Utah: U.S. Geological Survey Bulletin 1787-Q, 37 p.

Gale, H. S., 1910, Coal fields of northwestern Colorado and northeastern Utah: U.S. Geological Survey Bulletin 415, p. 179-203.

Garrigues, R. S., and Barnum, B. E., 1980, Geologic map and coal sections of the Rangely NE Quadrangle, Rio Blanco and Moffat Counties, Colorado: U.S. Geological Survey Open-File Report OF-80-274, Scale 1:24,000.

Gibling, M. R., 2006, Width and thickness of fluvial channel bodies and valley fills in the geological record: A literature compilation and classification: Journal of Sedimentary Research, v. 76, p. 731-770.

Green, G. N., 1992, The digital geologic map of Colorado in ARC/INFO format: U.S. Geological Survey Open-File Report 92-0507, 9 p.
<http://pubs.usgs.gov/of/1992/ofr-92-0507>.

Gomez-Veroiza, C., and Steel, R. J., 2010, Iles clastic wedge development and sediment partitioning within a 300-km fluvial to marine Campanian transect (3 m.y.), Western Interior Seaway, southwestern Wyoming and northern Colorado: AAPG Bulletin, v. 94, No. 9, p. 1349-1377.

Johnson, R. C., 1989, Geologic history and hydrocarbon potential of Late Cretaceous-age, low-permeability reservoirs, Piceance basin, western Colorado: U.S. Geological Survey Bulletin 1787-E. 51 p.

Jones, J. R. Jr., 1984, Reservoir characterization for numerical simulation of Mesaverde meanderbelt sandstone, northwestern Colorado: M.S. Thesis. The University of Texas at Austin. 115 p.

Kammerer, J. C., 1990, Largest rivers in the United States: U.S. Geological Survey Open-File Report 87-242, 2 p.

Hettinger, R. D., and Kirschbaum, M. A., 2002, Stratigraphy of the Upper Cretaceous Mancos Shale (Upper Part) and Mesaverde Group in the southern part of the Uinta and Piceance basins, Utah and Colorado: U.S.G.S. Geologic Investigations Series I-2764. 21 p.

Liu, S. F., Nummendal, D., Yin P. G., and Luo, H. J., 2005, Linkage of Sevier thrusting episodes and Late Cretaceous foreland basin megasequences across southern Wyoming (USA): Basin Research, v. 17, p. 487-506.

- Lunt, I. A., and Bridge J. S., 2004, Evolution and deposits of a gravelly braid bar, Sagavanirktok River, Alaska: *Sedimentology*, v. 51, p. 415-432.
- Nelson, K. H., 1984, Estuarine and anastomosing fluvial systems of the Lower Mesaverde Group, northwestern Colorado: M. A. Thesis. The University of Texas at Austin. 151 p.
- Ogg, J. G., Agterberg, F. P., and Gradstein, F. M., 2004, Chapter 19: The Cretaceous period. *in* Gradstein, F. M., Ogg, J. G., and Smith, A. G. *eds.* A geologic time scale 2004. Cambridge University Press. p. 344-383.
- Payne, J. B., 1982, Anastomosing and meandering fluvial systems Mesaverde Group (Campanian), northwest Colorado: M.A. Thesis, The University of Texas at Austin. 144 p.
- Plint, G. A., McCarthy, P. J., and Faccini, U. F., 2001, Nonmarine sequence stratigraphy: Updip expression of sequence boundaries and systems tracts in a high-resolution framework, Cenomanian Dunvegan Formation, Alberta foreland basin, Canada: *AAPG Bulletin*, v. 85, No. 11, p. 1967-2001.
- Ponten, A., and Plink-Bjorklund, P., 2007, Depositional environments in an extensive tide-influenced delta plain, Middle Devonian Gauja Formation, Devonian Baltic basin: *Sedimentology*, v. 54, p. 969-1006.
- Pranter, M. J., Cole, R. D., Panjaitan, H., and Sommer, N. K., 2009, Sandstone-body dimensions in a lower coastal-plain depositional setting: Lower Williams Fork Formation, Coal Canyon, Piceance basin, Colorado: *AAPG Bulletin*, v. 93, No. 10, p. 1379-1401.
- Ritzma, H. R., 1969, Tectonic resume, Uinta Mountains. *in* Lindsay, J. B., Salwerowicz, F. A., and Callaghan, E. *eds.* Geologic guidebook of the Uinta Mountains: Utah's maverick range: Sixteenth Annual Field Conference, Intermountain Association of Geologists, p. 57-63.
- Rodgers, R. R., 1998, Sequence analysis of the Upper Cretaceous Two Medicine and Judith River Formations, Montana: Nonmarine response to the Claggett and Bearpaw Marine Cycles: *Journal of Sedimentary Research*, v. 68, No. 4, p. 615-631.
- Schwendeman, K. M., In press, Sequence stratigraphy of the Campanian Castlegate Bentonite through Iles Formation interval through well-log analysis in the Piceance basin, northwestern Colorado: M.S. Thesis. University of Colorado-Boulder.
- Shanley, K. W., and McCabe, P. J., 1994, Perspectives on the sequence stratigraphy of continental strata: *AAPG Bulletin*, v. 78, No. 4, p. 544-568.

- Shanley, K. W., McCabe, P. J., and Hettinger, R. D., 1992, Tidal influence in Cretaceous fluvial strata from Utah, USA: A key to sequence stratigraphic interpretation: *Sedimentology*, v. 39, p. 905-930.
- Sprinkel, D. A., 1999, Digital geologic resources atlas of Utah: Utah Geological Survey, Bulletin 129DF.
- Tooth, S., 2005, Splay formation in the lower reaches of ephemeral rivers on the northern plains of arid central Australia: *Journal of Sedimentary Research*, v. 75, p. 636-649.
- Westergard, B. E., Mulvihill, C. I., Ernst, A. G., and Baldigo, B. P., 2005, Regionalized equations for bankfull-discharge and channel characteristics of streams in New York state: Hydrologic region 5 in central New York. *Scientific Investigations Report 2004-5247*. p. 16.
- White, H., Cole, R., Stancel, S., Lee, C., and MacMillan, L., 2008, "Window" outcrop analogs for Greater Natural Buttes Field, Uinta basin, Utah. *in* Longman, M. W. and Morgan, C. D. *eds.* *Hydrocarbon systems and production in the Uinta basin, Utah: Rocky Mountain Association of Geologists and Utah Geological Association Publication 37*, p. 209-235.
- Wray, L., Apeland, A. D., Hemborg, H., Thomas, B., Cheryl A., Morgan, M. L., and Young, G. B. C., 2005, Shapefiles for the 2002 oil and gas fields map of Colorado: Colorado Geological Survey, Open-File Report 05-9, CD-ROM.